

# Advances in wide-bandgap III-V solar cells

Cite as: Appl. Phys. Rev. **12**, 031309 (2025); doi: [10.1063/5.0273566](https://doi.org/10.1063/5.0273566)

Submitted: 31 March 2025 · Accepted: 25 June 2025 ·

Published Online: 17 July 2025



Stephanie Tomasulo<sup>1,a)</sup>  and Minjoo Larry Lee<sup>2,a)</sup> 

## AFFILIATIONS

<sup>1</sup>U.S. Naval Research Laboratory, Washington, District of Columbia 20375, USA

<sup>2</sup>The Grainger College of Engineering, Holonyak Micro and Nanotechnology Laboratory, Department of Electrical and Computer Engineering, and Department of Materials Science and Engineering, University of Illinois Urbana-Champaign, Urbana, Illinois 61801, USA

<sup>a)</sup>Authors to whom correspondence should be addressed: [stephanie.tomasulo.civ@us.navy.mil](mailto:stephanie.tomasulo.civ@us.navy.mil) and [mllee@illinois.edu](mailto:mllee@illinois.edu)

## ABSTRACT

III-V multi-junction solar cells have yielded the highest solar cell efficiencies for nearly three decades and recently achieved record efficiencies approaching 40% under standard conditions and 50% under concentrated sunlight. Such high efficiencies are currently only possible using four or more junctions to partition the broad solar spectrum into bins where each subcell efficiently collects a narrow range of photon energies. High-efficiency, wide-bandgap (1.7–2.2 eV) absorbers play a crucial role in multi-junction solar cells by efficiently converting visible photons into electrons and delivering them at high voltage. Since all subcells are interconnected in series, the widest bandgap junction produces both the highest voltage and highest power in the stack. Wide-bandgap absorbers also present the greatest materials challenges in the stack, including high aluminum content, lattice mismatch, lack of heterojunction barriers, and the sensitivity of phosphides to defects such as vacancies and oxygen. We review the history, current status, and opportunities for wide-bandgap III-V solar cells, ranging from ~1.7 eV for the top subcell of III-V/Si hybrid tandems to >2.2 eV for the top subcell of a 6+ junction stack. Future directions and recommendations to overcome remaining materials and device challenges will be discussed.

Published under an exclusive license by AIP Publishing. <https://doi.org/10.1063/5.0273566>

19 July 2025 05:24:42

## TABLE OF CONTENTS

I. INTRODUCTION.....	1
A. Motivation for wide-bandgap solar cells.....	1
B. Background on PV device physics and cell design.....	2
C. Background on epitaxial growth methods.....	4
D. Traits of wide-bandgap absorber materials.....	5
II. 1.7 EV JUNCTIONS: TOP CELLS FOR DUAL-JUNCTION CELLS AND UPRIGHT METAMORPHIC TRIPLE-JUNCTION CELLS ON GE.....	7
A. GaInAsP .....	7
B. Al <sub>x</sub> Ga <sub>1-x</sub> As x < 0.25 .....	8
C. Metamorphic Ga <sub>1-x</sub> In <sub>x</sub> P, x > 0.5 .....	9
D. Metamorphic GaAs <sub>y</sub> P <sub>1-y</sub> , y ≈ 0.70–0.85 .....	10
E. Summary and recommendations for future work on 1.7 eV junctions .....	13
III. 1.8–1.9 EV JUNCTIONS: TOP CELLS FOR GAAS/GE-BASED 3–4J CELLS .....	14
A. Lattice-matched GaInP.....	14
B. Al-rich Al <sub>x</sub> Ga <sub>1-x</sub> As (x ≈ 0.25–0.40) .....	16
C. Metamorphic GaAs <sub>y</sub> P <sub>1-y</sub> , y ≤ 0.6 .....	18
D. Summary and recommendations for future work on 1.8–1.9 eV junctions .....	18

IV. >1.9 EV JUNCTIONS: TOP CELLS FOR 4J AND BEYOND.....	18
A. AlGaInP .....	18
B. Metamorphic Ga <sub>1-x</sub> In <sub>x</sub> P, x < 0.5 .....	21
C. GaP .....	23
D. Summary and recommendations for future work on >1.9 eV top cells.....	24
V. NEW MATERIALS SYSTEMS FOR WIDE-BANDGAP PV APPLICATIONS.....	24
A. InAlAsSb .....	24
B. Metamorphic AlInP .....	25
C. GaNPAs .....	25
D. Summary and recommendations for future work on new materials systems .....	27
VI. CONCLUSION.....	27
SUPPLEMENTARY MATERIAL .....	27

## I. INTRODUCTION

### A. Motivation for wide-bandgap solar cells

III-V multi-junction solar cells have been investigated for decades due to their high conversion efficiency ( $\eta$ ) and radiation tolerance.

The high cost associated with III-V substrates, growth, and processing has historically limited them to space photovoltaics (PV), where an order of hundreds of kW/year to low MW/year of production satisfies much of the global demand.<sup>1</sup> Due to their high specific power density, III-V multi-junction devices are also attractive for defense applications such as portable power and unmanned aerial vehicles.<sup>2,3</sup> High specific power density is also a potential enabler for vehicle-integrated PV (i.e., PV electric vehicles), where a recent analysis suggests that 35% efficient cells could facilitate 30 km of driving per day without charging provided an average irradiance of 4 kWh/m<sup>2</sup> day.<sup>4</sup> Concentrator PV (CPV), where the incoming sunlight is focused down to a small area, enabling miniaturization of the expensive III-V solar cells, was heavily investigated from the late 1970s through the 2010s, though research and development in this field has nearly ceased at the time of writing. Recently, the emphasis of III-V PV research has pivoted to finding methods to reduce the cost of substrates, growth, and cell processing.<sup>5–10</sup> If successful, the high energy yield and reliability of III-V multi-junction solar cells will enable them to compete effectively in area-constrained applications by surpassing the Si  $\eta$  limit of ~29.5%.<sup>11</sup>

Wide-bandgap solar cells (defined in this review as having a bandgap energy  $E_g = 1.7\text{--}2.2\text{ eV}$ , corresponding to cutoff wavelengths of ~555–730 nm) are critical for multi-junction devices as they produce the highest voltage and, hence, the highest power in the stack. This paper will focus specifically on wide-bandgap III-V solar cells, and we direct the reader to many excellent reviews covering the full multi-junction stack.<sup>12–17</sup> Figure 1 plots the record  $\eta$  under standard (1-sun) test conditions as a function of year for single-crystal solar cell technologies: Si single-junction, GaAs single-junction, and multi-junction with three or more junctions. Multi-junction solar cells have held the record for the highest  $\eta$  of all solar cell technologies since the 1990s. This is achieved by splitting the absorption of the solar spectrum into discrete portions to reduce transmission and thermalization, the major loss contributors in single-junction solar cells. For a material with a given  $E_g$ , photons with energy  $h\nu < E_g$  will transmit through the material, leading to the aforementioned transmission loss. For  $h\nu$  slightly above the  $E_g$ , photons will be absorbed with minimal energy loss, while for  $h\nu \gg E_g$

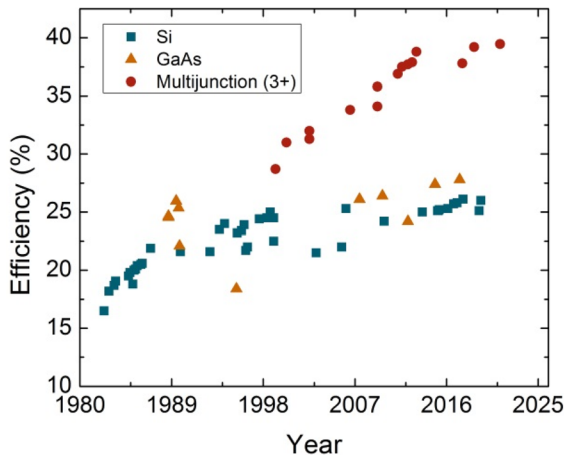


FIG. 1. Record solar cell  $\eta$  under standard (1-sun) test conditions as a function of year for crystalline Si single-junction, GaAs single-junction, and multi-junction (three or more junctions) solar cells. The data for this plot are courtesy of the National Renewable Energy Laboratory, Golden, CO.

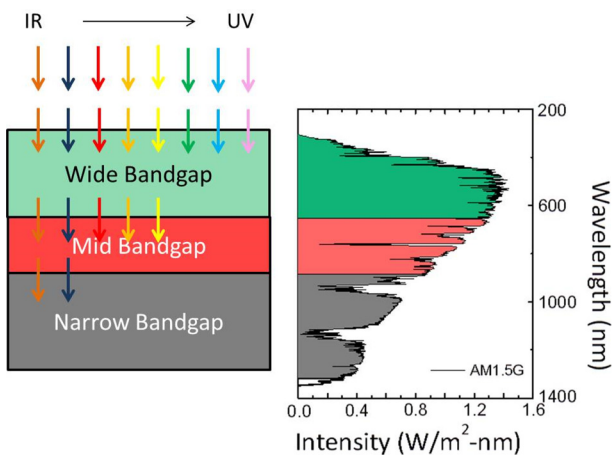


FIG. 2. Principle behind multi-junction solar cell operation. Solar cells with different  $E_g$  are stacked from the widest bandgap on top to the narrowest bandgap on the bottom, allowing high-energy photons to be absorbed in the top subcell while lower-energy photons pass through to the underlying subcells where they can be collected. In this generalized example, each subcell in the cross-sectional schematic (left) efficiently collects the portion of the AM 1.5G solar spectrum (right) with the corresponding color.

electrons are excited too far into the conduction band, leading to thermalization (losing energy to heat via phonon interactions) of the electron back to the band edge. Figure 2 provides a schematic of how multi-junction solar cells overcome these intrinsic losses in which high-energy photons are collected in the top junction, allowing lower-energy photons that would have been lost to transmission to be collected by the underlying subcells; the subcells are electrically interconnected using tunnel junctions. In other words, each subcell efficiently converts a small portion of the solar spectrum, unlike in a single-junction solar cell, which must balance transmission and thermalization losses, inherently limiting  $\eta$  to ~33%.<sup>18</sup> Just as one must choose the appropriate  $E_g$  for a single-junction device to balance these losses, it is also critical to choose the subcell  $E_g$  values judiciously for multi-junction devices to minimize losses while ensuring current matching. In principle, partitioning the spectrum to maximize  $\eta$  is relatively straightforward and was described by C. Henry in 1980.<sup>19</sup> Accordingly, wider-bandgap materials are required in the upper cells for optimum spectral utilization.<sup>20</sup> There have been many demonstrations of high- $\eta$  multi-junction solar cells, including the current records exceeding  $\eta = 47\%$  (under concentration)<sup>21–23</sup> and space PV under the AM0 spectrum with  $\eta > 31\%$ .<sup>24,25</sup>

## B. Background on PV device physics and cell design

Solar cell efficiency is defined as  $\eta = \frac{P_{\text{out}}}{P_{\text{in}}} = \frac{V_{\text{oc}}I_{\text{sc}}FF}{P_{\text{in}}}$ , where  $P_{\text{out}}$  is the maximum power out and  $P_{\text{in}}$  is the power of the incident spectrum integrated over all wavelengths. The most commonly used values for  $P_{\text{in}}$  are for terrestrial AM1.5G = 1000.4 W/m<sup>2</sup> and space AM0 = 1366.1 W/m<sup>2</sup>.<sup>26</sup>  $V_{\text{oc}}$  is the open circuit voltage, which is the voltage at zero current and is expressed as  $V_{\text{oc}} \approx \frac{nkT}{q} \ln\left(\frac{J_{\text{sc}}}{J_0}\right)$  where  $n$  is the diode ideality factor,  $J_0$  is the dark current density, and  $J_{\text{sc}}$  is the short circuit current density, as elaborated below. Ideally,  $V_{\text{oc}}$  increases with increasing  $E_g$  and can be considered a measure of the quasi-Fermi level (QFL) splitting between the n- and p-regions.<sup>27</sup> The  $J_{\text{sc}}$  is the

current density at zero volts and represents the density of incident photons converted to collected electrons and holes;  $J_{sc}$  decreases with increasing  $E_g$  due to increased transparency. Low surface recombination velocities and long minority carrier diffusion lengths ( $L_{n,p}$ ) are essential for high  $J_{sc}$ ;  $L = \sqrt{D\tau}$  where the diffusivity  $D = \frac{kT}{q}\mu$ ,  $\mu$  is the minority carrier mobility, and  $\tau$  is the minority carrier lifetime. Finally, the fill factor (FF) is the ratio of the area under the lighted current-voltage (LIV) curve compared to the rectangle formed by the corners of  $J_{sc}$  and  $V_{oc}$ , i.e., the “squareness” of the LIV curve. Parameters favoring a high FF at 1-sun operation include a diode ideality factor  $n = 1$  near the operating point,<sup>28</sup> low emitter sheet resistance (e.g.,  $<1000 \Omega/\square$ ) and low overall series resistance (e.g.,  $<1 \Omega\text{cm}^{-2}$ ),<sup>29</sup> and long diffusion lengths to avoid field-assisted carrier collection.<sup>30</sup>

While  $\eta$  is the primary consideration,  $V_{oc}$  is often used as a solar cell figure of merit due to its relatively weak sensitivity to the incident spectrum and the performance of anti-reflection coatings (ARC). However, as  $V_{oc}$  inherently varies with  $E_g$  it can only be used to compare devices with the same  $E_g$ . King *et al.* introduced the bandgap-voltage offset  $W_{oc} = \frac{E_g}{q} - V_{oc}$  to represent the distance between the QFLs and their respective bandages and to provide a  $E_g$ -independent figure of merit.<sup>27</sup> Thus, the lower the  $W_{oc}$  the better the cell performance. While researchers typically seek  $W_{oc} \approx 0.4 \text{ V}$  for high- $\eta$ , wide-bandgap cells, much higher values are common in the literature due to the materials challenges described below. Note, however, that very low  $W_{oc}$  values approaching the radiative limit of 0.30–0.35 V have been demonstrated for record- $\eta$  GaAs and Si solar cells.<sup>21</sup> Throughout this review, when efficiencies cannot be readily compared due to differences in  $E_g$  or reflectance, we rely on  $W_{oc}$  as a figure of merit to ascertain the technical maturity of each absorber material.

Virtually all III-V single-junction solar cells rely on a p-n junction to separate electrons from holes, with the addition of important barrier layers that surround the device to minimize recombination at surface defects and heavily doped contact layers for power extraction. The band alignment of the barrier layers should enable majority carriers to flow to the contacts with minimal voltage loss while redirecting minority carriers back to the p-n junction, i.e., a “carrier-selective contact.”<sup>31</sup> On the front side of the solar cell, the window layer (WL) acts as the top barrier and should be as transparent as possible; for middle cells, the WL must have  $E_g$  greater than or equal to the cell directly above to prevent parasitic absorption. On the back side, the back surface field (BSF) provides the bottom barrier layer, ideally possessing higher doping and  $E_g$  than the absorber.

In addition to barrier layers, the placement of the junction within the absorber has proven to be an important design factor, as seen in the schematics in Fig. 3. Front-junction (FJ) solar cells are the historical and most common design, with a thick base ( $\geq 0.5 \mu\text{m}$ ) and a thin emitter ( $\sim 20\text{--}200 \text{ nm}$ ), placing the junction closer to the surface. In this design, minority carriers generated deep in the base by absorption of photons with  $h\nu$  only slightly above the  $E_g$  must have minority carrier diffusion length on the order of micrometers to reach the junction and be collected. The most common polarity is n<sup>+</sup>-on-p, such that the minority carriers in the base are electrons with higher mobility and, hence, longer diffusion lengths. High majority electron mobility is also critical for maintaining a low emitter sheet resistance of  $\sim 500\text{--}1000 \Omega/\square$  with low thickness.<sup>29</sup> The rear homo- or hetero-junction (RHJ), instead, flips the conventional design to a thick emitter and thin base to place the junction at the back of the cell, often with a wider-

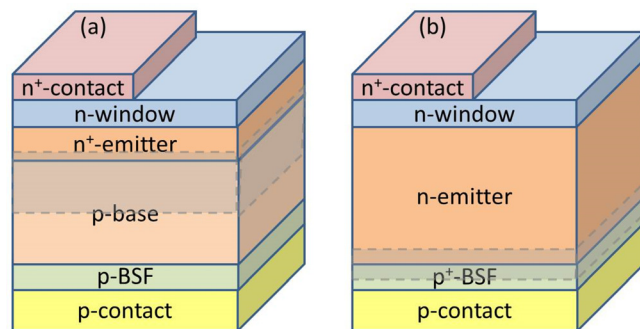


**FIG. 3.** Cross-sectional schematics of (a) front-junction and (b) rear-heterojunction device designs. Gray area represents depletion region thickness.

bandgap material for the thin base; all RHJ devices reported to date have been n-on-p.<sup>32–34</sup> The thick emitter is doped more lightly than in the FJ case (typically  $1\text{--}5 \times 10^{17} \text{ cm}^{-3}$ ) to allow longer minority hole lifetime and diffusion length; low emitter sheet resistance is maintained despite the reduced doping due to the increased thickness.<sup>32,35,36</sup> RHJ cells excel when combined with photon recycling, where a metal mirror/reflector at the back of the device permits spontaneously emitted photons to be re-absorbed, leading to increased excess carrier concentration and QFL splitting.<sup>36</sup> Placing the junction at the back of the device in a wider-bandgap material reduces dark current and improves radiative efficiency, leading to power conversion efficiency improvements with photon recycling.<sup>32,33</sup> However, it should be noted that photon recycling typically has little relevance for top subcells due to the difficulty of growing single-crystal, omni-directional reflectors.

In addition to the above-mentioned single-junction design factors, for multi-junction devices, one must also consider the interplay of lattice-matching and current-matching when selecting multiple absorber materials. First, to prevent the formation of  $\eta$ -degrading defects (namely, threading dislocations, described further below), all subcell materials are typically chosen to have approximately the same lattice constant as the starting substrate, which constrains the available  $E_g$  combinations. For instance, when using GaAs or Ge as the starting substrate, there is no conventional, lattice-matched absorber with  $E_g = 1 \text{ eV}$ , forcing the use of a non-ideal  $E_g$  combination. Second, when connecting the subcells in series, it is important to prioritize current-matching, as the total device current will be limited by the lowest current-generating junction. Ideally, one would choose materials with  $E_g$  values leading to closely matched currents in each junction, but this is not always possible due to the competing priority of lattice-matching. To overcome this limitation, one can thin down overproducing cells (increasing transmission) to improve current balance across all junctions. Another option to achieve current-matching with ideal  $E_g$  combinations is to sacrifice the lattice-matching constraint. Lattice mismatch introduces threading dislocations, which contribute to deep-level trap states in the bandgap. The increased trap density increases non-radiative recombination and decreases minority carrier lifetime, leading to increased dark current (lower  $V_{oc}$ ) and decreased diffusion length (lower  $J_{sc}$ ). Compositinally graded buffers (CGB) reduce the threading dislocation density (TDD) by bridging the lattice mismatch between the substrate and solar cell absorber material via many low-mismatch layers.<sup>37–42</sup> These CGBs have been shown to enable TDD in the range of  $10^5\text{--}10^6 \text{ cm}^{-2}$ , and GaAs solar cells with this level of TDD have only

slight degradation to  $\eta$ .<sup>43,44</sup> Furthermore, CGBs enable the inverted metamorphic [IMM, Figs. 4(c)–4(e)] design with record-breaking  $\eta$ .<sup>23</sup> For example, in the case of Fig. 4(e), the lattice mismatch is overcome by CGBs (between subcells 4–3, 3–2, and 2–1, where subcell 1 has the lowest  $E_g$ ) and enables a multi-junction stack with a nearly optimal  $E_g$  combination. By growing the device upside down (inverted), the first three subcells can be grown lattice-matched to the GaAs substrate before introducing the CGB and increased TDD.

Figure 4 provides cross-sectional schematics of highly investigated multi-junction solar cell structures: (a) Si tandems with  $\eta \approx 23\%-25\%$ ,<sup>45,46</sup> (b) 3J lattice-matched with  $\eta = 34.1\%$ ,<sup>47</sup> (c) 3J IMM with  $\eta = 37.9\%$ ,<sup>21,48</sup> (d) 4J IMM with  $\eta = 45.6\%$  (690 suns),<sup>49,50</sup> and (e) 6J IMM with  $\eta = 47.1\%$  (143 suns).<sup>23</sup> Note that the top subcell (or even the top two in the 6J case) requires materials with  $E_g \geq 1.7$  eV. These sub-cells are depicted with a thick border and bold-face font in Fig. 4 and will be covered, along with many others, in this review. We note that in addition to these monolithic approaches, wafer-bonding has also led to high-efficiency multi-junction devices.<sup>51,52</sup>

### C. Background on epitaxial growth methods

Advances in wide-bandgap solar cells have come hand-in-hand with advances in epitaxial growth techniques, chief among them metalorganic chemical vapor deposition (MOCVD)<sup>53</sup> and molecular beam

epitaxy (MBE).<sup>54</sup> MOCVD is also frequently referred to as metalorganic vapor phase epitaxy (MOVPE). More recently, there has been a resurgence of interest in halide or hydride vapor phase epitaxy (both are referred to as HVPE), which is among the oldest epitaxial growth techniques.<sup>55</sup> A brief description of each method is given below to provide context to the device results, and the reader is referred to the books and review articles cited above for more comprehensive information.

In MOCVD, the substrate is held on a rotating susceptor that may be heated by lamps, RF coils, or resistive heating. Group-III metalorganic and group-V hydride precursor gases are diluted in an H<sub>2</sub> carrier and flowed vertically or horizontally across the substrate surface; the highest possible purity is used for all precursors, and the hydride and H<sub>2</sub> are typically purified a final time before injection into the reactor (i.e., “point of use” purification). The precursor molecules diffuse through a static boundary layer where they can adsorb on the wafer surface and pyrolyze; a prototypical reaction is  $\text{Ga}(\text{CH}_3)_3 + \text{AsH}_3 \rightarrow \text{GaAs} + 3\text{CH}_4$ . A large excess of hydride typically flows to compensate for group-V desorption, and a nearly perfect 1:1 stoichiometry can be maintained over a wide range of conditions because excess group-V does not adsorb well on the surface. The growth chamber is typically held at a pressure of ~0.1–1 atmospheres, and reported substrate temperatures ( $T_{\text{sub}}$ ) vary from ~400–800 °C, with 500–650 °C being typical for most III–V solar absorbers. Growth rates

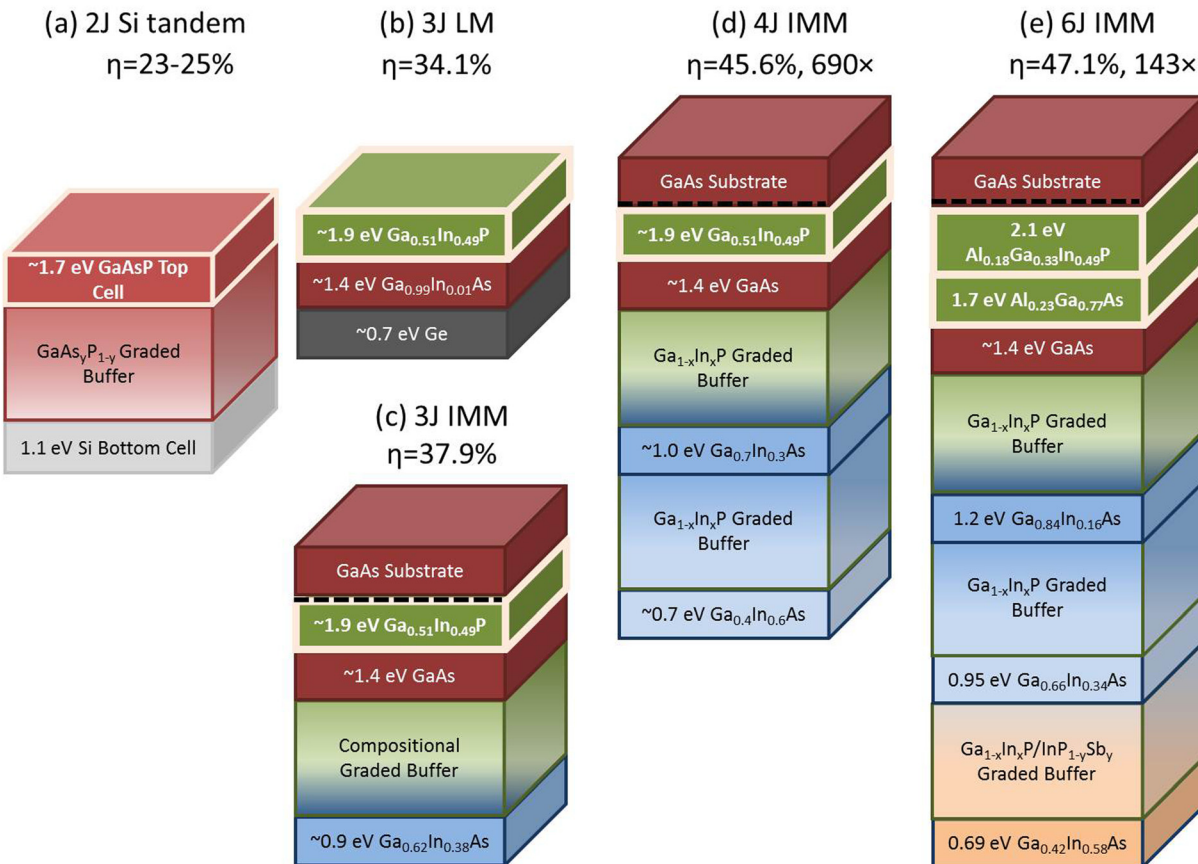


**FIG. 4.** General schematics for most common high- $\eta$  multi-junction solar cells: (a) GaAsP/Si,<sup>45,46</sup> (b) 3J LM (lattice-matched),<sup>47</sup> (c) 3J IMM,<sup>21,48</sup> (d) 4J IMM,<sup>49,50</sup> and (e) 6J IMM.<sup>23</sup> The black dotted lines represent where the substrate is ultimately removed. This review covers the wide-bandgap subcells outlined by a thick border with bolded text.

of  $1\text{--}4 \mu\text{m}/\text{h}$  are typical, but recent work has demonstrated that high- $\eta$  GaAs solar cells can be grown at  $>100 \mu\text{m}/\text{h}$  with excellent surface morphology and device performance.<sup>56</sup> To the authors' knowledge, all commercial III-V solar cells (and LEDs) are grown by MOCVD and have been for decades.

In MBE, a rotating substrate is heated radiatively in ultrahigh vacuum conditions (ideally  $10^{-10}$  Torr or less). Ultra-high purity elemental sources (e.g., metallic Ga and As) are evaporated or sublimated from independent sources and travel without collisions to the substrate (e.g., as beams of Ga atoms and As<sub>2</sub> molecules), where they can be adsorbed directly without diffusion through a boundary layer. A reaction of  $2\text{Ga} + \text{As}_2 \rightarrow 2\text{GaAs}$  proceeds on the surface without any other reaction byproducts. Growth rates of  $0.1\text{--}2 \mu\text{m}/\text{h}$  are typical in MBE, and we could not find any reported attempts to achieve significantly higher growth rates. However, we anticipate that a limit exists where the group-V beam flux is excessively high and the growth rate becomes limited by gas phase collisions.<sup>57</sup> While Solar Junction Corp. held a number of CPV  $\eta$  records in the 2010s using MBE-grown devices,<sup>58</sup> to our knowledge, no high-volume commercial solar cells are grown by MBE.

Finally, in HVPE, the wafer is held on a susceptor in a quartz tube furnace at 1 atm and exposed to flows of group-V hydrides and group-III chlorides that are formed *in situ* by passing HCl vapor over crucibles of molten Ga or In; AlCl<sub>3</sub> can be synthesized outside the reactor by passing HCl over solid Al at  $400^\circ\text{C}$ <sup>59</sup> and prototypical reactions include  $\text{GaCl} + \text{AsH}_3 \rightarrow \text{GaAs} + \text{HCl} + \text{H}_2$  and  $\text{GaCl} + \frac{1}{4}\text{As}_4 + \frac{1}{2}\text{H}_2 \rightarrow \text{GaAs} + \text{HCl}$ . The historical problem of poor interface control has been overcome using dynamic multi-chamber systems.<sup>55,60</sup> A combination of high growth rates ( $>100 \mu\text{m}/\text{h}$ ), high material quality, and reduced precursor cost make HVPE promising for future commercial applications.

As this review will show, all techniques appear to be capable of overcoming the challenges of growing high- $\eta$ , wide-bandgap solar cells. MOCVD and MBE were commercially developed in the 1970s and 1980s for their ability to create abrupt heterojunction interfaces used in lasers and transistors, which set them apart from HVPE and liquid phase epitaxy. Today, MOCVD and MBE dominate the literature on III-V solar cell growth. Although the final devices may be similar, MOCVD, MBE, and HVPE take significantly different routes in terms of both thermodynamics and kinetics, and the high efficiencies achieved by each highlight their versatility and the dedication of the research community.

#### D. Traits of wide-bandgap absorber materials

As this review focuses on III-V wide-bandgap solar cells, it is important to note some common themes among them. First, attaining a material with a high  $E_g$  requires alloys with Al, P, or both, which significantly affects both band structure and carrier transport. In III-Vs, the character of valence band states is dominated by the anion,<sup>61</sup> and hence, valence bands for III-phosphides differ widely from III-arsenides. For example, wide-bandgap phosphides have low bulk hole mobilities (compare  $\mu_{\text{hole}}^{\text{GaAs}, \text{max}} \sim 450 \text{ cm}^2/\text{Vs}$  with  $\mu_{\text{hole}}^{\text{GaP}, \text{max}} \sim 150 \text{ cm}^2/\text{Vs}$ ) and high effective masses ( $m_{\text{hh}, \text{GaAs}} \sim 0.51 m_0$  vs  $m_{\text{hh}, \text{GaP}} \sim 0.79 m_0$ ); alloy scattering leads to even lower hole mobility for GaInP with  $\mu_{\text{hole}}^{\text{GaInP}, \text{max}} \sim 50 \text{ cm}^2/\text{Vs}$ . This can be seen in Fig. 5 where we compare (a) electron and (b) hole mobilities of  $\text{Al}_x\text{Ga}_{1-x}\text{As}$ <sup>62</sup> and  $\text{Ga}_{0.51}\text{In}_{0.49}\text{P}$ .<sup>63,64</sup> While the electron mobilities are very comparable for both  $\text{Al}_x\text{Ga}_{1-x}\text{As}$  and  $\text{Ga}_{0.51}\text{In}_{0.49}\text{P}$ ,  $\text{Ga}_{0.51}\text{In}_{0.49}\text{P}$  hole mobilities are clearly much lower than those of  $\text{Al}_x\text{Ga}_{1-x}\text{As}$ . On the other hand, III-

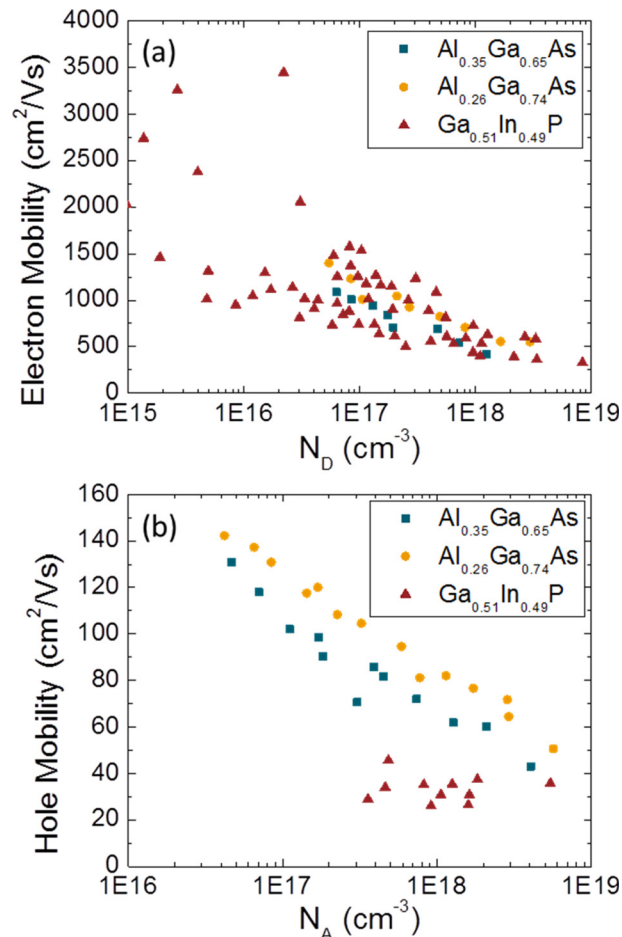
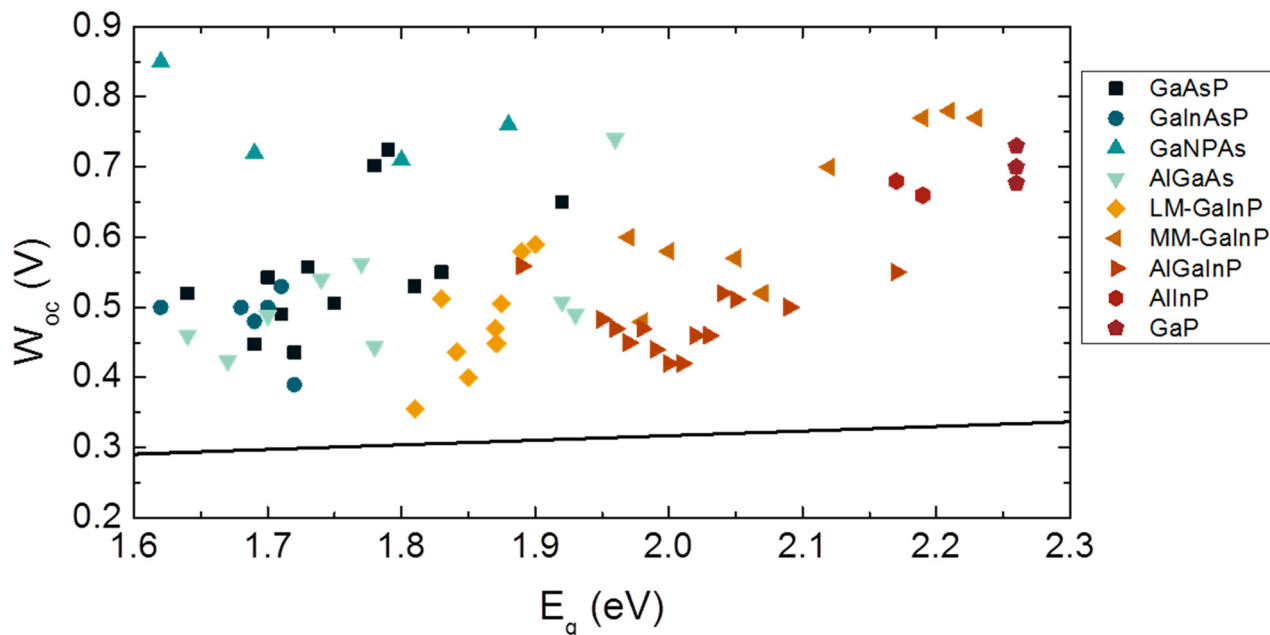


FIG. 5. (a) Electron and (b) hole mobility of  $\text{Al}_{0.35}\text{Ga}_{0.65}\text{As}$ ,  $\text{Al}_{0.26}\text{Ga}_{0.74}\text{As}$ ,<sup>62</sup> and  $\text{Ga}_{0.51}\text{In}_{0.49}\text{P}$ .<sup>63,64</sup> While the electron mobilities of all three materials are comparable, the hole mobility of  $\text{Ga}_{0.51}\text{In}_{0.49}\text{P}$  is clearly lower than that of  $\text{Al}_x\text{Ga}_{1-x}\text{As}$ .

phosphides benefit from stronger absorption than GaAs, potentially due to higher effective masses leading to higher joint density of states.<sup>65</sup>

Al-containing alloys also suffer from reduced electron and hole mobility due to alloy scattering, as seen when comparing carrier mobilities in AlGaAs vs GaAs.<sup>66,67</sup> However, a more challenging problem relates to the high strength of Al-O bonds, resulting in a propensity to form oxygen-related defects. This bond strength affects everything from precursor purity to epitaxial layer purity and will be discussed in Sec. II B. DX centers in n-type material also lead to reduced performance in Al-containing absorbers.<sup>68</sup>

These band structure and composition effects illustrate important trends observed in III-AsP materials as a function of  $E_g$ . The material with the highest  $E_g$  of the cubic III-Vs is  $\text{Al}_{0.52}\text{In}_{0.48}\text{P}$  with  $E_g \approx 2.3 \text{ eV}$ . As such, absorbers with  $E_g > 2.1 \text{ eV}$  will have barrier layers with inherently low barrier heights. Additionally, n-AlGaInP suffers from both poor majority electron mobility, which can harm FF, and poor minority hole mobility, precluding demonstration of RHJ cells with  $E_g > 1.9 \text{ eV}$ .<sup>69</sup> Finally, surface recombination velocity for minority electrons in p-type absorbers tends to be higher than minority holes in n-type absorbers.<sup>70</sup>



**FIG. 6.** Lowest-reported  $W_{oc}$  as a function of  $E_g$  for relevant wide-bandgap PV materials. Black line represents theoretical limits under AM1.5G from Ref. 18. See [supplementary material](#) for table of data including citations.

Another commonality among wide-bandgap III-V solar cells is that many suffer from high  $W_{oc}>0.5$  V due to high trap densities and elevated dark current densities ( $J_{01}, J_{02}$ ). While radiative limit and detailed balance calculations suggest that  $W_{oc}$  should increase slightly with increasing  $E_g$ , the experimental values significantly exceed those expected from theory. To visualize this, Fig. 6 plots the lowest-reported experimental  $W_{oc}$  as a function of  $E_g$  along with theoretical limits under AM1.5G (black line) from Ref. 18. Lattice-matched GaInP is a clear exception, likely due to its technological maturity relative to the other wide-bandgap PV materials. Even still, typical GaInP FJ designs have  $W_{oc} \sim 0.42$  V (~0.44 V) on non-absorbing (absorbing) substrates,<sup>32</sup> while the best GaAs cells have  $W_{oc}$  down to 0.32 V on non-absorbing substrates or 0.34 V on absorbing substrates.<sup>36</sup> The generally higher  $W_{oc}$  values observed for wide-bandgap solar cells reflect the higher defect concentration of these materials and their relative

immaturity in some cases. Lower-than-ideal FFs are another side effect of elevated  $W_{oc}$  values, constituting a potent “one-two punch” for wide-bandgap solar cells. Compounding the FF problem, the relatively low electron mobility of wide-bandgap phosphides can lead to high emitter sheet resistance, the combination of very low  $n/J_{01}$  values and high trap densities lead to  $n=2$  diode behavior for 1-sun operation, and low diffusion lengths can lead to field-assisted carrier collection.

This article reviews the current progress of wide-bandgap solar cells for incorporation into high-efficiency multi-junction devices. Despite the many challenges of these materials, tremendous progress has been achieved, both by continual improvements in materials growth and by adjusting cell designs to account for defects and other non-idealities. We will cover top cells for dual-junction Si-tandems with  $E_g = 1.7$  eV (Sec. II), top cells for traditional lattice-matched triple-junction cells with  $E_g = 1.8\text{--}1.9$  eV (Sec. III), top cells for 4+ junctions with  $E_g > 1.9$  eV (Sec. IV), and novel material systems for wide-bandgap PV (Sec. V). Figure 7 summarizes the layout of this review in the form of a  $E_g$  vs. lattice constant diagram, and Table I provides the highest reported single-junction efficiencies achieved to date for each  $E_g$  range.

**TABLE I.** Summary of highest single-junction  $\eta$  achieved to date in each  $E_g$  range covered in this review.

$E_g$ (eV)	Material	$W_{oc}$ (V)	AM1.5G $\eta$ (%)
2.0	LM-Al <sub>0.12</sub> Ga <sub>0.39</sub> In <sub>0.49</sub> P on GaAs (MOCVD)	0.44	14.8 <sup>69</sup>
1.9	LM-Ga <sub>0.51</sub> In <sub>0.49</sub> P grown on GaAs (MOCVD)	0.34	22.0 <sup>21</sup>
1.7	LM-GaInAsP on GaAs (MOCVD)	0.47	21.5 <sup>71</sup>

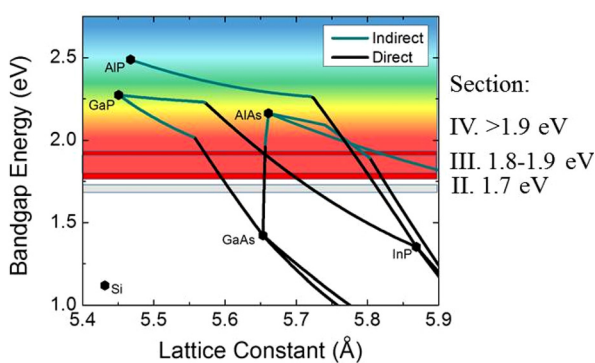


**FIG. 7.**  $E_g$  vs. lattice constant of relevant III-V materials for wide-bandgap PV. Highlighted  $E_g$  ranges correspond to each section of this review.

## II. 1.7 eV JUNCTIONS: TOP CELLS FOR DUAL-JUNCTION CELLS AND UPRIGHT METAMORPHIC TRIPLE-JUNCTION CELLS ON Ge

The laboratory  $\eta$  record for single-junction Si solar cells, the most mature PV technology, is 27.4%.<sup>21</sup> With a theoretical limit of 29.5%,<sup>11</sup> Si has relatively little room for further improvement, which has spurred global efforts on multi-junction solar cells to provide efficiencies exceeding 30%. The most efficient dual-junction (2J) or tandem cells with proven stability are presently based on 1.9 eV Ga<sub>0.51</sub>In<sub>0.49</sub>P/1.4 eV GaAs and succeed in surpassing the single-junction  $\eta$  limits at 32.8%.<sup>21</sup> However, it has long been appreciated that a 1.7 eV/1.1 eV tandem could offer significantly higher  $\eta$  due to a more ideal match with the solar spectrum. Such a device can theoretically achieve AM1.5G  $\eta \approx 37\%$  vs  $\eta \approx 35\%$  for the 1.9/1.4 eV stack.<sup>72</sup> Despite these potential advantages, 1.7 eV/1.1 eV tandem solar cells face inherent materials challenges due to the lack of a lattice-matched pair with these  $E_g$  values; GaAs substrates lack a high-performance, lattice-matched 1.1 eV absorber material, while InP substrates lack a 1.7 eV absorber. As such, virtually all schemes for spectrally matched III-V (or Si) tandem solar cells rely on lattice-mismatched junctions that can be combined either by metamorphic (MM) growth or mechanical stacking/wafer bonding. While Si offers a technologically mature and low-cost option for the bottom junction, integration of III-V junctions with Si presents significant challenges due to both lattice and thermal mismatch. However, recent developments in low-defect GaP/Si growth<sup>73–75</sup> provide a path toward epitaxial integration of a high- $\eta$  III-V top cell with an underlying Si bottom cell. 1.7 eV junctions are also of great interest as the top cell for upright MM triple-junction (3J) cells consisting of 1.7 eV GaInP/1.2 eV GaInAs/0.66 eV Ge.<sup>76,77</sup> In this section, we review the progress toward spectrally matched tandem solar cells, focusing on different  $\sim 1.7$  eV III-V top cell materials in order of highest efficiency to date: GaInAsP, AlGaAs, GaInP, and GaAsP.

### A. GaInAsP

Development of lattice-matched 1.7 eV Ga<sub>0.68</sub>In<sub>0.32</sub>As<sub>0.34</sub>P<sub>0.66</sub> (hereafter GaInAsP) on GaAs as a top cell for mechanical stacking on Si<sup>78</sup> got off to a strong start in 1993, with active-area efficiencies of  $\sim 21.5\%$  (under AM0) and  $W_{oc} = 0.54$  V for MOCVD-grown cells reported by Sharps *et al.* at Research Triangle Institute. Despite the high efficiencies reported in 1993, relatively little detail was provided

on the effect of growth conditions and the potential challenges resulting from the GaInAsP miscibility gap on cell performance. National Renewable Energy Laboratory (NREL) researchers revisited GaInAsP in the mid-2010s<sup>71,79–82</sup> recognizing its potential as an Al-free second subcell in 4-junction cells. They investigated GaInP/GaInAsP FJ devices on GaAs substrates grown by both MOCVD and HVPE, though the efficiencies of the HVPE-grown devices were hampered by the lack of a WL and ARC<sup>79</sup>; the range of AM1.5G results for all doping levels investigated are listed in Table II. Future studies on HVPE growth of 1.7 eV GaInAsP would undoubtedly benefit from the recent development of Al-containing window layers using AlCl<sub>3</sub>.<sup>59</sup>

NREL investigated a variety of MOCVD growth conditions and designs of GaInAsP cells, finding suppressed phase separation through the use of a low  $T_{sub}$  and (001) substrates offcut toward (111) A.<sup>81</sup> Varying the base layer thickness from 1.0–1.5  $\mu m$  led to little change in  $J_{sc}$  while increasing to 2.0  $\mu m$ , caused a clear degradation to long-wavelength external quantum efficiency (EQE), suggesting a minority carrier diffusion length around 1.5–2.0  $\mu m$ . Increasing the base doping from  $1 \times 10^{17}$  to  $4 \times 10^{17} \text{ cm}^{-3}$  led to increased  $V_{oc}$  with little change to  $J_{sc}/\text{EQE}$ . In contrast, dropping the base doping to  $2 \times 10^{15} \text{ cm}^{-3}$  increased long-wavelength collection, decreased short-wavelength collection, and reduced  $V_{oc}$  and FF. The best-performing cell utilized a 1  $\mu m$  base with p-doping of  $1 \times 10^{17} \text{ cm}^{-3}$ , resulting in  $W_{oc} = 0.51$  V,  $J_{sc} = 16.94 \text{ mA/cm}^2$ , FF = 0.864,  $\eta = 17.2\%$  measured under AM1.5D, 100 W/cm<sup>2</sup>.<sup>80</sup> Building off these results, the authors next added an ARC and switched to a n-i-p cell design to increase the depletion width and boost long-wavelength EQE.<sup>71</sup> For devices with i-region thicknesses of 1.0–1.4  $\mu m$ , the cell properties were comparable. However, when increasing to an i-region thickness of 1.7  $\mu m$ , the FF dropped due to field-assisted current collection and depletion region recombination. The authors also observed increased series resistance in this device. For the devices with 1.0–1.4  $\mu m$  thick i-regions, the combined benefits of the design change and ARC introduction led to an improved  $\eta$  of 18.0–18.1%, arising mostly from an improved  $J_{sc} = 18.3\text{--}18.4 \text{ mA/cm}^2$  while  $W_{oc}$  remained constant and FF decreased slightly to 0.823–0.825. In 2018, this group developed a 1.7/1.1 eV IMM 2J device using GaInAsP/GaInAs.<sup>82</sup> Further optimization to the top GaInAsP cell through replacement of the homojunction BSF with higher- $E_g$  AlGaInP and optimization of the base layer doping level ( $2\text{--}3 \times 10^{16} \text{ cm}^{-3}$ ) led to significantly improved  $W_{oc}$  and  $J_{sc}$  values of 0.39 V and 19.5 mA/cm<sup>2</sup>.

TABLE II. Summary of GaInAsP (lattice-matched to GaAs) solar cell results with different variables—base p-doping level,  $N_A$ , base thickness,  $t_b$ , and intrinsic layer thickness,  $t_i$ .

Growth method	$E_g$ (eV)	$V_{oc}$ (V)	$W_{oc}$ (V)	$J_{sc}$ (mA/cm <sup>2</sup> )	FF	$\eta$ (%)	Variable	citation
HVPE, no window, no ARC	1.7	1.09	0.61	9.5	0.809	8.4	$N_A = 4.1 \times 10^{16} \text{ cm}^{-3}$	79
	1.7	1.11	0.59	9.3	0.816	8.4	$N_A = 5.4 \times 10^{16} \text{ cm}^{-3}$	
	1.7	1.09	0.61	9.4	0.807	8.3	$N_A = 9.9 \times 10^{16} \text{ cm}^{-3}$	
MOCVD, 1 um base, window, ARC	1.69	1.18	0.51	16.94	0.864	17.2	$t_b = 1.0 \mu m$	80
	1.68	1.18	0.50	16.10	0.861	16.3	$t_b = 1.5 \mu m$	
	1.69	1.18	0.51	14.66	0.862	14.9	$t_b = 2.0 \mu m$	
MOCVD, 1E17 base doping, window, ARC	1.69	1.21	0.48	15.93	0.859	16.6	$N_A = 4 \times 10^{17} \text{ cm}^{-3}$	80
	1.71	1.18	0.53	15.17	0.839	15.1	$N_A = 1 \times 10^{17} \text{ cm}^{-3}$	
	1.69	1.17	0.52	17.25	0.762	15.4	$N_A = 2 \times 10^{15} \text{ cm}^{-3}$	
MOCVD, n-i-p, ARC	1.7	1.19	0.51	18.4	0.823	18.0	$t_i = 1.0 \mu m$	71
	1.7	1.20	0.50	18.3	0.825	18.1	$t_i = 1.4 \mu m$	
	1.7	1.19	0.51	18.2	0.763	16.5	$t_i = 1.7 \mu m$	

(extracted from the 2J device via electroluminescence spectra), respectively. When combined with the underlying GaInAs cell, the authors demonstrated a 2J  $\eta$  of 32.6%, barely behind the III-V  $\eta$  record of 32.9% held by a 1.9 eV GaInP/GaAs tandem with strain-balanced quantum wells in the bottom cell to improve current-matching.<sup>83</sup>

### B. $\text{Al}_x\text{Ga}_{1-x}\text{As}$ $x < 0.25$

The first 2J solar cell with a tunnel junction interconnect was demonstrated by Bedair *et al.* at Research Triangle Institute and North Carolina State University in 1979.<sup>84</sup> The 9%-efficient tandem utilized a spectrally mismatched 1.65 eV  $\text{Al}_{0.2}\text{Ga}_{0.8}\text{As}$  top cell on GaAs, all grown by liquid phase epitaxy (LPE). The materials challenges of AlGaAs alloys in device active regions include oxygen-related defects and DX centers in n-type layers. Nevertheless, with a direct bandgap that can be tuned from 1.40–1.97 eV, AlGaAs has been explored as a top cell for Si-based tandems via mechanical stacking or epitaxial integration with thermal cycle annealing (TCA) to reduce TDD. The idea was initially explored in the 1980s when Gale *et al.* at MIT Lincoln Laboratory developed 1.65 eV  $\text{Al}_{0.2}\text{Ga}_{0.8}\text{As}$  cells on GaAs by MOCVD.<sup>85</sup> The device design utilized a thin  $\sim 50$  nm emitter, no WL, and an oxide layer for an ARC. AM1 results revealed  $W_{oc} = 0.55$  V,  $J_{sc} = 14.6 \text{ mA/cm}^2$ , and  $FF = 0.76$  for  $\eta = 12.9\%$ . The authors stated that most of the loss came from the poor minority carrier collection from carriers generated via long-wavelength photons, suggesting that either the minority carrier diffusion length was much less than the base thickness or the  $1.7 \mu\text{m}$  base was insufficiently thick. A year later, Virshup *et al.* at Varian Research Center developed  $\text{Al}_{0.2}\text{Ga}_{0.8}\text{As}$  cells by MOCVD with a graded bandgap (1.64 to 1.72 eV) throughout the emitter to produce a 4000 V/cm field, effectively lengthening the short hole diffusion lengths in n-AlGaAs.<sup>86</sup> This design enabled cells with  $\eta = 19.2\%$  (AM2), via  $W_{oc} = 0.46$  V,  $J_{sc} = 14.5 \text{ mA/cm}^2$ , and  $FF = 0.83$ .

Nearly a decade later, researchers at the Nagoya Institute of Technology developed a monolithic  $\text{Al}_x\text{Ga}_{1-x}\text{As}/\text{Si}$  2J device grown via MOCVD at a high  $T_{sub}$  of  $800^\circ\text{C}$  and utilized TCA to improve the crystalline quality of the  $\text{Al}_x\text{Ga}_{1-x}\text{As}$ ;<sup>87–89</sup> the use of high  $T_{sub}$  is common for AlGaAs solar cells as a method to reduce O concentration, [O]. They first developed single-junction  $\text{Al}_x\text{Ga}_{1-x}\text{As}$  devices with  $x = 0.15$  and  $x = 0.22$ . The peak QE degraded from 80% to 65% due to the slight increase in Al content, likely due to increased [O]. Similar to Ref. 86, the authors employed a graded bandgap emitter (by grading  $x$  from 0.15 to 0.30) to improve  $J_{sc}$  of the top cell. In doing so, they produced an  $\text{Al}_{0.15}\text{Ga}_{0.85}\text{As}$  cell with AM0  $\eta = 11.9\%$  ( $V_{oc} = 0.953$  V,  $W_{oc} \approx 0.7$  V,  $J_{sc} = 23.0 \text{ mA/cm}^2$ ,  $FF = 0.734$ ) and a Si-based tandem cell with  $\eta = 19.9\%$ .<sup>87</sup>

Yazawa *et al.* at Hitachi further probed the effect of O-incorporation on  $\text{Al}_{0.22}\text{Ga}_{0.78}\text{As}$  solar cells by growing  $\text{Al}_{0.22}\text{Ga}_{0.78}\text{As}$  cells via MBE with various  $T_{sub}$  (580–700 °C).<sup>90</sup> They found [O] to be minimized for  $T_{sub} = 660^\circ\text{C}$  (via secondary ion mass spectrometry, SIMS), corresponding to the highest  $\eta$  device of the series with  $\eta = 13.7\%$  ( $V_{oc} = 1.2$  V,  $W_{oc} \approx 0.54$  V,  $J_{sc} = 12 \text{ mA/cm}^2$ ,  $FF = 0.8$ ). The remaining samples had  $<2\times$  higher [O] than the sample grown at  $T_{sub} = 660^\circ\text{C}$ , but nevertheless suffered from reduced  $\eta \leq 8\%$ , revealing the strong effect O-incorporation has on solar cell performance.

In the 2010s, Heckelman *et al.* at Fraunhofer ISE, investigated the possibility that incremental advancements to growth technology could enable reduced [O] in Al-containing devices grown by MOCVD.<sup>91</sup> For example, due to improvements in the purity of the metalorganic

**TABLE III.** Summary of recent  $\text{Al}_x\text{Ga}_{1-x}\text{As}$  solar cell results from Fraunhofer ISE.<sup>91</sup>

Al content, x	$E_g$ (eV)	$V_{oc}$ (V)	$J_{sc}$ ( $\text{mA/cm}^2$ )	FF	$W_{oc}$ (V)
0.00	1.42	1.041	21.2	0.827	0.379
0.05	1.49	1.089	19.8	0.834	0.401
0.20	1.67	1.246	15.8	0.859	0.424

precursor trimethylaluminum (TMAI), they expected samples to have oxygen-related defect concentrations below  $10^{13} \text{ cm}^{-3}$ , a  $>5$  order of magnitude improvement compared to the AlGaAs grown in the 80s and 90s.<sup>90,92</sup> To investigate the effect of this dramatic improvement to material quality on solar cell properties, the authors grew  $\text{Al}_x\text{Ga}_{1-x}\text{As}$  single-junction solar cells with varied Al contents ranging from 0% to 37% ( $E_g = 1.42$ –1.90 eV,  $x > 25\%$  discussed in Sec. III B). Deep level transient spectroscopy (DLTS) revealed a large number of defects between 100 and 200 K for the highest Al contents explored in the work, which the authors associated with Te-related DX centers. Additional non-DX-center-related defects were present in all samples and nearly independent of Al concentration, implying the Al precursor was of high quality. However, short-wavelength internal quantum efficiency (IQE) degraded with increasing Al content, implying that the formation of DX centers could not be fully alleviated by the improved purity of TMAI. Table III summarizes the results as a function of Al content.

The group at Fraunhofer ISE further analyzed  $\text{Al}_x\text{Ga}_{1-x}\text{As}$  cells grown with two different TMAI sources: one with low O content (0.4 ppm) and one with deliberately elevated O content (97 ppm).<sup>93</sup> Both Al sources yielded AlGaAs layers with [O] below the SIMS detection limit. However, the solar cells grown with the higher O content TMAI underperformed slightly compared to cells grown with the lower O content TMAI. A slight degradation to long-wavelength IQE was observed for samples with  $x = 0.05$  and  $x = 0.20$  when grown with the lower-purity TMAI (Fig. 8), along with two additional DLTS peaks that shifted toward mid-gap as Al content increased. Increasing Al content also led to a drop in peak IQE, even for the samples grown with the high-purity TMAI source. These results suggest that solar cell

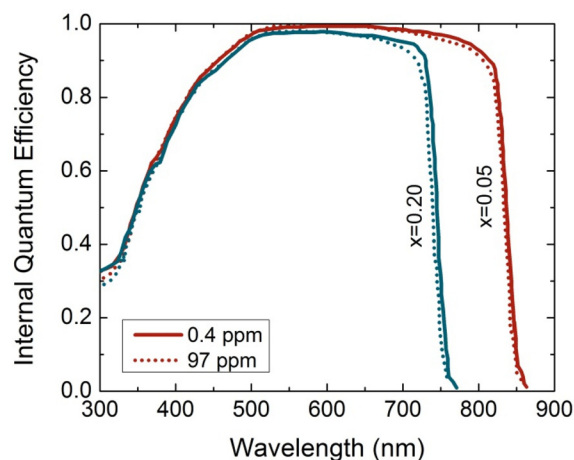


**FIG. 8.** IQE of  $\text{Al}_x\text{Ga}_{1-x}\text{As}$  solar cells from Ref. 93 revealing slight degradation of cells with  $x \leq 0.20$  at long wavelengths when lower-quality Al source is used during growth. Adapted from Ref. 93.

performance may still be adversely affected even in cases where the [O] is below the SIMS detection limit.

Onno *et al.* at University College London investigated the effect of  $T_{\text{sub}}$  on MBE-grown 1.7 eV  $\text{Al}_{0.22}\text{Ga}_{0.78}\text{As}$  solar cells.<sup>94</sup> The authors grew  $\text{Al}_{0.22}\text{Ga}_{0.78}\text{As}$  at various  $T_{\text{sub}}$  ranging from 580 to 660 °C and observed a “forbidden” growth window at  $T_{\text{sub}} = 600$  °C characterized by a degradation of surface morphology (3× increase in RMS roughness compared to samples grown at surrounding  $T_{\text{sub}}$ ), confirming previous reports of such a “forbidden”  $T_{\text{sub}}$  window for  $\text{Al}_x\text{Ga}_{1-x}\text{As}$  ( $x > 0.2$ ).<sup>95,96</sup> Both the smoothest surface morphology and highest PL intensity were observed for the sample grown at  $T_{\text{sub}} = 620$  °C. Solar cell properties trended with surface roughness, with the most efficient cell grown at  $T_{\text{sub}} = 620$  °C and the least efficient cell grown at  $T_{\text{sub}} = 600$  °C. The best performing cell had  $\eta = 7.77\%$ ,  $W_{\text{oc}} = 0.488$  V,  $J_{\text{sc}} = 7.85$  mA/cm<sup>2</sup>, and FF = 0.817.

More recently, Slimane *et al.* from Institut Photovoltaïque d’Île-de-France investigated MBE-grown 1.7 eV cells with a p-Al<sub>0.25</sub>Ga<sub>0.75</sub>As base and n-Ga<sub>0.51</sub>In<sub>0.49</sub>P emitter, obtaining  $W_{\text{oc}} = 0.438$  V and  $\eta = 18.7\%$ .<sup>97</sup> MBE growth of GaAs/AlGaAs is highly mature, and the record low-temperature two-dimensional electron gas mobility in MBE ( $\sim 57 \times 10^6$  cm<sup>2</sup>/Vs<sup>98</sup>) dramatically exceeds what is possible in MOCVD ( $\sim 2 \times 10^6$  cm<sup>2</sup>/Vs<sup>99</sup>) due to the higher purity that can be achieved in MBE when ultra-stringent maintenance procedures are followed. However, MBE has no apparent advantage over MOCVD for the growth of  $\text{Al}_x\text{Ga}_{1-x}\text{As}$  solar cells tested under standard conditions. Additional work on wider-bandgap  $\text{Al}_x\text{Ga}_{1-x}\text{As}$  ( $x > 0.25$ ) solar cells is described below in Sec. III B.

Ultimately, exploration of  $\text{Al}_x\text{Ga}_{1-x}\text{As}$  solar cells with  $x < 0.25$  revealed several important considerations, including:

- Introducing a graded composition profile to the emitter produces a drift field that can partially counteract the short diffusion length of holes in n-AlGaAs while also boosting  $V_{\text{oc}}$ .<sup>86</sup>
- Increasing  $x$  in  $\text{Al}_x\text{Ga}_{1-x}\text{As}$  from 0.15 to 0.22 results in peak EQE degradation from 80% to 65%, likely due to increased [O]<sup>87</sup> and DX centers.
- A 2× increase in [O] led to a >5% (absolute) drop in  $\eta$ , highlighting the significant impact of unintentional O-incorporation.<sup>90</sup>
- Even if [O] is below the SIMS detection limit, O-related defects can still hamper device performance.<sup>93</sup>

### C. Metamorphic $\text{Ga}_{1-x}\text{In}_x\text{P}$ , $x > 0.5$

Hoffman *et al.* at Essential Research, Inc. used MOCVD to demonstrate the first MM  $E_g = 1.65$  eV  $\text{Ga}_{1-x}\text{In}_x\text{P}$  ( $x \sim 0.65$ ) cell at Fall MRS 1998.<sup>100</sup> Their MM-GaInP cells were grown without AlInP barrier layers and achieved an impressive  $V_{\text{oc}}$  ( $W_{\text{oc}}$ ) of 1.16 V (0.49 V) under AM0 testing; interestingly, their lattice-matched 1.85 eV GaInP cells (also unpassivated) exhibited a slightly higher  $W_{\text{oc}}$  of 0.53 V, despite the near absence of threading dislocations. A second report on MM  $E_g = 1.67$  eV  $\text{Ga}_{0.35}\text{In}_{0.65}\text{P}$  cells grown on a step-graded 1.18 eV  $\text{Ga}_{0.83}\text{In}_{0.17}\text{As}$  buffer on GaAs was published by Dimroth *et al.* at Fraunhofer in 2000. They used MOCVD to attain 2J  $\text{Ga}_{0.35}\text{In}_{0.65}\text{P}/\text{Ga}_{0.83}\text{In}_{0.17}\text{As}$  efficiencies of 25.1% and 21.6% under the AM1.5G and AM0 spectra, respectively, despite estimated TDDs in the  $10^7$  cm<sup>-2</sup> range.<sup>101</sup> While the performance of the individual subcells was not reported, we can infer a top cell  $V_{\text{oc}}$  of ~1.15 V ( $W_{\text{oc}} \sim 0.52$  V) based on a paper from earlier that year describing just the bottom  $\text{Ga}_{0.83}\text{In}_{0.17}\text{As}$  cell.<sup>102</sup> High EQEs hovering around 90% were attained, though losses were noted at short wavelengths due to

absorption from the direct-gap AlGaInP window. By 2009, Fraunhofer had grown the same materials on an active Ge junction and achieved a 3J AM1.5D  $\eta = 31.6\%$  and a concentrated  $\eta = 41.1\%$ , a record at the time.<sup>76</sup> 4J AlGaInP/AlGaInAs/GaInAs/Ge space solar cells have now been commercialized for space applications,<sup>103</sup> though again, details on the growth, TDD, and individual subcell performance have not been published.

In 2023, Kim *et al.* used MBE to grow the first 1.7 eV MM GaInP RHJ solar cells.<sup>104</sup> Using a straightforward 6-step CGB grown at  $T_{\text{sub}} = 500$  °C, they were able to achieve TDDs as low as  $6 \times 10^5$  cm<sup>-2</sup> in the  $\text{Ga}_{0.85}\text{In}_{0.15}\text{As}$  cap layers, which were fully relaxed due to the incorporation of a  $\text{Ga}_{0.81}\text{In}_{0.19}\text{As}$  overshoot layer. With the help of rapid thermal annealing (RTA), the authors achieved remarkably long time-resolved photoluminescence (TRPL) lifetimes in n-Ga<sub>0.63</sub>In<sub>0.17</sub>P double heterostructures of 28 ns, longer than lattice-matched n-Ga<sub>0.51</sub>In<sub>0.49</sub>P double heterostructures grown in the same chamber (12.2 ns), indicating superior defect tolerance in In-rich MM-GaInP; the long lifetimes in MBE-grown MM GaInP are reminiscent of the low  $W_{\text{oc}}$  values in MM-GaInP demonstrated by Hoffman *et al.* in 1998.<sup>100</sup> Figure 9 shows the

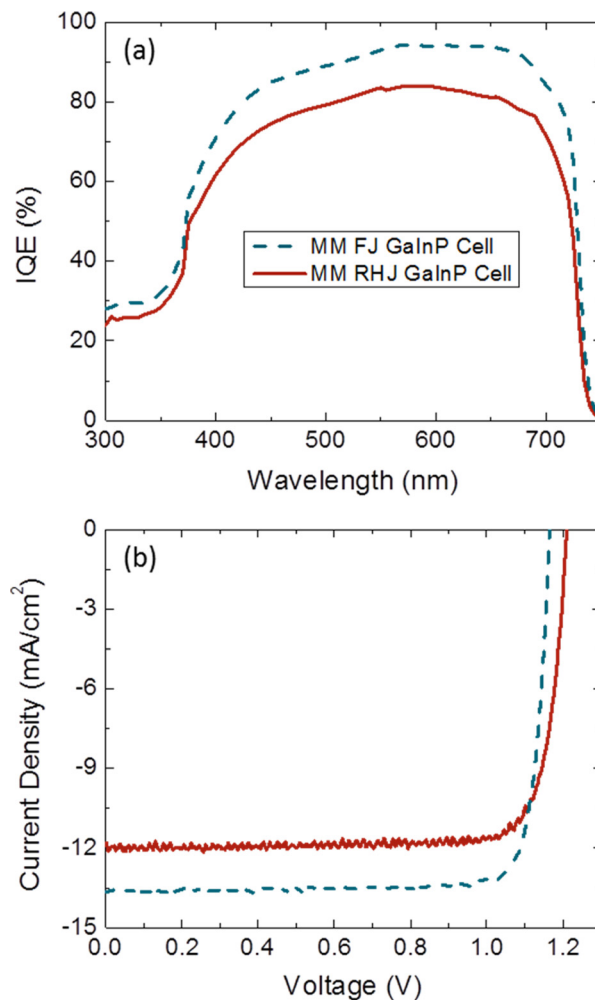


**FIG. 9.** (a) EQE and (b) LIV comparing uncoated FJ (dashed) and RHJ (solid) 1.7 eV MM-GaInP cells.<sup>104</sup> Adapted from Ref. 104.

(a) IQE and (b) LIV comparing FJ and RHJ cell configurations with  $E_g = 1.68$  eV. They noted that FJ cells had lower  $V_{oc}$  (1.17 vs 1.21 V) and higher  $J_{sc}$  (13.73 vs 11.8 mA/cm<sup>2</sup>). Thus, despite the long lifetime and relatively low  $W_{oc}$  of 0.47 V, MBE-grown MM GaInP RHJ cells have considerable room for improvement.

### D. Metamorphic GaAs<sub>y</sub>P<sub>1-y</sub>, $y \approx 0.70\text{--}0.85$

The most explored approach to epitaxial III-V/Si tandem cells uses MM-GaAs<sub>y</sub>P<sub>1-y</sub> as the III-V subcell. While GaAs<sub>y</sub>P<sub>1-y</sub> offers the desired bandgap ( $E_g = 1.6\text{--}1.8$  eV for  $y \approx 0.70\text{--}0.85$ ), its lattice mismatch with Si of 2.9%–3.4% induces  $\eta$ -degrading threading dislocations.<sup>43,105</sup> The binary end point GaP, on the other hand, possesses only 0.4%–0.5% lattice mismatch with Si, and fully strained GaP-on-Si templates are commercially available.<sup>106,107</sup> Using GaP as a starting point enables the growth of a GaAs<sub>y</sub>P<sub>1-y</sub> CGB to the desired lattice constant, thus overcoming the lattice mismatch and enabling sufficiently low TDD ( $< 1 \times 10^7$  cm<sup>-2</sup>) to demonstrate high- $\eta$  devices via optimized III-V on Si growth<sup>106,107</sup> and CGB design/growth.<sup>21,108</sup>

Our historic review of MM-GaAsP begins with Barton and Olsen, who first explored GaAs<sub>y</sub>P<sub>1-y</sub> solar cells in the late 1970s using HVPE-grown material from the already-mature visible light emitting diode (LED) market.<sup>109</sup> Although the device design was optimized for LEDs rather than solar cells, they demonstrated a 2.08 eV GaAs<sub>0.35</sub>P<sub>0.65</sub> device on GaP with  $V_{oc} = 0.65$  V ( $W_{oc} = 1.43$  V),  $J_{sc} = 3.16$  mA/cm<sup>2</sup>, and FF = 0.77. They additionally presented a 1.90 eV GaAs<sub>0.6</sub>P<sub>0.4</sub> device on GaAs with  $V_{oc} = 0.89$  V ( $W_{oc} = 1.01$  V),  $J_{sc} = 6.34$  mA/cm<sup>2</sup>, and FF = 0.78. While not optimized for PV operation, they provided an early proof of concept for GaAs<sub>y</sub>P<sub>1-y</sub> solar cells and, noting the significant increase in  $W_{oc}$  with increased P content, a first indication that as the material becomes more GaP-like (i.e., P-rich), solar cell performance suffers. However, little work followed these initial demonstrations until nearly a decade later.

Noting that the optical transparency of a GaP substrate would enable mechanical stacking to a bottom Si solar cell and renewed motivation for GaAs<sub>y</sub>P<sub>1-y</sub> solar cell investigation, Fraas *et al.* began fabricating GaAs<sub>0.7</sub>P<sub>0.3</sub> solar cells on GaP substrates in 1985.<sup>110</sup> Starting with HVPE-grown GaAs<sub>0.35</sub>P<sub>0.65</sub>/GaP LED wafers as templates, the authors used MOCVD to perform a rough compositional grade from GaAs<sub>0.35</sub>P<sub>0.65</sub> to GaAs<sub>0.70</sub>P<sub>0.30</sub>, terminating the structure with a p-on-n GaAs<sub>0.7</sub>P<sub>0.3</sub> solar cell. Their best device exhibited  $\eta = 15.4\%$  under 30 suns. Two years later at the IEEE Photovoltaic Specialists Conference, Negley *et al.* presented results for a GaAs<sub>y</sub>P<sub>1-y</sub> on GaP solar cell with  $E_g = 1.97$  eV.<sup>111</sup> Their best device, a metal-insulator-semiconductor structure grown by LPE with an indium-titanium-oxide front contact, exhibited  $\eta = 10.6\%$ . They then fabricated the first mechanically stacked, 2J, 4-terminal solar cells with GaAs<sub>y</sub>P<sub>1-y</sub> as the top cell but did not report any results from this device. At the same conference, Vernon *et al.* at Spire Corporation reported the effect of different CGB designs on cell performance for MOCVD-grown GaAs<sub>0.8</sub>P<sub>0.2</sub> cells on GaAs substrates, finding that thicker CGBs led to better device characteristics.<sup>112</sup> Their highest- $\eta$  device possessed an 8  $\mu\text{m}$  thick CGB with TDD =  $1.7 \times 10^6$  cm<sup>-2</sup> and AM1.5G  $\eta = 17.8\%$  with  $W_{oc} = 0.45$  V ( $E_g = 1.69$  eV). Unfortunately, these cells suffered from degradation linked to uncontrolled oxidation of the Al-rich WL. The authors projected that these cells could achieve  $\eta > 19\%$  with an improved WL. Wanlass *et al.* at NREL also explored various schemes for GaAs<sub>y</sub>P<sub>1-y</sub> CGBs grown by MOCVD on GaAs substrates, comparing TDD to

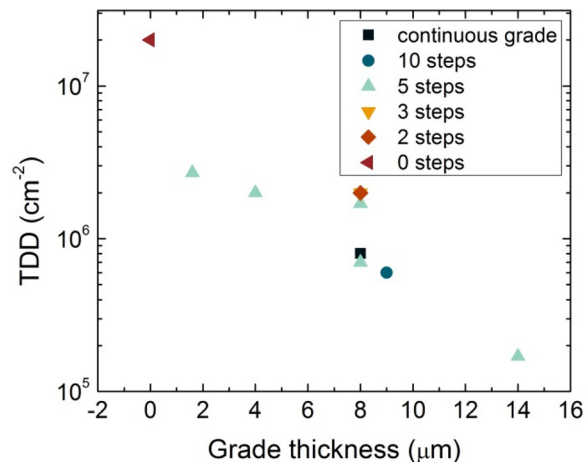


FIG. 10. TDD (measured by electron beam induced current) of GaAsP on GaAs vs grade thickness showing trend of strong TDD reduction with increased thickness.<sup>112,113</sup>

solar cell performance of GaAs<sub>0.74</sub>P<sub>0.26</sub> shallow homojunction cells.<sup>113</sup> Various grades were explored, and, similar to Vernon *et al.*,<sup>112</sup> thicker grades with more steps led to the lowest TDD and highest  $\eta$ . However, they found that buffers thicker than 8  $\mu\text{m}$  and changing from five steps to a continuous grade had little effect on TDD or device performance, indicating a point of diminishing returns in CGB design. Their best devices exhibited  $\eta = 8.87\text{--}9.12\%$  and possessed TDD (on GaAs) in the high  $10^5$  cm<sup>-2</sup> range. Figure 10 plots the TDD as a function of CGB thickness and number of steps for the references,<sup>112,113</sup> revealing a clear decrease in TDD with increased CGB thickness and demonstrating the importance of CGB design. Figure 11 then plots  $\eta$  as a function of TDD for these two references, showing that  $\eta$  is relatively insensitive to TDD below  $2 \times 10^6$  cm<sup>-2</sup>. These initial efforts proved that GaAs<sub>y</sub>P<sub>1-y</sub> is a viable option for a 1.7 eV solar cell and that the CGB design strongly impacts TDD and device performance.

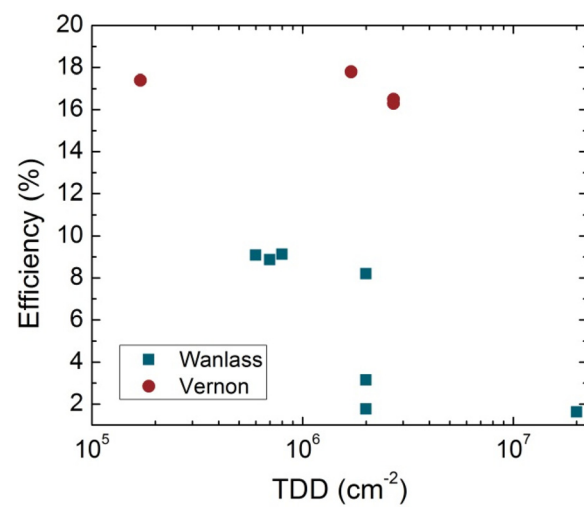


FIG. 11. Effect of TDD on GaAsP single-junction solar cell  $\eta$ . The relatively weak trend for  $TDD < 2 \times 10^6$  cm<sup>-2</sup> indicates that factors other than TDD can influence GaAsP cell  $\eta$ .<sup>112,113</sup>

Throughout the 1990s and 2000s, research progressed from  $\text{GaAs}_y\text{P}_{1-y}$  cells on GaP or GaAs substrates toward  $\text{GaAs}_y\text{P}_{1-y}$  cells on Si substrates. Hayashi *et al.* at Nagoya explored the effects of TCA and the use of a  $\text{GaAs}_y\text{P}_{1-y}$  CGB on the  $\eta$  of  $\text{GaAs}_{0.7}\text{P}_{0.3}$  solar cells on Si grown by MOCVD.<sup>114</sup> They found that performing a TCA after the GaP deposition and in the middle of the  $\text{GaAs}_y\text{P}_{1-y}$  CGB led to decreased TDD in cross-sectional transmission electron microscopy. The best devices used both a CGB and TCA, resulting in  $\eta(\text{AM}0) = 5.5\%$  ( $W_{\text{oc}} = 0.847$  V,  $J_{\text{sc}} = 10.41 \text{ mA/cm}^2$ , and  $\text{FF} = 0.77$ ). Geisz *et al.* at NREL used MOCVD to introduce a nearly lattice-matched  $\text{GaN}_{0.02}\text{P}_{0.98}$  layer following GaP nucleation on Si to annihilate antiphase domains.<sup>73</sup> Following the  $\text{GaN}_{0.02}\text{P}_{0.98}$  layer, the authors graded from GaP to  $\text{GaAs}_{0.7}\text{P}_{0.3}$ , varying the step thickness in the CGB and base thickness in the solar cell design (no ARC). All cells investigated by Geisz *et al.* possessed TDD  $\sim 1 \times 10^8 \text{ cm}^{-2}$ , about two orders of magnitude higher than the threshold at which III-V cell performance typically degrades.<sup>43</sup> Doubling the graded buffer step thickness from 0.25 to  $0.50 \mu\text{m}$  led to a reduction in TDD from  $1.7 \times 10^8$  to  $9.7 \times 10^7 \text{ cm}^{-2}$  and an  $\eta$  improvement from 8.2 to 8.7%. Doubling the base thickness from 1 to  $2 \mu\text{m}$ , on the other hand, led to a greater improvement, enabling  $\eta = 9.8\%$  (thin CGB,  $W_{\text{oc}} = 0.725$  V,  $J_{\text{sc,AM1.5G}} = 13 \text{ mA/cm}^2$ ,  $\text{FF} = 0.77$ ).

Fundamental research on GaP/Si growth continued, and by the early 2010s, GaP/Si was being commercialized by NAsP III-V GmbH (NAsP) and produced in-house at Ohio State University (OSU), leading to a resurgence in  $\text{GaAs}_y\text{P}_{1-y}/\text{Si}$  2J solar cell research. OSU developed a GaP/Si nucleation method using migration-enhanced epitaxy, enabling 1.7 eV  $\text{GaAs}_y\text{P}_{1-y}$  single-junction solar cells on Si using TDD =  $2 \times 10^8 \text{ cm}^{-2}$   $\text{GaAs}_y\text{P}_{1-y}$  CGB templates<sup>115</sup> and then produced 1.75 eV  $\text{GaAs}_y\text{P}_{1-y}$  cells on Si with  $\eta(\text{AM}0) = 7.0\%$  and  $W_{\text{oc}} = 0.71$  V.<sup>116</sup> Transitioning the virtual substrate growth from MBE to MOCVD while simultaneously refining the growth of the  $\text{GaAs}_y\text{P}_{1-y}$  CGB led to significant reduction in TDD to the high  $10^6 \text{ cm}^{-2}$  range.<sup>117</sup>  $\text{GaAs}_y\text{P}_{1-y}$ -on-Si single-junction solar cells ( $E_g \approx 1.72 \text{ eV}$ ) grown on these improved templates exhibited  $\eta(\text{AM1.5G}) = 9.5\%$  and  $W_{\text{oc}} \approx 0.62$  V. The OSU group also investigated the impact of switching to a RHJ design in the hopes of improving defect tolerance.<sup>118</sup> They grew both FJ and RHJ single-junction devices on GaAs substrates but found the FJ device to exceed the performance of the RHJ design due to greatly improved  $J_{\text{sc}}$ . In parallel with this work on single-junction  $\text{GaAs}_y\text{P}_{1-y}$  devices, the OSU group began the development of 2J  $\text{GaAs}_y\text{P}_{1-y}/\text{Si}$  solar cells. In 2016, Grassman *et al.* demonstrated 2J  $\text{GaAs}_{0.75}\text{P}_{0.25}/\text{Si}$  devices by both MOCVD and MBE on  $\text{GaAs}_y\text{P}_{1-y}$  CGB templates with TDD  $\approx 10^7 \text{ cm}^{-2}$  and showed that MOCVD-grown cells outperformed those grown by MBE.<sup>119</sup> The authors suggested that the reduced  $\eta$  in the MBE-grown device resulted from dopant diffusion in the tunnel junction (TJ) during the growth of the  $\text{GaAs}_y\text{P}_{1-y}$  top cell. In contrast, the MOCVD-grown device employed a more stable TJ design with heavy carbon doping on the p-side. Ultimately, the MOCVD-grown 2J device yielded  $\eta(\text{AM1.5G}) = 13.1\%$ , far exceeding any previously demonstrated  $\text{GaAs}_y\text{P}_{1-y}/\text{Si}$  tandem cell.

Two years later, the OSU group presented an improved 2J device in which most aspects of the growth/design were optimized to achieve a record-breaking  $\eta = 20.1\%$  and  $V_{\text{oc}} = 1.673$  V.<sup>120</sup> Adjustments to the design of the Si subcell led to  $\eta = 21.8\%$  a year later.<sup>121</sup> Performing loss analysis on their previous cell ( $\eta = 21.8\%$ ) led Lepkowski *et al.* to focus on improving TDD and increasing the top cell  $E_g$ .<sup>122</sup> Comparing

single-junction  $\text{GaAs}_y\text{P}_{1-y}$  cells on Si (TDD =  $2 \times 10^7 \text{ cm}^{-2}$ ) to identical cells on GaAs (TDD =  $1-2 \times 10^6 \text{ cm}^{-2}$ ) revealed a  $2 \text{ mA/cm}^2$  current loss, a 120 mV voltage loss, and a 6% absolute loss in FF due to the elevated TDD on Si. These losses highlight the need for further reduction to TDD to fully take advantage of the 2J architecture on Si. That said, reducing the TDD to  $9 \times 10^6 \text{ cm}^{-2}$  and increasing top cell  $E_g$  to 1.72 eV resulted in a certified  $\eta = 23.4\%$  with a  $V_{\text{oc}} = 1.73$  V,  $J_{\text{sc}} = 17.34 \text{ mA/cm}^2$ , and  $\text{FF} = 0.777$ . Later, the OSU group introduced a strained-layer  $\text{GaAs}_y\text{P}_{1-y}/\text{GaP}$  superlattice structure during the initial relaxation of GaP on Si, which, combined with an optimized  $\text{GaAs}_y\text{P}_{1-y}$  CGB, enabled GaAsP top cells on Si with TDD down to  $3 \times 10^6 \text{ cm}^{-2}$ , showing excellent promise for future  $\eta$  improvements.<sup>123</sup>

In parallel, Lee's group (initially at Yale University and later at the University of Illinois) investigated  $\sim 1.7 \text{ eV}$   $\text{GaAs}_y\text{P}_{1-y}$  solar cells grown on GaP substrates and commercial GaP/Si templates by MBE. They first developed 1.71 eV  $\text{GaAs}_{0.73}\text{P}_{0.27}$  solar cells on GaP with TDD =  $6.3 \times 10^6 \text{ cm}^{-2}$ ,  $W_{\text{oc}} = 0.56$  V, and  $\eta = 6.5\%$ .<sup>124</sup> Following the development of single-junction  $\text{GaAs}_y\text{P}_{1-y}$  solar cells on GaP, they then compared various  $E_g \approx 1.7 \text{ eV}$   $\text{GaAs}_{0.72}\text{P}_{0.28}$  device structures on both GaP and GaP/Si templates.<sup>125</sup> The authors found the TDD on GaP/Si ( $1.0-1.3 \times 10^7 \text{ cm}^{-2}$ ) exceeded that on GaP ( $6.4-7.6 \times 10^6 \text{ cm}^{-2}$ ) by  $\sim 2\times$ , though this was the lowest reported TDD on Si by an order of magnitude at the time of publication. Lang *et al.* also interrogated the effect of device polarity on LIV characteristics and found the devices to be insensitive to this design parameter,<sup>125</sup> contrary to the results of Andre *et al.* for MM GaAs cells on Si.<sup>44</sup> Following these growths, the authors used x-ray reciprocal space mapping to optimize the CGB structure, producing n+/p 1.71 eV  $\text{GaAs}_y\text{P}_{1-y}$  single-junction cells with TDD =  $9.2 \times 10^6 \text{ cm}^{-2}$ . This slight reduction to TDD enabled a  $V_{\text{oc}} = 1.12$  V, yielding a  $W_{\text{oc}} = 0.59$  V, the lowest  $W_{\text{oc}}$  reported at the time.<sup>125</sup>

Nay Yaung *et al.* at Yale University then investigated the effect of GaP relaxation on GaP/Si templates on TDD and  $\text{GaAs}_y\text{P}_{1-y}$  solar cell performance.<sup>126</sup> The authors ultimately found a moderate  $T_{\text{sub}} = 505^\circ\text{C}$  during GaP nucleation minimized TDD, counter to Fitzgerald's dislocation dynamics model, which stipulates that increased  $T_{\text{sub}}$  leads to increased dislocation glide velocities and thus reduced TDD.<sup>37</sup> However, at  $T_{\text{sub}} > 505^\circ\text{C}$  for GaP on GaP/Si growth, dislocation nucleation begins to dominate, resulting in increased TDD. In addition to  $T_{\text{sub}}$ , the authors probed the effect of growth rate on TDD, finding that decreasing the growth rate from 1.0 to  $0.25 \mu\text{m/h}$  reduced TDD slightly, as expected from Ref. 37. However, further growth rate reduction to  $0.1 \mu\text{m/h}$  caused an increase in TDD, perhaps resulting from dislocation nucleation during the extended growth time. The combination of  $T_{\text{sub}} = 505^\circ\text{C}$  and  $0.5 \mu\text{m/h}$  enabled GaP/Si templates with TDD  $< 2 \times 10^6 \text{ cm}^{-2}$ . Armed with the knowledge of how to minimize the starting TDD, the authors investigated the effect of  $T_{\text{sub}}$  and grading rate ( $\xi = \frac{a_{\text{sub}} - a_{\text{film}}}{d_{\text{film}}} \times 100\%$ ,  $d = \text{CGB thickness}$ ) of the  $\text{GaAs}_y\text{P}_{1-y}$  CGB on TDD. They found a  $T_{\text{sub}}$  window of  $575-600^\circ\text{C}$  for which the TDD was minimized. Above this window, dislocation nucleation dominates, and below it, dislocation glide velocity is reduced, each resulting in increased TDD. Reducing  $\xi$  to  $0.38\%-\mu\text{m}^{-1}$  had the largest impact on TDD, ultimately providing  $\text{GaAs}_y\text{P}_{1-y}$  on Si possessing TDD =  $4.2 \times 10^6 \text{ cm}^{-2}$ <sup>126</sup> a  $2\times$  reduction compared with previous results.<sup>125</sup> Combining the optimized GaP homoepitaxy  $T_{\text{sub}} = 505^\circ\text{C}$ , optimized  $\text{GaAs}_y\text{P}_{1-y}$  CGB  $T_{\text{sub}} = 575^\circ\text{C}$ , and low  $\xi = 0.38\%-\mu\text{m}^{-1}$ , the authors reported single-junction 1.7 eV  $\text{GaAs}_{0.77}\text{P}_{0.23}$  solar cells on Si with  $\eta = 12.0\%$  and  $W_{\text{oc}} = 0.55$  V.

The Lee Group then improved the 1.7 eV  $\text{GaAs}_{0.77}\text{P}_{0.23}$  solar cell design, improved material quality, and added an optimized ARC.<sup>127</sup> These cells exhibited improved  $\eta = 15.33\%$  and  $W_{oc} = 0.543$  V. By integrating a Si bottom cell to provide the full 2J solar cell, the group obtained  $\eta = 20\%$  for a device with  $TDD = 8 \times 10^6 \text{ cm}^{-2}$ .<sup>108</sup> They also investigated avenues for further 2J improvement, such as increased  $\text{GaAs}_y\text{P}_{1-y}$   $T_{sub}$  to improve carrier collection and backside random pyramid texturing of the Si bottom cell to enhance light trapping as a pathway to higher  $\eta$ .<sup>108</sup> Fan *et al.* further pushed the 2J  $\eta$  to 25% by focusing on the interface between the TJ and the BSF of the 1.7 eV  $\text{GaAs}_{0.77}\text{P}_{0.23}$  top cell.<sup>45,128</sup> Electron beam-induced current measurements revealed a network of dark-line defects at a depth of 1–2  $\mu\text{m}$ , and TEM confirmed the presence of misfit dislocations at the BSF/base interface. By incorporating a 500 nm spacer layer of  $\text{GaAs}_y\text{P}_{1-y}$  (where  $y$  is identical to that of the active region) between the TJ and the BSF and changing the BSF from  $\text{Ga}_{0.66}\text{In}_{0.34}\text{P}$  to  $\text{Al}_{0.3}\text{Ga}_{0.7}\text{As}_{0.77}\text{P}_{0.23}$ , the authors obtained a 3× reduction in the dark-line defects, leading to a significant increase to the  $\text{GaAs}_{0.77}\text{P}_{0.23}$  top cell EQE. The single-junction  $\eta$  increased by 2.3% absolute due to a slight increase to FF and a  $2 \text{ mA/cm}^2$  increase to  $J_{sc}$ . Incorporating this technique into the 2J device enabled a tandem  $J_{sc} = 18.8 \text{ mA/cm}^2$ ,  $V_{oc} = 1.646$  V, and  $FF = 0.81$ , leading to the  $\eta = 25\%$  cell mentioned above. Saenz *et al.* demonstrated similar benefits when replacing GaInP with AlGaAs barriers (both lattice-matched to GaAs) in GaAs solar cells on V-grooved Si, including a significant reduction in misfit dislocation density and an increase in TRPL lifetime.<sup>129</sup> Based on findings from III-V lasers on Si,<sup>130</sup> they attributed misfit dislocation formation at GaInP/GaAs interfaces to disparities in dislocation velocity in the two materials, which causes differences in dislocation glide length during cooldown. In contrast, the similar dislocation velocities of AlGaAs and GaAs, due to the absence of atomic size mismatch, mitigate this effect.

Recognizing the need to alter cell designs to account for threading dislocations, both OSU and the University of Illinois recently demonstrated concepts that could significantly boost the  $J_{sc}$  of  $\text{GaAs}_y\text{P}_{1-y}$  on Si top cells toward  $20 \text{ mA/cm}^2$  and beyond. Considering that  $J_{sc}$  of the current-record Si solar cell is  $42.35 \text{ mA/cm}^2$ , a GaAsP top cell would ideally deliver  $\sim 21 \text{ mA/cm}^2$ . Li *et al.* made the first experimental demonstration of an MBE-grown  $\text{Al}_{0.8}\text{Ga}_{0.2}\text{AsP}/\text{GaAsP}$  distributed Bragg reflector on Si.<sup>131</sup> Building on previous simulation studies,<sup>132</sup> they showed that a  $\sim 2 \mu\text{m}$  DBR with 20 repeats could attain a peak reflectance of 88% (in air) with little or no effect on TDD and surface roughness. Li then used simulations to show the potential to raise  $J_{sc}$  from 18.24 to  $19.23 \text{ mA/cm}^2$  with a thin 700 nm absorber.

Kasher *et al.* showed that the benefits of the lattice-matched AlGaAsP BSF demonstrated by Fan *et al.* also extend to MOCVD-grown GaAsP on Si solar cells and further added a gradient in base doping from  $3 \times 10^{16} \text{ cm}^{-3}$  near the junction to  $3 \times 10^{17} \text{ cm}^{-3}$  near the BSF; the purpose of the doping gradient was to introduce a small drift field to improve carrier collection without greatly increasing  $J_{02}$ .<sup>133</sup> In addition to the expected benefit in IQE, the doping gradient also enabled a record-low  $W_{oc}$  of 0.44 V, creating a near-term path to 30%-efficient GaAsP/Si tandem cells.

An alternative method to integrate III-V PV onto Si utilizes a  $\text{Si}_{1-x}\text{Ge}_x$  CGB instead of  $\text{GaAs}_y\text{P}_{1-y}$ . This approach requires the bottom cell be made of the cap  $\text{Si}_{1-x}\text{Ge}_x$  composition rather than the Si substrate due to the lack of transparency in the SiGe CGB; combining a 1.6 eV  $\text{GaAs}_y\text{P}_{1-y}$  cell and a 1.0 eV  $\text{Si}_{1-x}\text{Ge}_x$  cell provides a maximum theoretical  $\eta$  of 36% under AM1.5G.<sup>72</sup> In a collaborative effort, Lee's group investigated  $\text{GaAs}_{0.82}\text{P}_{0.18}$  ( $E_g = 1.64$  eV) single-junction

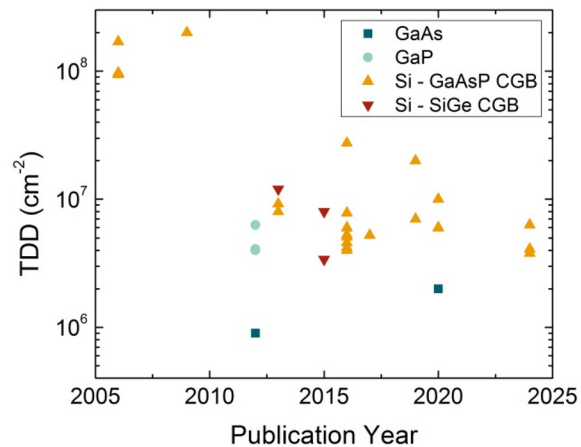


**FIG. 12.** TDD vs Publication year for  $\text{GaAs}_y\text{P}_{1-y}$  ( $y \approx 0.75$ ) on various substrates. Significant effort has led to over an order of magnitude improvement TDD for GaAsP on Si CGBs.

solar cells grown by MOCVD on  $\text{Si}_{0.2}\text{Ge}_{0.8}/\text{Si}$  ( $E_g = 0.79$  eV) virtual substrates. While the TDD exceeded  $10^7 \text{ cm}^{-2}$ , the authors achieved a low  $W_{oc} = 0.52$  V and  $\eta = 8.2\%$ .<sup>134</sup> By optimizing the III-V on SiGe initiation and SiGe CGBs, Milakovich *et al.* reduced the TDD down to  $\sim 2.0 \times 10^6 \text{ cm}^{-2}$ , resulting in what at the time was the lowest  $W_{oc}$  of 0.48 V obtained for p-on-n  $\sim 1.7$  eV  $\text{GaAs}_y\text{P}_{1-y}$  cells on Si.<sup>135</sup> Schmieder *et al.* produced 2J  $\text{GaAs}_{0.79}\text{P}_{0.21}/\text{Si}_{0.18}\text{Ge}_{0.82}$  cells using an *in situ* stress sensor during MOCVD growth to ensure lattice matching at  $T_{sub}$  and control TDD. This method resulted in  $TDD = 8 \times 10^6 \text{ cm}^{-2}$ , and a 2J device with  $V_{oc} = 1.458$  V.<sup>136</sup>

Figure 12 summarizes the progress in TDD reduction since 2005 for  $\text{GaAs}_y\text{P}_{1-y}$  on various substrates and CGBs. We see that starting on a III-V substrate or using a group-IV CGB enables TDD  $< 10^7 \text{ cm}^{-2}$  to be obtained in a straightforward manner. However, to achieve similar TDD for the desired  $\text{GaAs}_y\text{P}_{1-y}$  CGB on Si required over

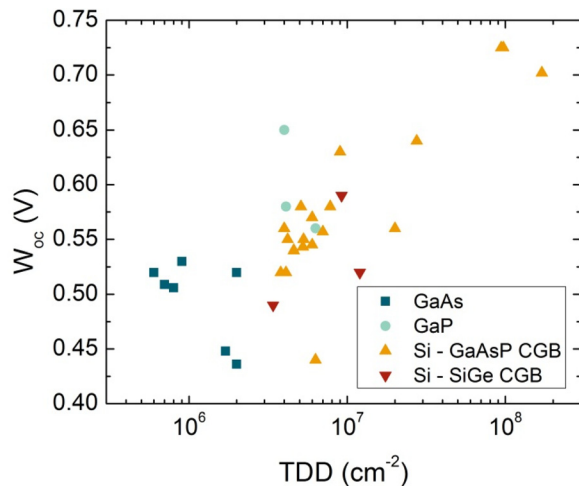


**FIG. 13.**  $W_{oc}$  vs TDD for single-junction  $\text{GaAs}_y\text{P}_{1-y}$  cells on various substrates measured under AM1.5G. Cells with  $W_{oc} > 1$  V excluded.  $W_{oc}$  is clearly linked to TDD, with decreasing TDD leading to decreased  $W_{oc}$ .

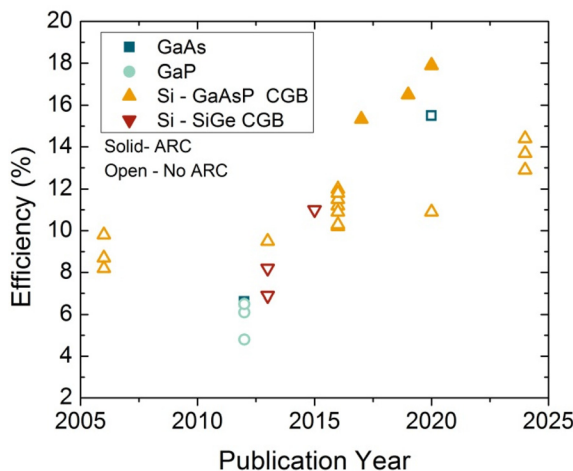


**FIG. 14.** Efficiency as a function of publication year for single-junction  $\text{GaAs}_y\text{P}_{1-y}$  cells (AM1.5G) on a variety of substrates. Excludes pre-2005 data. Improvements to TDD and solar cell design over two decades have led to a nearly 2 $\times$  increase in  $\eta$  for devices on Si substrates.

a decade of optimization of the GaP on Si initiation and CGB design and growth conditions. Such optimization enabled a nearly 100 $\times$  reduction in TDD of  $\text{GaAs}_y\text{P}_{1-y}$  on Si. The impact of this reduction is clearly seen in Fig. 13, which depicts the strong dependence of  $\text{GaAs}_y\text{P}_{1-y}$  single-junction  $W_{oc}$  on TDD. With current TDD levels in the mid-to-high- $10^6 \text{ cm}^{-2}$  range, the  $\text{GaAs}_y\text{P}_{1-y}$  cell performance remains limited, and continued reduction to  $TDD \leq 10^6 \text{ cm}^{-2}$  is likely necessary to achieve 2J  $\eta$  approaching 30%.<sup>122</sup> Figures 14 and 15 show  $\eta$  as a function of publication year for single- and dual-junction devices, respectively. Both have benefited from two decades' worth of effort but remain short of their theoretical maxima. Beyond TDD improvement, further  $\eta$  gains will require improved photon management (e.g., optimized grid coverage and reduced TJ absorption) to increase  $J_{sc}$  and reduced recombination at the GaP/Si interface to improve  $V_{oc}$  of the Si cell.<sup>108</sup>

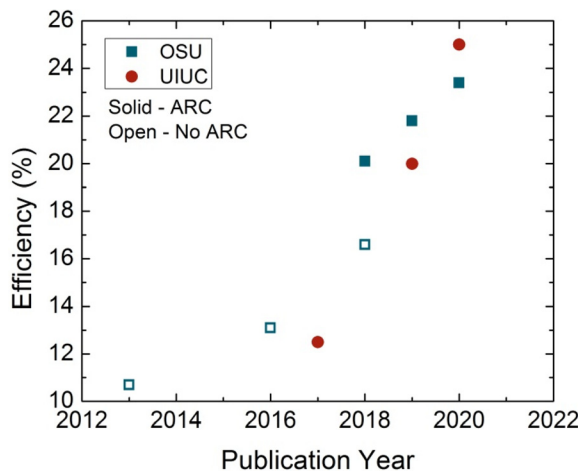


**FIG. 15.**  $\text{GaAs}_y\text{P}_{1-y}/\text{Si}$  2J AM1.5G  $\eta$  as a function of publication year. A significant increase in 2J tandem  $\eta$  shows a path for these devices to surpass  $\eta$  of single-junction Si solar cells.

## E. Summary and recommendations for future work on 1.7 eV junctions

To date, the highest- $\eta$  1.7 eV cells have employed lattice-matched  $\text{GaInAsP}$ <sup>71</sup> and  $\text{AlGaAs}$  on GaAs,<sup>97</sup> though MM-GaAsP on Si<sup>133</sup> and MM- $\text{Ga}_{1-x}\text{In}_x\text{P}$  ( $x > 0.5$ ) on GaAs<sup>104</sup> closely approach the  $W_{oc}$  values achieved in  $\text{AlGaAs}$ . However, one of the main applications of absorbers in this  $E_g$  range is stacking with a 1.1 eV bottom cell, which cannot be achieved solely at the GaAs lattice constant. As such, recent work has focused on materials that can be integrated with a Si subcell. Although pairing a 1.7 eV absorber with Si also requires lattice-mismatched growth, the low cost and technological maturity of Si make it an attractive option. For epitaxial III-V/Si tandems to reach  $\eta > 30\%$ , a 20%-efficient III-V top cell is likely needed. To date, the best such cells grown on Si have been GaAsP at  $\eta = 17.6\%$ , leveraging an improved understanding of GaP on Si nucleation and MM growth.<sup>45</sup> In addition to optimizing the device design and optical management, we recommend continued research to understand and reduce threading dislocation formation during III-V on Si initiation, CGB growth, and even cooldown<sup>130</sup> to further improve device performance. Alternatively, 1.7 eV  $\text{GaInAsP}$  and  $\text{AlGaAs}$  could be reconsidered for epitaxial Si-based tandems despite requiring higher lattice mismatch.

Most investigations of 1.7 eV solar cells have utilized MOCVD and MBE, with both techniques capable of producing low- $W_{oc}$  and high- $\eta$  cells. We anticipate that with sufficient time and investment, HVPE will also be able to produce high- $\eta$   $\text{GaInAsP}$ ,  $\text{AlGaAs}$ , and  $\text{GaAsP}$  solar cells. Table IV summarizes the current-best  $W_{oc}$  values for each material system and growth technique. While  $\text{GaInAsP}$  leads, Table IV indicates that  $\text{AlGaAs}$  and  $\text{GaAsP}$  are equally viable 1.7 eV absorber materials for high- $\eta$  sub-cells, which is in stark contrast to the case for wider- $E_g$  absorbers (Secs. III and IV) where lattice-matched (Al)GaInP dominates.

## III. 1.8-1.9 eV JUNCTIONS: TOP CELLS FOR $\text{GaAs}/\text{Ge}$ -BASED 3-J CELLS

Absorber materials with  $E_g = 1.8$ -1.9 eV are relevant for the top cell of 3J AM1.5G devices and the top cell in concentrator 4J solar cells.<sup>137</sup> Triple-junction designs on GaAs and Ge emerged primarily for space applications due to the superior radiation hardness of III-V cells compared to Si,<sup>138</sup> and such designs require top cells with  $E_g \sim 1.8$ -1.9 eV.<sup>20</sup> This section will explore PV materials with  $E_g \approx 1.8$ -1.9 eV, with Sec. III A covering  $\text{GaInP}$ , Sec. III B covering  $\text{AlGaAs}$ , and Sec. III C covering MM-GaAsP.

**TABLE IV.** Lowest  $W_{oc}$  values currently achieved for each 1.7 eV absorber material and growth technique used to achieve said value

Absorber material	Method	$W_{oc}$ (V)
$\text{GaInAsP}$ <sup>82</sup>	MOCVD	0.39
$\text{GaInAsP}$ <sup>79</sup>	HVPE	0.59
$\text{AlGaAs}$ <sup>91</sup>	MOCVD	0.424
$\text{AlGaAs}$ <sup>97</sup>	MBE	0.438
$\text{GaAsP}$ <sup>133</sup>	MOCVD	0.44
$\text{GaAsP}$ <sup>134</sup>	MBE	0.52
$\text{GaInP}$ <sup>104</sup>	MBE	0.47

### A. Lattice-matched GaInP

$\text{Ga}_{1-x}\text{In}_x\text{P}$  ( $x \approx 0.5$ , GaInP hereafter) has been the wide-bandgap absorber of choice for 3J devices for over 20 years, as it is both lattice-matched to GaAs and possesses reasonably good spectral matching with a GaAs middle cell. Furthermore, its  $E_g$  can be tuned from 1.8–1.9 eV via ordering when grown by MOCVD, providing another knob for current-matching aside from top-cell thinning.<sup>139</sup> As discussed in greater detail below, GaInP is also considerably more radiation-tolerant than GaAs, making it well suited for space applications.

MOCVD growth of GaInP and AlGaInP was initially developed in the mid-1980s to replace Al-rich AlGaAs in red visible lasers and high-efficiency LEDs.<sup>140</sup> Researchers at NREL first investigated GaInP solar cells in the context of a lattice-matched 2J GaInP/GaAs cell in the early 1990s. While not the ideal  $E_g$ -combination for two junctions (see Sec. II), it has the benefits of being lattice-matched, Al-free, and theoretically capable of achieving  $\eta \approx 35\%$  (1-sun, AM1.5G).<sup>72</sup> They found that MOCVD growth conditions (e.g.,  $T_{\text{sub}}$ , V/III ratio, and growth rate) had little effect on minority carrier diffusion length. In contrast, mismatch strain strongly and asymmetrically impacted  $J_{\text{sc}}$ ; tensile strain caused a rapid decrease beyond what would be expected for increased  $E_g$ , while compressive strain caused an increase commensurate with the decreased  $E_g$ . After just a few years of work, the authors fabricated a 2J device with  $V_{\text{oc}} = 2.29$  V,  $J_{\text{sc}} = 13.6 \text{ mA/cm}^2$ , and FF = 0.87, yielding  $\eta = 27.3\%$  (AM1.5G, very comparable to record AlGaAs/GaAs results<sup>141</sup>).<sup>142</sup> Further work focused on improving grid design, top surface passivation, and back surface passivation,<sup>143</sup> and Fig. 16 shows the device schematic and LIV curve. Reducing grid coverage from 4.9% to 1.9% without loss to FF led to a 0.8% absolute increase in  $\eta$ . To improve front surface passivation, the authors changed the AlInP WL dopant from selenium to silicon and introduced a “point-of-use phosphine purifier.” These changes led to decreased oxygen contamination and improved short-wavelength EQE. BSFs were then introduced to both subcells; the GaAs subcell employed a thin GaInP BSF, while wider-bandgap, disordered GaInP provided the BSF for the top subcell. These changes together produced a 2J device with record-breaking  $\eta = 29.5\%$  ( $V_{\text{oc}} = 2.385$  V,  $J_{\text{sc}} = 14.0 \text{ mA/cm}^2$ ) within 3 years of the first demonstration.

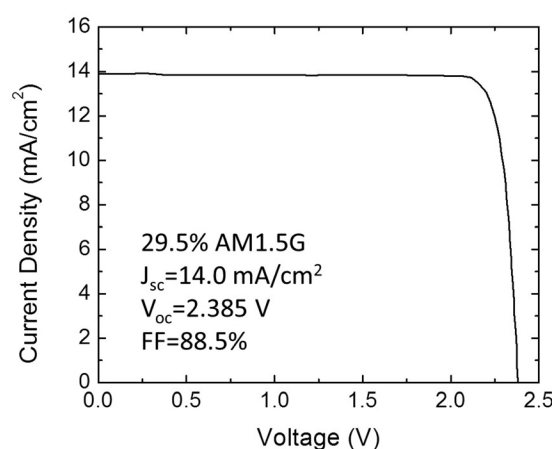
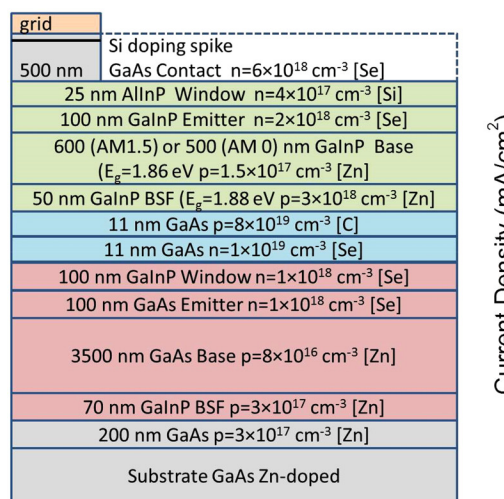


FIG. 16. (a) Layer schematic of record-breaking  $\eta = 29.5\%$  GaInP/GaAs 2J cell from 1994. (b) LIV characteristic under AM1.5G illumination. Adapted from Ref. 143.

Following NREL’s early success, commercial entities began investigating GaInP as a potential top cell material. In 1993, Spectrolab obtained a single-junction AM0 record of  $\eta = 15.3\%$  ( $V_{\text{oc}} = 1.299$  V,  $J_{\text{sc}} = 18.39 \text{ mA/cm}^2$ , FF = 0.866).<sup>144</sup> By testing the radiation hardness of GaInP under electron energies of 0.7, 1.0, and 2.0 MeV with fluences ranging from  $5 \times 10^{14} \text{ e/cm}^2$  and  $1 \times 10^{16} \text{ e/cm}^2$ , the authors showed that GaInP possesses superior radiation tolerance compared with GaAs, confirming initial radiation tolerance tests performed by Kurtz *et al.*<sup>145</sup> Lockheed Martin then reported GaInP/GaAs cells on Ge in production in 1996.<sup>146</sup> In 1999, Spectrolab activated the Ge substrate as a bottom junction to develop GaInP/GaAs/Ge 3J, radiation-hard devices that offered 60%–75% more end-of-life power than high- $\eta$  Si cells at 60 °C.<sup>147</sup> Similarly, in 2001, TECSTAR reported highly radiation-tolerant GaInP/GaAs/Ge cells.<sup>148</sup> Takamoto *et al.* at Japan Energy Corporation and Japan Energy Research Center Company developed a GaInP/GaAs tandem cell with >30% AM1.5G  $\eta$  by optimizing the TJ structure and reducing dopant diffusion.<sup>149</sup> At the time of this writing, the highest- $\eta$  3J solar cells on record all employ a GaInP top cell, providing  $\eta \geq 44\%$  under concentration.<sup>21,150</sup>

The mid-1990s also saw the advent of valved phosphorus crackers with greatly improved flux stability<sup>151</sup> for MBE growth of visible optoelectronics, prompting research on MBE growth of GaInP solar cells. In the early 2000s, OSU examined GaInP cells on GaAs as a pathway toward high- $\eta$  III-V cells on Si substrates.<sup>152</sup> Andre investigated single-junction GaInP cells grown at  $T_{\text{sub}} = 490$  °C on GaAs with both n-on-p and p-on-n polarities. While previously reported GaInP solar cells were grown by MOCVD at  $T_{\text{sub}} = 600$ –750 °C,<sup>142</sup> MBE growth of GaInP is typically done at  $T_{\text{sub}} \leq 510$  °C due to indium desorption and the inability to supply adequate  $P_2$  flux while remaining in a molecular flow pressure regime. A momentary RTA at 875 °C caused  $J_{\text{sc}}$  to increase by 15% for n<sup>+</sup>/p cells and 26% for p<sup>+</sup>/n cells. EQE spectra of these devices revealed that annealing enhances the base minority carrier lifetime in the n<sup>+</sup>-on-p cell and enhances EQE across all wavelengths for the p<sup>+</sup>-on-n design. The author also found that increasing the base doping from  $5 \times 10^{16}$  to  $2 \times 10^{17} \text{ cm}^{-3}$  in the n<sup>+</sup>-on-p design significantly improved  $V_{\text{oc}}$ , increasing from 1.210 to 1.275 V. However, the higher-doped base hampered the carrier

collection, resulting in a drop in  $J_{sc}$  from 8.55 to 6.56 mA/cm<sup>2</sup>. In the case of the p<sup>+</sup>-on-n design, reducing the emitter thickness from 200 to 50 nm resulted in increased  $J_{sc}$ , enabling a device with  $J_{sc} \approx 8.2$  mA/cm<sup>2</sup> and  $V_{oc} \approx 1.3$  V.

With the emergence of IMM cells in the late '00s, Steiner *et al.* compared MOCVD-grown GaInP single-junction solar cells grown inverted *vs.* upright.<sup>153</sup> By growing inverted, the contact layer, WL, and emitter essentially undergo an anneal during the growth of the thick base layer (and ultimately the additional junctions) that those layers do not experience during an upright growth. The time and temperature can increase dopant diffusion from the highly doped layers (emitter/window/contact) into the lower-doped base layer, causing both an increased contact resistance as well as a shift of the junction depth, which the authors confirmed through SIMS measurements of identical solar cell structures with opposite growth directions. While the structures were identical, the authors noted that they have two different growth processes and doping levels depending on the growth direction, though no specific growth process differences were provided.

In the early 2010s, Suzhou Institute of Nano-tech and Nanobionics and Sony investigated GaInP solar cells lattice-matched to GaAs grown by solid-source MBE.<sup>154,155</sup> One factor motivating the investigation of MBE-grown GaInP was the emergence of high- $J_{sc}$  1.0 eV InGaAsN (exclusively grown by MBE) junctions to serve as the bottom cell in a 1.9 eV/1.4 eV/1.0 eV 3J cell. MOCVD-grown GaInP solar cells had historically been more efficient than their MBE counterparts, and the reason had been attributed to a higher density of defect states due to the lower growth temperature (~470 °C vs ~700 °C), as well as the still-maturing nature of phosphide MBE. Using conventional MBE growth conditions, the authors obtained a  $E_g = 1.875$  eV GaInP solar cell with  $V_{oc} = 1.37$  V ( $W_{oc} = 0.505$  V),  $J_{sc} = 13.5$  mA/cm<sup>2</sup> and FF = 0.88 ( $\eta = 16.4\%$ ).<sup>154</sup> While the low growth temperature may impact the material quality of MBE-grown GaInP, it can be balanced by the clean ultrahigh vacuum environment, which decreases the background carrier density, enabling high-quality solar cell growth even at low  $T_{sub}$ . The same group then explored the effect of  $T_{sub}$  and found that growing at 512 °C *vs* 487 °C led to improvements across all solar cell figures of merit (see Table V).<sup>155</sup> When growing In-containing materials at such high temperatures, it is important to note that the In sticking coefficient may drop below 1, requiring special attention to composition calibration and  $T_{sub}$  variations during growth (as the In composition will become dependent on  $T_{sub}$  in this case).

In 2013, a significant breakthrough in lattice-matched GaInP once again came from NREL.<sup>32</sup> Geisz *et al.* integrated photon recycling<sup>36,156</sup> into their GaInP solar cells lattice-matched to GaAs, resulting in a boost to  $V_{oc}$  and a record-breaking  $\eta = 20.8\%$ . This work compared a traditional FJ single-junction solar cell structure with a RHJ design where a much thinner depletion region is placed deep into the cell by using a low-doped, thick (1 μm) n-type emitter on a wider-bandgap BSF. Recall from Sec. I that the RHJ design improves photon recycling. To investigate this, Geisz *et al.* placed the depletion region

into the AlGaInP BSF at the rear of the solar cell. They then varied the amount of back-side reflection; cells were grown either upright (where the GaAs substrate absorbs all of the emitted photons that enter it, thereby providing poor back reflectance) or inverted with varying thickness of an absorbing Al<sub>0.2</sub>Ga<sub>0.8</sub>As contact layer between the cell and a back reflector. They found that  $V_{oc}$  increased with increasing back reflectance due to strong photon recycling, resulting in longer carrier lifetime and reduced  $J_{02}$  from the RHJ design. This led to an extremely low  $W_{oc}$  of 0.35 V, and AM1.5G measurements revealed  $V_{oc} = 1.455$  V,  $J_{sc} = 16.0$  mA/cm<sup>2</sup>, FF = 0.893, resulting in  $\eta = 20.8\%$ . Recent solar cell efficiency tables show that NREL has further achieved a RHJ GaInP single-junction cell with tensile-strained AlInP with  $\eta = 22\%$  (AM1.5G).<sup>157</sup>

In 2020, Hinojosa *et al.* at Universidad Politécnica de Madrid investigated the feasibility of doping the thick emitter of a GaInP RHJ device solely using the Te memory effect.<sup>158</sup> This memory effect is the phenomenon of Te continuing to incorporate even after the Te flow has been turned off in MOCVD. In this case, the device was grown inverted (recall from Steiner *et al.*<sup>153</sup> that care must be taken when growing inverted), and the top GaAs contact layer was heavily doped with Te. The Te memory effect was then used to n-dope the thick emitter. The Te pulls double duty as it also acts as a surfactant that disorders the GaInP, widening the device's bandgap and increasing the  $V_{oc}$ . To enable comparison with more conventional GaInP solar cells, the authors also grew a Si-doped RHJ and a Si-doped FJ. Table VI compares the results from these devices. The benefit of switching to a RHJ design is immediately apparent when comparing the Si-doped FJ with the Si-doped RHJ.  $W_{oc}$  decreased from 0.539 to 0.448 V with minimal impact on  $J_{sc}$ , suggesting that the minority carrier diffusion lengths are longer than the 850 nm thick emitter. When switching the RHJ emitter dopant from Si to Te, the  $E_g$  increased as expected from the now disordered GaInP, and the  $V_{oc}$  for this device was the highest observed in this work at 1.418 V. However, the increase in  $V_{oc}$  was not commensurate with the increased  $E_g$  and led to a slight rise in  $W_{oc}$  in the Te-doped case. Although the Te-doped RHJ did not outperform the Si-doped device, it did show that using the Te memory effect in MOCVD is a feasible pathway to obtain high-performance solar cells while increasing the  $E_g$  in CuPt-ordered GaInP.

In the 2010s, HVPE (discussed in depth in Sec. IC) reemerged as a technique for the growth of high- $\eta$  III-V solar cells with the potential for greatly reduced cost due to a combination of high growth rate, lower-cost precursors, and high precursor utilization.<sup>55,159</sup> Although HVPE is an old technique, the first 1.9 eV GaInP solar cells grown by HVPE were reported in 2017 by Schulte *et al.* at NREL.<sup>160</sup> At the time, Al-containing films grown by HVPE were not widely available, so the authors were limited to an  $\eta$  of just 12.8% due to the lack of wide-bandgap passivation layers. By 2018, the NREL team had boosted  $\eta$  to 15.2% by eliminating Fe-related contamination from their HVPE

**TABLE VI.** Comparison of RHJ vs FJ design and Si vs Te emitter doping in MOCVD-grown GaInP solar cells from Ref. 158.

TABLE V. MBE-grown GaInP FJ solar cell figures of merit as a function of $T_{sub}$ . <sup>155</sup>				
$T_{sub}$ (°C)	$V_{oc}$ (V)	$J_{sc}$ (mA/cm <sup>2</sup> )	FF	$\eta$ (%)
487	1.271	12.2	0.80	12.4
512	1.377	13.6	0.88	16.6

Design	$E_g$ (eV)	$V_{oc}$ (V)	$W_{oc}$ (V)	$J_{sc}$ (mA/cm <sup>2</sup> )
Si emitter doping, FJ	1.838	1.313	0.539	14.98
Si emitter doping, RHJ	1.841	1.404	0.448	14.63
Te emitter doping RHJ	1.873	1.418	0.460	13.66

reactor, attaining a remarkable  $V_{oc}$  of 1.41 V ( $W_{oc} = 0.47$  V) despite the lack of any surface passivation.<sup>161</sup> The next major advance for HVPE was the development of Al-containing layers using  $AlCl_3$  as a precursor gas.<sup>162,163</sup> Despite the high  $V_{oc}$  that was possible with excellent bulk material quality, the attainment of high QE still required  $AlInP$  window layers. The current 2J  $GaInP/GaAs$   $\eta$  record for HVPE stands at 28.3%,<sup>6</sup> while the single-junction  $GaInP$  record is 17.3%.<sup>164</sup>

While incorporating a RHJ design and photon recycling has led to significant improvements to single-junction devices, it becomes less impactful in a multi-junction scheme where a back reflector cannot be incorporated. As such, it is important to continue to find avenues for improvement to FJ  $GaInP$  solar cells. This led France *et al.* at NREL to explore the effect of post-growth annealing on  $GaInP$  solar cell performance.<sup>165</sup> The authors found that simply annealing for 30 min at 620 °C or 725 °C (by growing an additional  $\mu m$  of  $GaAs$  at the end of the growth) led to an increase in  $W_{oc}$  from 0.484 to >0.500 V. However, inserting an  $AlGaAs:C/GaAs:Se$  TJ between the device and the  $GaAs$  annealing layer improved performance, causing both improved QE and reduction of  $W_{oc}$  to 0.405 V. This TJ acted as a defect injection layer and also reduced the CuPt ordering, increasing the  $E_g$ . The authors speculate that the introduction of defects from the TJ effectively complements or neutralizes the Zn-related defects native to the p-doped  $GaInP$  base layer. For example, a group-III vacancy and a group-III interstitial could potentially passivate each other. By adding the defect injection layer and post-growth anneal, the authors attained a FJ  $GaInP$  solar cell with  $\eta = 19.8\%$  without a back reflector.

In 2022, Sun *et al.* at the University of Illinois published the first study on  $GaInP$  RHJ cells grown by MBE.<sup>35</sup> Sun observed strong improvements in the TRPL lifetime of both n- and p-type double heterostructures with RTA. However, for n- $GaInP$  with  $n_o \geq 2 \times 10^{18} \text{ cm}^{-3}$ , PL intensity and lifetime were sharply degraded by RTA. By understanding the combined effects of doping and RTA on optical quality, as well as delta doping in the window for improved surface passivation, Sun achieved  $W_{oc}$  values of 0.494 and 0.442 V in FJ and RHJ devices, respectively, the best values for MBE-grown  $GaInP$  and comparable to MOCVD-grown cells on absorbing substrates. Following up on this work, Li *et al.* showed that n- $GaInP$  double heterostructures grown on  $GaAs/Si$  by MBE could attain TRPL lifetimes as high as 11.7 ns despite a TDD of  $9.4 \times 10^6 \text{ cm}^{-2}$ , the highest value for any III-V material on Si; for comparison, n- $GaInP$  double heterostructures grown lattice-matched on  $GaAs$  exhibited TRPL lifetimes of 14.6 ns.<sup>166</sup> Taking advantage of the apparent defect tolerance of n- $GaInP$ , they went on to demonstrate  $GaInP$  RHJ cells with  $V_{oc}$  values of 1.29 and 1.22 V with corresponding TDDs of  $1.0 \times 10^7 \text{ cm}^{-2}$  and  $2.7 \times 10^8 \text{ cm}^{-2}$ , respectively. While further work is still needed to demonstrate  $GaInP$  RHJ cells on Si with high  $J_{sc}$ , the prospect of high- $\eta$  cells despite high TDD warrants further investigation to aid in the quest for low-cost substrate technology.

At the time of writing, the highest- $\eta$  2J III-V solar cells still rely on  $GaInP/GaAs$  technology, superficially resembling cells from 28 years ago. The increase to 32.8% ( $V_{oc} = 2.568$  V,  $J_{sc} = 14.56 \text{ mA/cm}^2$ ,  $FF = 0.877$ ),<sup>21</sup> was primarily achieved through increased  $V_{oc}$ . While a detailed comparison of NREL's 1994 cell with the current record cell is not possible due to limited published details from LG Electronics, we speculate that much of the  $\eta$  boost can be attributed to thin film cell processing with a backside mirror for improved photon recycling. Therefore, despite various complexities (e.g., sensitivity to mismatch

strain and oxygen,  $E_g$  dependence on ordering and substrate offcut, and pyrophoric residual deposits, etc.), by the early 1990s,  $GaInP$  was already established as the gold-standard absorber material for  $E_g = 1.8\text{--}1.9$  eV. In late 2020, a new 2J record of  $\eta = 32.9\%$  was achieved by NREL.<sup>83</sup> They achieved this through the same  $GaInP/GaAs$  baseline structure but incorporated strain-balanced  $GaAsP/GaInAs$  multiple quantum wells into the  $GaAs$  bottom cell to improve current matching.

Despite its maturity, our review shows that the growth of 1.8–1.9 eV  $GaInP$  solar cells with high performance is challenging due to the effects of ordering and annealing, along with inherently low minority hole mobility. However, researchers over time have proven that MOCVD, MBE, and HVPE are all capable of growing cells with similar  $V_{oc}$  and FF values ( $J_{sc}$  and  $\eta$  values depend sensitively on junction thickness and antireflection coatings), implying similar dark current and trap densities among the three techniques. The ability to grow high-quality material using any method is notable considering the widely disparate growth temperature in MBE vs MOCVD, the low V/III ratio and high growth rate of HVPE, and the wide differences in source materials/chemistry (Table VII). We nevertheless anticipate that MOCVD will remain the commercial growth method of choice in the near future due to its relative maturity and well-developed equipment ecosystem.

## B. Al-rich $Al_xGa_{1-x}As$ ( $x \approx 0.25\text{--}0.40$ )

$Al_xGa_{1-x}As$  was an obvious initial choice for the top cell of a 3J device as it possesses the desired  $E_g$  and is nearly lattice-matched to  $GaAs$  and Ge substrates over its entire composition range. Continuing from Sec. II B, we now investigate results for Al-rich  $Al_xGa_{1-x}As$  solar cells with  $E_g \approx 1.8\text{--}1.9$  eV ( $x \approx 0.25\text{--}0.40$ ).

Initial work on higher-Al content  $Al_xGa_{1-x}As$  ( $x > 0.25$ ) solar cells began in the 1980s.<sup>92,141,167\text{--}169</sup> LaRue *et al.* developed an  $Al_{0.32}Ga_{0.68}As/GaAs$  (1.82 eV/1.42 eV) 2J solar cell by MOCVD using a metal “groove” interconnect instead of a TJ.<sup>168,170</sup> The  $x = 0.32$  composition was chosen as the highest- $E_g$  material attainable with high QE (decreasing QE occurs for  $E_g > 1.82$  eV due to the direct-indirect transition around 1.92 eV). Given the non-ideal  $E_g$  combination in this tandem design, the authors used an optically thin (1.2  $\mu m$ )  $AlGaAs$  top cell to provide current matching in the ultimate 2J device. This technique led to AM1.5G 2J results of  $V_{oc} = 2.1$  V,  $J_{sc} = 12.0 \text{ mA/cm}^2$ ,  $FF = 0.63$ ,  $\eta = 15.7\%$ . Subsequently, the first  $Al_{0.4}Ga_{0.6}As/GaAs$  2J solar cell to exceed 20% efficiency ( $V_{oc} = 2.1$  V,  $J_{sc} = 13.8 \text{ mA/cm}^2$ ,  $FF = 0.70$ ,  $\eta = 20.2\%$ ) was demonstrated by Amano *et al.* at NTT Electrical Communications Laboratories in 1987 via MBE.<sup>171</sup>

**TABLE VII.** Best-reported  $V_{oc}$ ,  $W_{oc}$ , and FF values of lattice-matched  $GaInP$  cells on  $GaAs$  substrates (except where noted) for different growth methods.

Growth method	Design	$V_{oc}$ (V)	$W_{oc}$ (V)	FF
HVPE <sup>164</sup>	RHJ	1.431	Not reported	0.863
MBE <sup>35</sup>	FJ	1.401	0.49	0.863
	RHJ	1.420	0.44	0.847
MOCVD <sup>32</sup>	FJ	1.406	0.44	0.883
	RHJ	1.413	0.43	0.881
MOCVD <sup>157</sup>	RHJ thin film	1.4695	Not reported	0.902

Chung *et al.* then developed the first  $\sim 1.9$  eV  $\text{Al}_{0.37}\text{Ga}_{0.63}\text{As}$  single-junction devices with  $\eta \approx 15\%$  grown by MOCVD.<sup>167</sup> Their device design employed an n-on-p structure with a linear doping gradient through the base and a combination of a uniform and graded doping in the emitter to improve minority carrier collection efficiency. The cells were AR-coated and measured under AM1.5G, yielding  $\eta = 14.9\%$ , with  $V_{oc} = 1.42$  V,  $J_{sc} = 12.04$  mA/cm<sup>2</sup>, and FF = 0.87. A year later, the same group cascaded this cell with a GaAs bottom cell.<sup>141</sup> The 2J device employed a “prismatic cover glass” to reduce obscuration from grid fingers as well as a three-terminal configuration to enable independent measurement of both subcells. Independently measuring the top  $\text{Al}_{0.37}\text{Ga}_{0.63}\text{As}$  cell revealed improved  $\eta$  to 16% due to an increased  $J_{sc}$ , likely from the addition of the cover glass. Cascading this cell with a GaAs bottom cell in a 2-terminal configuration resulted in the highest- $\eta$  2J device at the time:  $V_{oc} = 2.4$  V,  $J_{sc} = 13.78$  mA/cm<sup>2</sup>, FF = 0.84,  $\eta = 27.6\%$ .

Around the same time, Amano *et al.* studied the effect of O-incorporation on high Al content  $\text{Al}_x\text{Ga}_{1-x}\text{As}$  solar cells grown by MBE.<sup>92</sup> SIMS revealed  $[\text{O}] \sim 10^{18}$  cm<sup>-3</sup> in  $\text{Al}_{0.4}\text{Ga}_{0.6}\text{As}$  layers compared with Al-free GaAs layers with  $< 8 \times 10^{16}$  cm<sup>-3</sup>. To evaluate the effect of [O], the authors grew two cells: 1 under “clean” conditions and the other under “not very clean” conditions. Clean conditions yielded  $\text{Al}_{0.4}\text{Ga}_{0.6}\text{As}$  layers with a 5× reduction in [O] compared with those grown under not very clean conditions. Furthermore, the authors found that [O] had a clear effect on solar cell properties as outlined in Table VIII. Increasing [O] from 0.7 to  $1.4 \times 10^{18}$  cm<sup>-3</sup> led to a decrease in  $J_{sc}$  from 6.0 to 4.4 mA/cm<sup>2</sup> due to a decrease in minority carrier diffusion length but had little effect on FF. Further increasing [O] to  $1.9 \times 10^{18}$  cm<sup>-3</sup> led to a severe degradation of FF to 0.25, resulting in  $\eta < 1\%$ . To investigate the reduction in [O] required to obtain high- $\eta$  AlGaAs devices, the authors grew lower-Al content  $\text{Al}_{0.2}\text{Ga}_{0.8}\text{As}$  cells. They obtained  $\eta = 12.9\%$  for  $\text{Al}_{0.2}\text{Ga}_{0.8}\text{As}$  cells with  $[\text{O}] \sim 10^{17}$  cm<sup>-3</sup> compared with  $\eta = 17.1\%$  for GaAs cells with  $[\text{O}] < 8 \times 10^{16}$  cm<sup>-3</sup>, suggesting [O] must be reduced below  $10^{17}$  cm<sup>-3</sup> for high- $\eta$  Al-containing devices.

More recently,  $\text{Al}_x\text{Ga}_{1-x}\text{As}$  has been reexamined for its potential to replace GaInP in conventional device designs to cut costs and address scarcity issues related to In. As noted in Sec. II B, Heckelmann *et al.* investigated the effect of improved TMAI purity on Al-containing solar cells grown by MOCVD; cells with  $x = 0.27$  and 0.37 are well suited for the top cell in a 3J device and are thus described here in more detail.<sup>91,93</sup> These cells continue the trend of increasing  $W_{oc}$  with increasing  $x$  (see Table IX). To address the degrading short-wavelength IQE with increasing Al content, the authors replaced the Te-doped n- $\text{Al}_{0.37}\text{Ga}_{0.63}\text{As}$  emitter with Si-doped n-GaInP, enabling a recovery of the short-wavelength IQE and a decrease in  $W_{oc}$  by 19 mV. The device improvement from replacing only the emitter suggests that some of the degradation with increasing Al content is due to

**TABLE VIII.**  $\text{Al}_{0.4}\text{Ga}_{0.6}\text{As}$  solar cell figures of merit as a function of [O] from Ref. 92.

[O] ( $\times 10^{18}$ cm <sup>-3</sup> )	$V_{oc}$ (V)	$J_{sc}$ (mA/cm <sup>2</sup> )	$\eta$ (%)
0.7	1.22	6.0	4.6
1.4	1.17	4.4	3.3
1.9	...	...	<1

**TABLE IX.**  $\text{Al}_x\text{Ga}_{1-x}\text{As}$  solar cell figures of merit as a function of Al content, x.<sup>91</sup>

Al content, x	$E_g$ (eV)	$V_{oc}$ (V)	$J_{sc}$ (mA/cm <sup>2</sup> )	FF	$W_{oc}$ (V)
0.27	1.78	1.336	13.7	0.868	0.444
0.37	1.92	1.393	10.4	0.858	0.527
0.37 (GaInP emitter)	1.92	1.412	11.7	0.888	0.508

the presence of Te-related DX centers, the energy level of which is located such that it drops below the conduction band minimum as the Al content exceeds 20%. Table IX summarizes the results as a function of Al content.

Heckelmann *et al.* then investigated the effect of Al precursors with low- and high-[O] (described in Sec. II B) and found that increasing to  $x = 0.37$  led to significant EQE degradation from  $\lambda = 500$ –650 nm (>10% absolute near the band edge) when grown with the high-[O] precursor compared with the identical sample grown with the higher-purity TMAI. DLTS of n- $\text{Al}_{0.37}\text{Ga}_{0.63}\text{As}$  revealed two defects associated with a DX center and an EL2 defect, which does not correlate with a crystal impurity. Power-dependent radiative PL on  $x = 0.37$  samples grown with both Al sources showed a shorter Shockley–Read–Hall lifetime for the sample with the more oxygen-contaminated Al source. Increasing Al content also led to a drop in peak IQE, even for the samples grown with the high-purity Al source. Thus, while gradual improvements in TMAI purity enable significantly improved lifetimes and diffusion lengths, the formation of DX centers in n-type  $\text{Al}_x\text{Ga}_{1-x}\text{As}$  remains difficult to mitigate for  $x > 0.3$ .

Despite meaningful improvements in MOCVD system design, precursor purity, and cell design, solar cell performance still decreases with increasing Al content. Even if O could be completely eliminated from AlGaAs, challenges related to DX centers and EL2 defects would likely still remain. Figure 17 plots the data from the three groups detailed above and shows an increase in  $W_{oc}$  with increasing Al content.

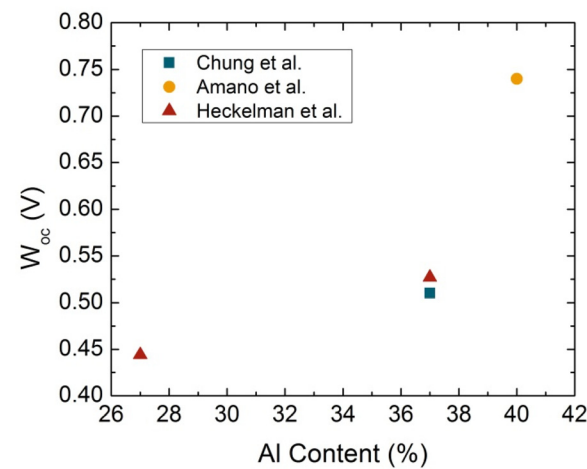


**FIG. 17.**  $W_{oc}$  vs Al content for wide-bandgap AlGaAs solar cells. Increasing Al content results in degraded solar cell performance as seen through an increase in  $W_{oc}$ .

### C. Metamorphic $\text{GaAs}_y\text{P}_{1-y}$ , $y \leq 0.6$

While mostly explored for use as the top junction in a Si-based tandem (Sec. II D),  $\text{GaAs}_y\text{P}_{1-y}$  could also be an option for wider-bandgap applications (i.e., top or second cell in 4+ junction devices) due to its direct bandgap up to  $\sim 2.0$  eV. As such,  $\text{GaAs}_y\text{P}_{1-y}$  solar cells with  $E_g > 1.9$  eV were investigated as early as 1978.<sup>109</sup> As noted in Sec. II D, Barton and Olsen first used material from the mature LED market (grown by HVPE<sup>172</sup>) to demonstrate  $E_g = 1.9$  eV  $\text{GaAs}_{0.60}\text{P}_{0.40}$  solar cells with  $\eta = 5.30\%$  ( $W_{oc} = 1.01$  V) and  $E_g = 2.08$  eV  $\text{GaAs}_{0.35}\text{P}_{0.65}$  solar cells with  $\eta = 1.9\%$  ( $W_{oc} = 1.43$  V).<sup>109</sup> TDD was not reported, though early studies of graded  $\text{GaAs}_y\text{P}_{1-y}$  used in LEDs reported TDD of  $0.1\text{--}4 \times 10^7 \text{ cm}^{-2}$ .<sup>173</sup> Negley *et al.* then developed  $\text{GaAs}_y\text{P}_{1-y}$  on GaP cells by LPE with  $E_g = 1.95$  eV and  $W_{oc} = 1.049$  V.<sup>111</sup> Decades later, the Lee Group at Yale demonstrated  $\text{GaAs}_{0.56}\text{P}_{0.44}$  solar cells on GaP substrates by MBE with  $E_g = 1.92$  eV and  $TDD = 4.0 \times 10^6 \text{ cm}^{-2}$ .<sup>124</sup> They obtained  $W_{oc} = 0.65$  V, a significant improvement over the initial devices from the '70s and '80s. However, lower- $E_g$   $\text{GaAs}_y\text{P}_{1-y}$  cells in the same study exhibited  $W_{oc}$  as low as 0.56 V despite an elevated  $TDD = 6.3 \times 10^6 \text{ cm}^{-2}$ , implying additional defect challenges exist when approaching GaP-like compositions (also observed for MM-GaInP discussed below in Sec. IV B).

### D. Summary and recommendations for future work on 1.8–1.9 eV junctions

While AlGaAs, GaAsP, and GaInP all possess the desired  $E_g$  for 3J devices based on GaAs and Ge substrates, the success of GaInP, along with its high radiation tolerance, has positioned it as the  $E_g \approx 1.9$  eV material of choice. This has led to both 2J and 3J record-breaking/holding devices grown primarily by MOCVD, with some records set by the now-defunct Solar Junction corporation using MBE.<sup>174</sup> Given that GaInP has long been the  $E_g \approx 1.8\text{--}1.9$  eV material of choice for 3J solar cells, it has benefited from significant maturing since its first demonstration in the early 1990s. Further evidence of GaInP's maturity can be seen in demonstrations of high- $\eta$  solar cells by HVPE, MOCVD, and MBE. While thin-film RHJ designs have nearly approached the Shockley–Quiesser limit, the inability to add a rear reflector in a multi-junction design requires further improvement to FJ schemes. Post-growth annealing appears to be an effective way for FJ devices to approach the efficiencies seen in RHJ devices.<sup>165</sup> AlGaAs, on the other hand, has historically been avoided in this  $E_g$  range due to the incorporation of O-related defects. However, the purity of Al source material has improved significantly over the last several decades, potentially enabling high- $\eta$  devices in the future. While MM-GaAsP possesses the appropriate  $E_g$  for the top cell in 3J and 4J devices, the degradation observed with increasing P content and  $E_g$  must be addressed for it to compete with GaInP and AlGaAs. We do not anticipate that any new III-V absorber will significantly outperform lattice-matched GaInP in this  $E_g$  range and recommend further work to understand the coupled effects of doping and annealing on GaInP device performance.

### IV. >1.9 eV JUNCTIONS: TOP CELLS FOR 4J AND BEYOND

As 3J cells matured, researchers moved toward 4–6 junction cell designs to obtain further  $\eta$  gains.<sup>23,51</sup> This increase in subcells invoked a recalculation of the optimum  $E_g$  combination and demonstrated the need for PV junctions with  $E_g$  exceeding 1.9 eV, as illustrated in the

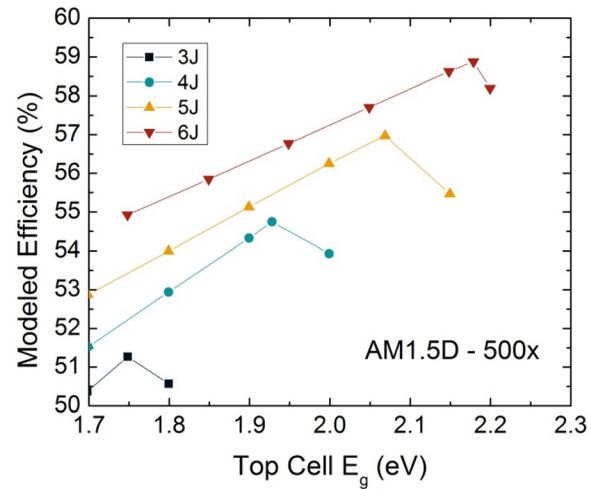


**FIG. 18.** Concentrator  $\eta$  as a function top cell  $E_g$  for devices with 3–6 junctions. Adapted from Ref. 20.

multi-junction  $\eta$  vs top-cell  $E_g$  plot in Fig. 18.<sup>20</sup> In this section, we discuss the most viable wide-bandgap materials that have served or could serve this purpose, specifically targeting AlGaInP (Sec. IV A), MM-GaInP (Sec. IV B), and GaP (Sec. IV C).

#### A. AlGaInP

Quaternary AlGaInP at a lattice constant  $a = 5.65\text{--}5.66 \text{ \AA}$  is a clear candidate for the top junction of a 4+ junction solar cell based on its tunable, direct  $E_g$  of 1.92–2.32 eV (Al content = 0% to 26%) while maintaining lattice-matching with GaAs or Ge. The lattice-matched  $(\text{Al}_x\text{Ga}_{1-x})_{0.51}\text{In}_{0.49}\text{P}$  compositions can be expressed as a ratio of the two ternary endpoints,  $\text{Ga}_{0.49}\text{In}_{0.51}\text{P}$  and  $\text{In}_{0.48}\text{Al}_{0.52}\text{P}$  to give  $(\text{In}_{0.48}\text{Al}_{0.52}\text{P})_x(\text{Ga}_{0.51}\text{In}_{0.49}\text{P})_{1-x}$ , and Fig. 19 plots the conduction

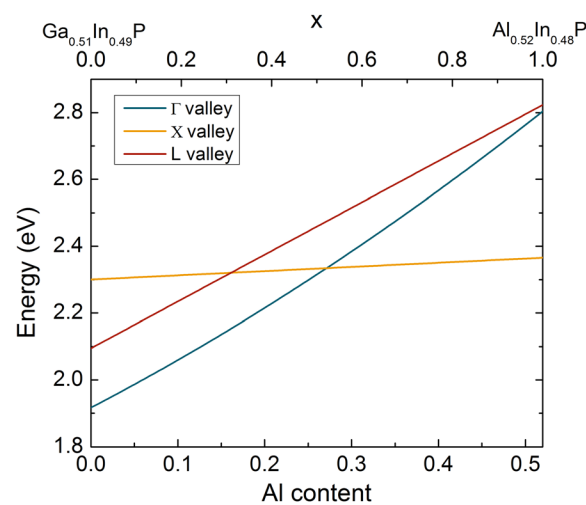


**FIG. 19.** Conduction band edge minima for AlGaInP lattice-matched to GaAs as a function of Al content, represented as  $(\text{Al}_{0.52}\text{In}_{0.48}\text{P})_x(\text{Ga}_{0.51}\text{In}_{0.49}\text{P})_{1-x}$  (top x-axis).

band valleys as a function of Al content ( $x$  on top x-axis) for AlGaInP lattice-matched to GaAs. While the lattice-matching and direct-bandgap range are attractive, the Al content poses a concern due to the propensity for Al to incorporate O-related defects<sup>175,176</sup> which have been shown to reduce solar cell  $\eta$  as in AlGaAs (Secs. II B and III B).<sup>90,92</sup>

AlGaInP was first explored for space PV applications in the early 2000s with wide-bandgap solar cells demonstrated in 2003.<sup>177</sup> Agui *et al.* at Sharp Corporation investigated MOCVD growth of  $E_g = 2.04$  eV and  $E_g = 1.96$  eV AlGaInP cells at substrate temperatures of 700–750 °C with Al contents of 0.14 and 0.08, respectively. They first found that increasing the cell thickness improved  $J_{sc}$  for both compositions, implying at least 2 μm thickness is required to obtain optically thick devices. Unfortunately,  $W_{oc}$  was found to increase with increasing Al content from 0.47 V for Al = 0.08 ( $E_g = 1.96$  eV) to 0.52 V for Al = 0.14 ( $E_g = 2.04$  eV).<sup>177</sup> Morioka *et al.* from Japan Aerospace Exploration Agency and Japan Atomic Energy Agency investigated the effect of base thickness (constant base doping,  $p = 3 \times 10^{16} \text{ cm}^{-3}$ ) and base doping level (constant base thickness = 1 μm) of  $\text{Al}_{0.1}\text{Ga}_{0.5}\text{In}_{0.4}\text{P}$  ( $E_g \approx 2.0$  eV) cells in 2006. The emitter thickness and doping were kept constant at 30 nm and  $n = 2 \times 10^{18} \text{ cm}^{-3}$ , respectively.<sup>178</sup> Similar to Ref. 177, they found that increasing base thickness led to increased  $J_{sc}$  up to 1.2 μm, suggesting either a minority carrier diffusion length of at least 1.2 μm or the cell becoming optically thick at this point;  $V_{oc}$  was unaffected by base thickness. When base doping was increased from  $2 \times 10^{16}$  to  $4 \times 10^{17} \text{ cm}^{-3}$ , an increase in  $V_{oc}$  and a decrease in  $J_{sc}$  were observed, presumably due to a narrower depletion region causing decreased  $J_{02}$  along with a decrease in field-assisted current collection, respectively; the base dopant was not noted, though based on the authors' use of MOCVD growth, Zn is the most likely candidate.<sup>178</sup> Soon after, CESI Ricerca explored the effect of Al content on material and device properties by varying the Al content in MOCVD-grown AlGaInP solar cells from 0% to 12%.<sup>179,180</sup> They found that  $J_{sc}$  trended down and  $V_{oc}$  generally trended upward, as expected for increasing  $E_g$ , despite some outliers. By optimizing the structure of the cell with Al = 10% ( $E_g \approx 1.97$  eV according to PL measurements performed in this work), the authors obtained a device with  $\eta = 13.6\%$  ( $V_{oc} = 1.436$  V,  $W_{oc} = 0.534$  V,  $J_{sc} = 15 \text{ mA/cm}^2$ , FF = 0.85), though the specific optimizations were not reported.

As 3J devices matured in the 2010s, the motivation for absorber materials with  $E_g > 2.0$  eV strengthened with increased demand for 4+ junction cells. For instance, Emcore developed a 2.05 eV AlGaInP cell for use as the top cell in 5–6 junction IMM applications.<sup>181</sup> They used a heterojunction design with a 1.9 eV GaInP emitter, resulting in the desired  $J_{sc} = 13.4 \text{ mA/cm}^2$  for 5-junction applications. However,  $V_{oc}$  only increased by 43 mV (as opposed to the expected 150 mV) compared with a 1.9 eV GaInP homojunction device. By switching to a homojunction AlGaInP cell with lower emitter doping and a wider-bandgap BSF, the authors obtained average AM0 results of  $V_{oc} = 1.537$  V ( $W_{oc} = 0.513$  V),  $J_{sc} = 11.8 \text{ mA/cm}^2$ , FF = 0.876, and  $\eta = 11.8\%$ .<sup>181</sup> The sensitivity of MOCVD-grown AlGaInP to n-type doping concentration seen by Cornfeld *et al.* partly foreshadowed Sun's observations of degradation in MBE-grown n-GaInP with  $n \geq 2 \times 10^{18} \text{ cm}^{-3}$  after RTA.<sup>35</sup> Interestingly, an RHJ top cell design consisting of an n-GaInP emitter on a p-AlGaInP base was explored by Steiner *et al.* as a way to maintain low emitter sheet resistance in CPV cells owing to the higher electron mobility in GaInP.<sup>29</sup>

Masuda *et al.* at Yale University investigated 2.0 eV AlGaInP solar cell performance as a function of substrate offcut and emitter thickness using MBE.<sup>182</sup> They found the O incorporation to be independent of offcut angle and that the only observed effect of increased substrate offcut was increased  $E_g$  (due to reduced CuPt ordering) along with a proportional increase in  $V_{oc}$ . To investigate the effect of emitter thickness, the authors removed the WL and performed sequential timed etches, measuring cell performance at each new thickness. Thinning the emitter from 100 to 40 nm resulted in increased  $J_{sc}$  via significant improvement in short wavelength EQE by bringing the depletion region closer to the front surface. Performing the same experiment on a  $E_g = 1.9$  eV GaInP cell lattice-matched to GaAs yielded a lower degree of  $J_{sc}$  improvement. Given the expected high front surface recombination velocity (due to the lack of a WL), the authors concluded that the minority carrier diffusion length in the emitter of the AlGaInP cell is shorter than that of the GaInP cell and  $< 100$  nm.<sup>182</sup> Based on the short minority carrier diffusion length in the AlGaInP emitter, the same group later focused on introducing a drift field near the front surface by adding a graded composition layer between the window and emitter layers.<sup>183</sup> This technique led to a  $2.5 \times$  increase in  $L_p$  while also enabling the removal of growth interrupts, resulting in improved IQE over all wavelengths and improved interfaces, respectively. The authors also explored the effect of MBE growth conditions, finding that  $T_{sub} = 490$  °C led to improved  $L_n$ , IQE, and  $V_{oc}$  while varying V/III and growth rate had little effect. They then altered the device design by reducing the emitter/grade thickness to 70 nm while increasing the base thickness to 1.5 μm to increase short wavelength collection and reduce transmission losses, respectively. These optimizations enabled improvements to both  $V_{oc}$  and IQE across all wavelengths. Finally, adding a post-growth anneal led to increases in  $J_{sc}$  and  $V_{oc}$ , and at the highest anneal temperature of 740 °C achieved  $W_{oc} = 0.52$  V,  $J_{sc} = 9.0 \text{ mA/cm}^2$ , and FF ≈ 0.85. In a subsequent study, Sun *et al.* switched from annealing within the MBE chamber to RTA and showed similar material improvements using short times and higher temperatures (e.g., 800–820 °C for 30 s–5 min). IQE of annealed (solid lines) and un-annealed (dashed lines) AlGaInP solar cells with  $E_g = 2.19$ –2.02 eV [Fig. 20(a)] reveal the improvement that can be attained with post-growth RTA. In addition, they systematically studied cells with  $E_g = 2.0$ –2.2 eV, showing strong degradation in  $W_{oc}$ , peak IQE, and FF as  $E_g$  increased.<sup>30</sup> Overall, the best RTA'd cell (without ARC) had  $E_g = 2.02$  eV,  $W_{oc} = 0.534$  V,  $J_{sc} = 8.46 \text{ mA/cm}^2$ , and FF = 0.87 [Fig. 20(b)].

Perl *et al.* at NREL then developed MOCVD-grown 2.0 eV AlGaInP solar cells, first investigating the growth conditions such as  $T_{sub}$  and dopant species.<sup>184</sup> Changing the emitter doping from Si to Se yielded increased IQE over all wavelengths (Fig. 21) accompanied by increased  $V_{oc}$ , though the mechanism was not clarified. Although not directly reported, we assume that Cornfeld *et al.* used Si as the n-type dopant in their earlier work, implying that multiple groups have observed challenges with material quality in Si-doped n-AlGaInP. Perl *et al.* then found that increasing  $T_{sub}$  to 780 °C improved cell performance, but further increases to  $T_{sub}$  resulted in degradation;  $E_g$  also increased with increasing  $T_{sub}$ , potentially due to decreased CuPt ordering or indium desorption. With  $T_{sub} = 780$  °C, the authors obtained an AlGaInP cell with  $E_g = 2.01$  eV,  $V_{oc} = 1.59$  V,  $W_{oc} = 0.42$  V,  $J_{sc} = 10.6 \text{ mA/cm}^2$ , and FF = 0.88, yielding AM1.5D  $\eta = 14.8\%$  (the highest  $\eta$  for a ~2.0 eV solar cell). Building on this work, the same

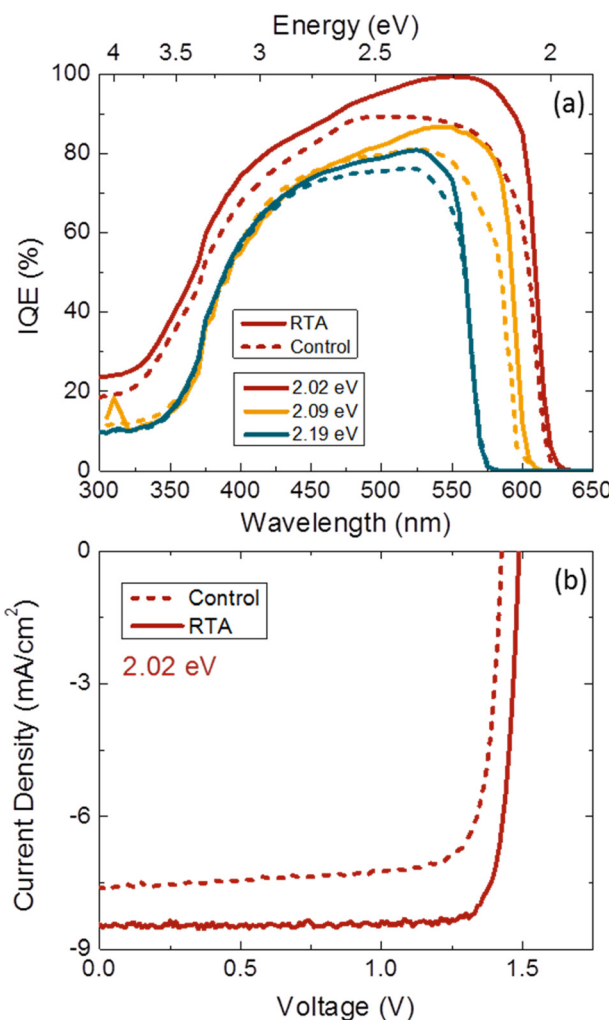


**FIG. 20.** MBE-grown AlGaNp solar cells. (a) IQE of 2.02–2.19 eV AlGaNp solar cells before (dashed) and after RTA (solid) showing that improvement in 2.09 and 2.19 eV cells is not as strong as in 2.02 eV cells, and (b) LIV of highest-performing cell after RTA before and after anneal ( $E_g = 2.02$  eV).<sup>30</sup> Adapted from Ref. 30.

group investigated additional growth conditions such as V/III and growth rate.<sup>69</sup> Increasing V/III improved short wavelength IQE, resulting from an increased minority carrier diffusion length in the n-type emitter (either due to reduced O-related defects or reduced emitter doping). Increasing the growth rate up to  $4\text{ }\mu\text{m/h}$  also resulted in improved IQE and  $V_{oc}$ , but increasing further to  $6\text{ }\mu\text{m/h}$  showed no change in IQE. However, they did observe a small change in  $V_{oc}$ , consistent with reduced O-related defects. Increasing the base thickness beyond the optical thickness had little effect on IQE, indicating a long diffusion length in the p-type base. Increasing the emitter thickness, on the other hand, decreased short wavelength IQE (also observed by Masuda *et al.*<sup>182</sup> described above). To counteract the short diffusion length in n-AlGaNp, they investigated the effect of doping concentration in the emitter, finding that decreasing from  $10^{18}$  to  $10^{17}\text{ cm}^{-3}$  resulted in consistent improvement to IQE. However, the minority

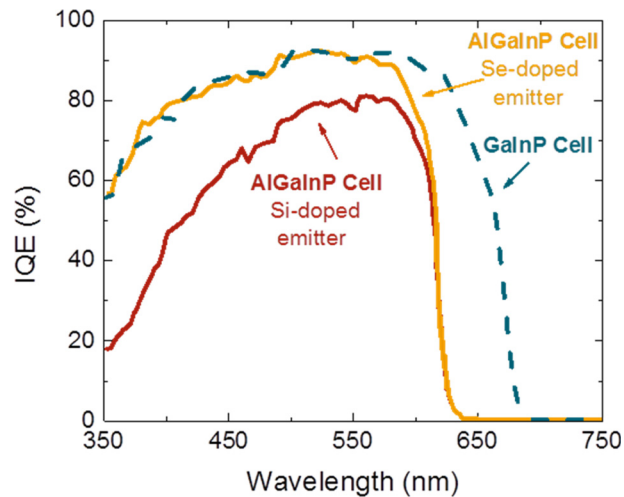


**FIG. 21.** IQE of AlGaNp solar cells grown by MOCVD using different n-type doping species. Switching from Si to Se led to significant improvement in IQE across all wavelengths.<sup>184</sup> Adapted from Ref. 184.

carrier diffusion length in the n-type emitter remained too short to employ a thick emitter and/or RHJ cell design. These results clearly indicate a significant difference in collection efficiency between n- and p-type AlGaNp. Finally, they varied the Al composition from 0% to 24% ( $E_g = 1.90$  to  $2.17$  eV). As shown in Fig. 22(a), increasing the Al content from 0% to 18% caused the peak IQE to drop by <8%, consistent with increased O-related defects and reduced effectiveness of heterojunction barriers as Al content of the cell increased. Increasing all the way to 24% Al, however, results in a much larger drop to peak IQE, potentially resulting from the direct-to-indirect crossover. Figure 22(b) shows the impact of increasing Al content on LIV ( $E_g = 1.90$ – $2.17$  eV). It is clear that the  $V_{oc}$  does not increase proportionally with the  $E_g$  beyond Al = 12%, likely due to the impact of increased O-contamination with increased Al content.

Wanlass *et al.* at NREL worked toward integrating a 1.95 eV AlGaNp cell into a 4J IMM device.<sup>185</sup> They began by optimizing upright n-on-p 1.95 eV AlGaNp single-junction solar cells. The IQE of these optimized cells peaked at 100% near the band edge and then dropped to 80% at shorter wavelengths. The high long-wavelength IQE implied that electron-hole-pairs generated deep in the cell ( $4\text{ }\mu\text{m}$  base) are collected, again suggesting a very long minority carrier diffusion length in the p-base. However, the IQE drop at shorter wavelengths may indicate losses resulting from a high density of O-related defects in the high Al content AlInP WL. The authors suggest that future improvements to short-wavelength IQE could be possible by thinning and reducing O-contamination in the WL. These single-junction cells achieved AM1.5D  $\eta = 16.7\%$ , with  $V_{oc} = 1.467$  V,  $W_{oc} = 0.483$  V,  $J_{sc} = 13.12\text{ mA/cm}^2$ , and  $FF = 0.865$ . Taking a step toward the full 4J IMM, they first integrated the 1.95 eV AlGaNp cell with a 1.55 eV AlGaAs cell, providing a 2J device. They obtained  $V_{oc} = 2.765$  V,  $J_{sc} = 14.15\text{ mA/cm}^2$ , and  $FF = 0.895$  under  $107\times$  concentration—showing promise for the full 4J structure.

These results prove that AlGaNp lattice-matched to GaAs can serve as a high-performance, wide-bandgap absorber in 4–6 junction

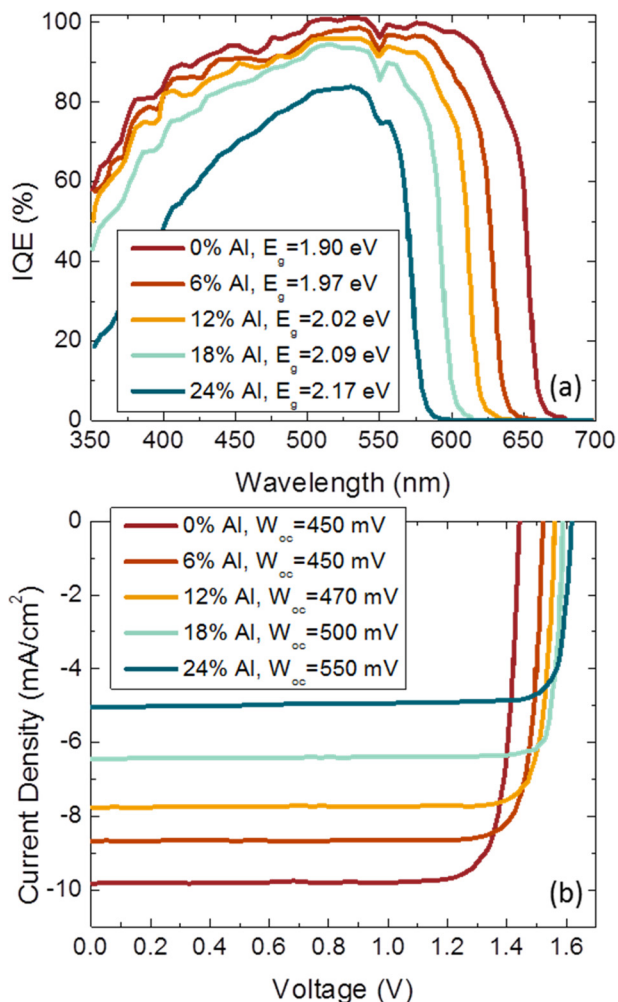


**FIG. 22.** (a) IQE and (b) LIV of MOCVD-grown AlGaInP solar cells showing excellent performance for  $E_g$  up to 2.02 eV.<sup>69</sup> Adapted from Ref. 69.

devices. Despite significant advances, the performance of AlGaInP cells remains limited by O-incorporation, leading to high  $W_{oc}$  and short minority carrier diffusion lengths in the n-type emitter. Some successful tactics to overcome these limitations included:

- Increasing the Al content ( $E_g$ ) to 6%–12% (1.97–2.02 eV) incurs only modest performance penalties, while higher Al content leads to steeper performance penalties.<sup>30,69</sup>

**TABLE X.** Comparison of AlGaInP solar cells grown by various methods.

Growth method	Al content (%)	$T_{sub}$ (°C)	Post-growth anneal	$E_g$ (eV)	$V_{oc}$ (V)	$W_{oc}$ (V)
MOCVD <sup>69</sup>	12	780	N/A	2.02	1.56	0.47
	18	780	N/A	2.09	1.59	0.50
MBE <sup>183</sup>	8	490	740 °C, 5'	2.02	1.50	0.52
MBE <sup>30</sup>	16	480	820 °C, 5'	2.09	1.51	0.59

- Thinning the emitter from 100 nm to 10s of nm improved short wavelength collection.<sup>69,182</sup>
- Introducing a graded-composition layer between the emitter and WL to provide a drift field near the surface of the device improved short wavelength collection.<sup>183</sup>
- Reducing the emitter doping level from  $10^{18}$  to  $10^{17} \text{ cm}^{-3}$  increased IQE overall.<sup>69</sup>
- In MBE, post-growth annealing improved minority carrier diffusion length in the p-base, leading to improved IQE and  $V_{oc}$ .<sup>183</sup>
- In MOCVD,<sup>69,184</sup>
  - Switching the n-type emitter dopant from Si to Se increased IQE over all wavelengths and increased  $V_{oc}$ .
  - Increasing growth rate up to 4  $\mu\text{m}/\text{h}$  increased IQE and  $V_{oc}$ .
  - Increasing V/III increased short wavelength IQE.
  - Increasing  $T_{sub}$  up to 780 °C improved cell performance overall as well as increased  $E_g$  likely due to reduced CuPt ordering.

In the future, greater understanding of trap formation in n-AlGaInP as a function of n-type doping concentration, doping species, and Al content could simplify cell design and also unlock the potential for wide-bandgap RHJ AlGaInP cells with higher  $V_{oc}$ . Table X summarizes AlGaInP solar cell results grown by both MOCVD and MBE. Note the wide disparity in  $T_{sub}$  values between MOCVD and MBE and the fact that MBE-grown cells can approach the low  $W_{oc}$  values seen in MOCVD-grown cells through the use of post-growth annealing at MOCVD-like growth temperatures. High temperature growth or post-growth annealing appears to be critical to eliminate traps and attain high performance in AlGaInP solar cells, though the atomic nature of the defects remains unclear.

## B. Metamorphic $\text{Ga}_{1-x}\text{In}_x\text{P}$ , $x < 0.5$

To avoid the impact of Al-related O-contamination, MM-Ga<sub>1-x</sub>In<sub>x</sub>P ( $x < 0.5$ , tensile mismatch with GaAs/Ge) has been explored as an alternative top cell material. Increasing the Ga content both increases the  $E_g$  and decreases the lattice constant. As wide-bandgap Ga<sub>1-x</sub>In<sub>x</sub>P is no longer lattice-matched to conventional substrates, mitigation of threading dislocations becomes necessary to obtain high- $\eta$  subcells. Similar to the MM-GaAs<sub>y</sub>P<sub>1-y</sub> described above (Sec. II D), compositional grading is utilized to obtain TDD  $< 10^7 \text{ cm}^{-2}$ . Furthermore, as the desired  $E_g$  possesses lattice constants between GaP and GaAs, either substrate can be employed (Fig. 23).

Steiner *et al.* first published MM-Ga<sub>1-x</sub>In<sub>x</sub>P single-junction solar cells in 2010.<sup>186</sup> These cells were grown by MOCVD on GaAs substrates using GaAs<sub>y</sub>P<sub>1-y</sub> CGBs to obtain devices with  $E_g = 1.98$  (Ga<sub>0.61</sub>In<sub>0.39</sub>P) and 2.07 eV (Ga<sub>0.69</sub>In<sub>0.31</sub>P). Increasing the lattice mismatch from 0.69% to 1.31% caused a TDD increase from  $2 \times 10^6$  to  $8 \times 10^6 \text{ cm}^{-2}$ . Table XI summarizes the results from these devices.

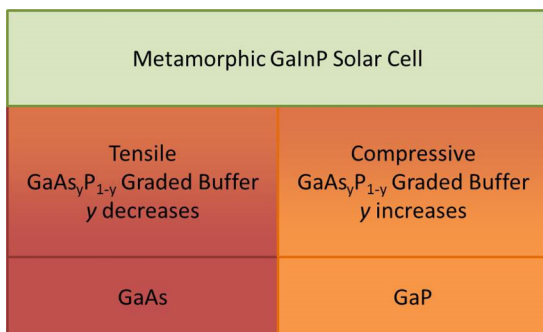


**FIG. 23.** Schematic demonstrating how the same MM-GaInP solar cell could be grown on either GaAs or GaP substrates.

While the  $V_{oc}$  increased with  $E_g$  as expected, the increase was not proportional, likely due to the increased TDD. This increase in  $W_{oc}$  (from 0.48 to 0.52 V) with  $E_g$  signals the first indication that maintaining high  $\eta$  while increasing  $E_g$  is challenging in MM- $Ga_{1-x}In_xP$ .

The Lee Group also explored MBE growth of  $Ga_{1-x}In_xP$  on  $GaAs_yP_{1-y}$  CGBs on GaAs substrates, focusing on the effect of the CGB design on TDD and  $\eta$ .<sup>187–190</sup> They discovered the formation of faceted trenches, deep crack-like grooves that promote non-radiative recombination, for  $\xi$  exceeding  $0.3\% \cdot \mu\text{m}^{-1}$ . However, by maintaining low grading rates ( $\sim 0.2\% \cdot \mu\text{m}^{-1}$ ), the authors sufficiently reduced the density of faceted trenches and maintained  $TDD < 2 \times 10^6 \text{ cm}^{-2}$  for 2.07 eV  $Ga_{0.64}In_{0.36}P$  cells.<sup>188</sup> In doing so, a constant  $W_{oc}$  of 0.58 V was obtained for In content ranging from 0.36–0.49, resulting in  $V_{oc}$  for the widest-bandgap  $Ga_{0.64}In_{0.36}P$  cell nearly comparable to that of AlGaInP cells with similar  $E_g$ .<sup>181</sup>

The same group then transitioned to compressive  $GaAs_yP_{1-y}$  CGBs on GaP (still grown by MBE) to better access wide-bandgap  $Ga_{1-x}In_xP$ , as the mismatch between GaP and  $Ga_{1-x}In_xP$  is lower than that between GaAs and  $Ga_{1-x}In_xP$  for  $x < 0.24$ .<sup>191,192</sup> Additionally, switching to compressive strain allowed for faster grading rates due to the lack of tensile-specific faceted trenches. They attained  $Ga_{1-x}In_xP$  solar cells with  $x = 0.18$ –0.30, resulting in  $E_g \approx 2.1$ –2.2 eV using grading rates of  $\sim 0.4\% \cdot \mu\text{m}^{-1}$  (2× faster than on GaAs). The PL spectra of the solar cells possessed a single peak for  $x$  as low as 0.24, but the spectrum for  $x = 0.18$  revealed two distinct peaks representing direct and indirect transitions and implying a crossover from direct to

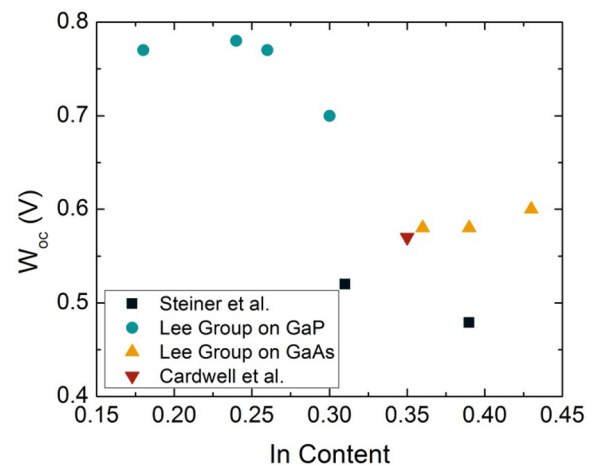


**FIG. 24.**  $W_{oc}$  vs. In content for MM-GaInP solar cells. Decreasing In content leads to degraded solar cell performance.

indirect bandgap near  $x = 0.18$ . Extracted  $E_g$  values from EQE measurements matched well with direct PL emission for all In contents explored in their work.<sup>192</sup> TDD for the devices on GaP substrates was slightly elevated compared to those on GaAs and ranged from  $2.3$ – $7.6 \times 10^6 \text{ cm}^{-2}$ ; the TDD increase trended with increasing mismatch (increasing  $x$ ).  $W_{oc}$  instead increased with decreasing  $x$  for all compositions explored on GaP with  $W_{oc} = 0.70$  V for  $x = 0.30$  ( $E_g = 2.1$  eV) and  $W_{oc} \approx 0.78$  V for  $x = 0.18$ –0.24 ( $E_g = 2.2$  eV). The lower  $W_{oc}$  for higher  $x$  (i.e., higher mismatch and TDD, Fig. 24, blue circles) implies that the elevated TDD is not entirely responsible for the high  $W_{oc}$  observed in the low In content devices on GaP. In fact,  $W_{oc}$  for  $x = 0.18$ –0.30 compares well with GaP solar cells *lattice-matched* to GaP where  $W_{oc} = 0.8$  V (discussed in depth in Sec. IV C). If TDD is not responsible for decreased solar cell performance of low-In content  $Ga_{1-x}In_xP$  devices, it is likely that there is an increased point defect density at these compositions. This trend of performance reduction as the material becomes more GaP-like was similarly observed in P-rich GaAsP (Secs. II D and III C), another indication that GaP and GaP-rich materials are challenging for PV applications. The high  $W_{oc}$  values in wide-bandgap phosphides imply that further work is necessary to arrive at optimized growth conditions with reduced In content, as all

**TABLE XI.** Summary of MM-GaInP solar cells in the literature. \* denotes ARC.

x	$E_g$ (eV)	$V_{oc}$ (V)	$W_{oc}$ (V)	$J_{sc}$ (mA/cm <sup>2</sup> )	FF	$\eta$ (%)	TDD ( $\times 10^6 \text{ cm}^{-2}$ )
0.39 <sup>186</sup>	1.98	1.50	0.48	11.06*	0.864	14.4	2.0
0.31 <sup>186</sup>	2.07	1.55	0.52	8.22*	0.845	10.7	8.0
0.43 <sup>187</sup>	1.97	1.37	0.60	7.80	0.79	8.44	0.7
0.39 <sup>187</sup>	2.00	1.42	0.58	7.30	0.80	8.29	1.6
0.36 <sup>188</sup>	2.07	1.49	0.58	6.75	0.81	8.14	1.0
0.30 <sup>192</sup>	2.12	1.42	0.70	3.65	0.75	3.89	7.6
0.24 <sup>192</sup>	2.21	1.43	0.78	2.75	0.73	2.87	4.0
0.18 <sup>192</sup>	2.23	1.46	0.77	2.29	0.74	2.47	2.3
0.35 <sup>193</sup>	2.07	1.48	0.59	5.29	0.80	6.25	1.0

devices in this study were grown with conditions optimized for  $x=0.49$  regardless of In content. Based on Faucher<sup>183</sup> and Sun's<sup>30</sup> results on AlGaInP solar cells, we speculate that significant performance improvements could be realized in MM-Ga<sub>1-x</sub>In<sub>x</sub>P with high-temperature annealing.

In 2015, Ohio State also investigated  $\sim 2.07$  eV Ga<sub>0.65</sub>In<sub>0.35</sub>P solar cells grown by MBE. These devices were grown on virtual GaAs<sub>y</sub>P<sub>1-y</sub>/GaAs substrates grown by MOCVD with TDD =  $1 \times 10^6$  cm<sup>-2</sup>.<sup>193</sup> Annealing their devices for 5 min at 680 °C under mixed As/P flux improved all solar cell metrics. Following anneal,  $W_{oc}$  improved from 0.68 to 0.59 V, resulting in an AM1.5G  $\eta = 6.25\%$ .

Ultimately, all work on wide-bandgap GaInP to date has revealed difficulty in obtaining high-performance solar cells with low In content. We expect that improvements could be made by optimizing growth conditions specifically for low In content GaInP as well as post growth annealing. Table XI summarizes the results for wide-bandgap MM-Ga<sub>1-x</sub>In<sub>x</sub>P solar cells in the literature.

### C. GaP

GaP is a binary option for wide-bandgap solar cells with  $E_{g,\text{indirect}} = 2.26$  eV and  $E_{g,\text{direct}} = 2.78$  eV (see band structure in Fig. 25). GaP solar cells suffer from poor absorption at photon energies of 2.26–2.78 eV and a lack of material options for an effective WL. However, given the simplicity of this binary option, researchers have been investigating its suitability for PV applications as early as the 1970s.

In addition to the wide-bandgap GaAs<sub>y</sub>P<sub>1-y</sub> that Barton and Olsen investigated above (Sec. IID), they explored GaP as a wide-bandgap PV material. Similar to their work with GaAs<sub>y</sub>P<sub>1-y</sub>, they used LED material to demonstrate a solar cell proof of concept. This device exhibited an  $\eta = 1.21\%$  via an  $V_{oc} = 1.37$  V,  $W_{oc} = 0.89$  V,  $J_{sc}$  ("AM1.5 83 mW/cm<sup>2</sup>") = 0.975 mA/cm<sup>2</sup>, and FF = 0.75.<sup>109</sup> It was not until the 2010s, when multi-junction solar cells were beginning to extend beyond three junctions (thus requiring materials with ever higher  $E_g$ ), that GaP was revisited as a potential wide-bandgap PV material.

Allen *et al.* demonstrated MBE-grown n-on-p GaP solar cells with  $V_{oc} = 1.53$  V,  $W_{oc} = 0.73$  V,  $J_{sc} = 0.959$  mA/cm<sup>2</sup>, and FF = 0.8.<sup>194</sup> They then used simulations matching the experimental LIV data to extract lifetime and mobility in each device layer. These simulations indicated a lower than expected  $\mu_n = 59$ – $64$  cm<sup>2</sup>/Vs for the p-GaP base. By simulating various potential improvements, the authors determined that front surface passivation, p-type lifetime improvement, and rear surface passivation would have the largest effects on  $\eta$  of GaP solar cells. As such, the authors added an ARC to improve the front surface passivation, boosting the one-sun results to  $\eta = 2.60\%$  via  $V_{oc} = 1.48$  V,  $W_{oc} = 0.78$  V,  $J_{sc} = 1.81$  mA/cm<sup>2</sup>, and FF = 0.77. They then measured

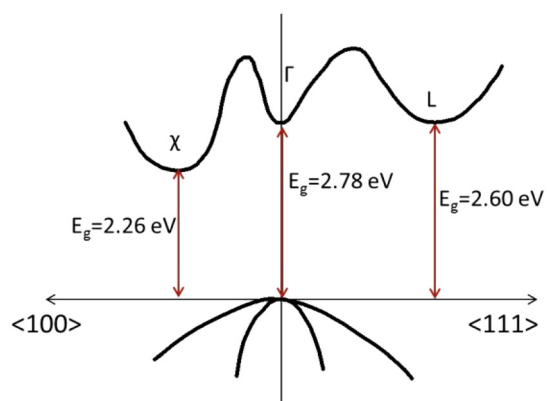


FIG. 25. GaP band structure, indirect with  $\Gamma$  valley only 0.52 eV higher than  $\chi$  valley.

this device under 10.7 suns, achieving a lower  $\eta = 2.05\%$  due to a decrease in FF from increased series resistance at higher current densities.<sup>195</sup>

Contemporary with the work above, Lu *et al.* also interrogated the suitability of GaP (grown by LPE) for PV applications, further probing the effect of device design on PV performance. Table XII summarizes the various designs studied and the accompanying results. The authors first looked at an n-on-p design with an 8  $\mu\text{m}$  base and a 1  $\mu\text{m}$  emitter yielding  $\eta = 1.29\%$ .<sup>196</sup> Fitting the IQE curve of this device revealed the major limitations to be low diffusion length in the n-type emitter and high surface recombination velocity. The authors thus flipped the polarity to provide a p-type emitter but found that a high  $J_{02}$  and low diffusion length in the base outweighed the improvement in emitter diffusion length, causing a decrease in overall performance. Returning to an n-on-p design, the authors further refined the GaP solar cell by reducing the emitter thickness from 1.0 to 0.8  $\mu\text{m}$ , changing the emitter dopant from Te to Sn (resulting in an increase in fitted minority carrier diffusion length in the emitter from 0.11 to 0.19  $\mu\text{m}$ ), and adding an ARC, ultimately obtaining  $\eta = 1.95\%$ . Further reducing the emitter thickness to 0.5  $\mu\text{m}$ , however, led to a significant increase in series resistance, causing FF to drop substantially.<sup>197</sup> In addition to adjusting the device design, the authors reduced the growth rate from 4 nm/s to 1.6 nm/s to improve material quality. Combined with the reduced emitter thickness, Sn emitter dopant, and addition of an ARC, the authors obtained  $\eta = 2.42\%$  with a  $V_{oc} = 1.55$  V,  $J_{sc} = 1.97$  mA/cm<sup>2</sup>, and FF = 0.794.<sup>198</sup> Finally, by adding an AlGaP WL,<sup>199</sup> Lu *et al.* improved the  $\eta$  of GaP solar cells to 2.9% owing to a reduction in surface recombination velocity from  $2 \times 10^6$  to  $1 \times 10^4$  cm/s.

TABLE XII. Summary of GaP solar cell results from Lu *et al.*<sup>196,197</sup>

Polarity	Base thickness ( $\mu\text{m}$ )	Emitter Thickness ( $\mu\text{m}$ )	Emitter Dopant	ARC?	$\eta$ (%)	$V_{oc}$ (V)	$J_{sc}$ (mA/cm <sup>2</sup> )	FF
n-on-p	8	1	Te	N	1.29	1.54	1.040	0.814
p-on-n	8	0.8	Zn	N	0.49	1.32	0.540	0.69
n-on-p	8	0.8	Sn	N	1.42	1.08	1.580	0.836
n-on-p	8	0.8	Sn	Y	1.95	1.50	1.583	0.822
n-on-p	8	0.5	Sn	Y	...	1.54	2.480	Low (high series resistance)

The Lee Group then investigated the effect of MBE  $T_{\text{sub}}$  and device design on GaP solar cell performance.<sup>200</sup> Vaisman *et al.* grew three identical GaP solar cells with  $T_{\text{sub}}$  of 465, 600, and 640 °C, finding the best results for  $T_{\text{sub}} = 600\text{--}640$  °C. They then added an AlGaP WL to a device grown at 600 °C, providing a 10% increase to  $J_{\text{sc}}$ . This enabled devices with  $\eta = 2.47\%$  without ARC, thus approaching the record  $\eta$  for a GaP solar cell (AR coated,  $\eta = 2.9\%$ , described above<sup>199</sup>). Figure 26 depicts the challenges of attaining high- $\eta$  GaP cells by plotting  $V_{\text{oc}}$  as a function of publication year for modern GaP solar cells. This shows that while there is clearly room for improvement, five years' worth of research has not led to significant strides. Despite the lack of Al and threading dislocations, GaP solar cells exhibit all of the same challenges as wide-bandgap AlGaInP, MM-GaInP, and P-rich MM-GaAsP, such as low minority hole diffusion length in the n-GaP emitter and the additional challenges of low majority/minority electron mobility. While its technological relevance may be limited, a fundamental understanding of performance-limited defects in GaP solar cells could yield insights that would apply to other wide-bandgap absorbers.

#### D. Summary and recommendations for future work on >1.9 eV top cells

Overall, AlGaInP FJ cells provide excellent performance for  $E_g$  up to 2.0 eV (~8%–12% Al, depending on degree of order), whereas, for  $E_g \geq 2.1$  eV, all absorbers exhibit significant degradation across all figures of merit. The improvement in MOCVD-grown AlGaInP cells with Se-doped emitters (as opposed to Si) is promising,<sup>69</sup> though no mechanism has been proposed. For both MM-GaInP and GaP, devices to date show that wider bandgap and lower In content lead to worse performance, despite low TDD and the lack of Al.

Given that these wider-bandgap phosphides are not as mature as those developed for 2J and 3J devices, there is ample room for improvement in the materials explored in this section. For AlGaInP, we recommend further research to improve bulk n-type material quality<sup>69</sup> and exploration of n-type delta doping to minimize sheet

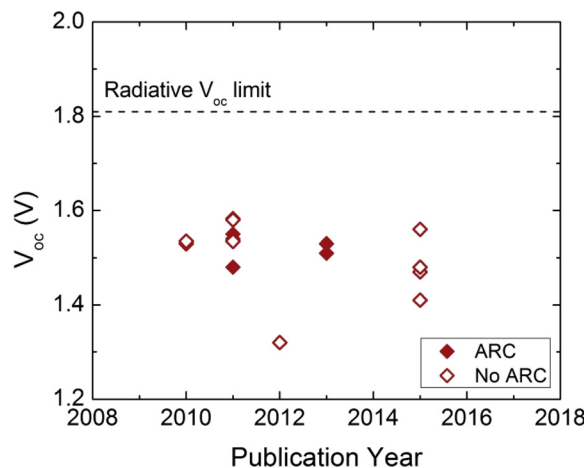


**FIG. 26.**  $V_{\text{oc}}$  as a function of publication year for modern GaP solar cells. Lack of clear improvement over 5 years indicates significant challenges with GaP PV material.

resistance while allowing the majority of the emitter to be lightly n-doped; challenges with Si-doped AlGaInP are reminiscent of those seen in MBE-grown GaInP with Si doping  $> 1 \times 10^{18} \text{ cm}^{-3}$ , which were alleviated by delta doping.<sup>35</sup> In the case of GaP and MM-GaInP, further work should investigate the growth conditions necessary for GaP and low-In content  $\text{Ga}_{1-x}\text{In}_x\text{P}$  devices to attain low  $W_{\text{oc}}$ , as well as post-growth annealing. Defect spectroscopy studies may elucidate whether impurities or intrinsic point defects are the predominant cause of high dark current in these devices. This information could subsequently inform the development of new growth strategies to enhance material quality. Finally, investigating why thermal annealing is so beneficial for MBE-grown AlGaInP and extending it to MM-GaInP and GaP could yield substantial performance benefits.

#### V. NEW MATERIALS SYSTEMS FOR WIDE-BANDGAP PV APPLICATIONS

In addition to the above-mentioned material systems, some less-common systems have been explored for wide-bandgap PV. This section highlights the novel and/or less-researched materials InAlAsSb (Sec. V A), MM-AlInP (Sec. V B), and GaNPAs (Sec. V C).

##### A. InAlAsSb

InAlAsSb is technologically relevant as it possesses the widest bandgap that can be grown lattice-matched to InP ranging from  $E_g \approx 1.45\text{--}1.80$  eV. Triple-junction devices on InP substrates are projected to achieve efficiencies  $>45\%$  under concentration, using lattice-matched materials for each subcell with  $E_g$  of 1.75, 1.17, and 0.74 eV as seen in Fig. 27.<sup>201,202</sup> While the bottom two junctions would be made of relatively mature materials such as  $\text{Ga}_{0.47}\text{In}_{0.53}\text{As}$  and  $\text{Ga}_{0.12}\text{In}_{0.88}\text{As}_{0.25}\text{P}_{0.75}$ , the top subcell requires use of the novel quaternary alloy InAlAsSb.

In the mid-2010s, the U.S. Naval Research Laboratory performed initial work on  $\text{In}_{0.31}\text{Al}_{0.69}\text{As}_{0.82}\text{Sb}_{0.18}$  ( $E_g = 1.57$  eV) grown by MBE.<sup>203</sup> The authors found that the PL emission energy, which typically approximates the  $E_g$ , was significantly lower than the  $E_g$  extracted

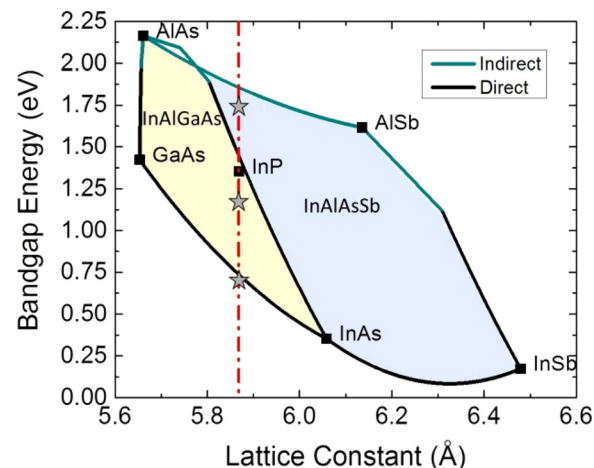


**FIG. 27.** III-V  $E_g$  vs lattice constant plot. Stars represent three subcells in a potential lattice-matched 3J on InP.<sup>203</sup> Reproduced with permission from Tomasulo *et al.*, in *IEEE Proceedings of the 42nd Photovoltaic Specialists Conference* (2015). Copyright 2015 IEEE.

from ellipsometry measurements and expected from theory, likely due to the presence of severe phase separation from unoptimized growth conditions. In practice, this would likely lead to low  $V_{oc}$  and limit the overall  $\eta$  of the ultimate 3J device. They found that relatively low  $T_{sub}$  ( $\sim 325^{\circ}\text{C}$ ) and relatively high group-V overpressure of  $3.2 \times 10^{-6}$  Torr resulted in increased PL emission energy, implying a reduction in phase separation from reduced adatom mobility.

The same group also investigated the effect of post-growth RTA on  $\text{In}_{0.42}\text{Al}_{0.58}\text{As}_{0.91}\text{Sb}_{0.09}$  ( $E_g = 1.47\text{ eV}$ ) on the PL emission energy.<sup>204</sup> The samples were annealed for 1 min each at temperatures ranging from 500 to  $650^{\circ}\text{C}$ , and it was found that the PL emission energy shifted from 1.33 eV as-grown to 1.42 eV following a  $650^{\circ}\text{C}$  anneal temperature. This suggests that in addition to optimizing MBE growth conditions, post-growth anneals can help to mitigate the presence of sub-bandgap states and shift the PL emission energy closer to the expected  $E_g$  value.

Finally, the authors used the lessons learned from Ref. 203 to develop  $\text{In}_{0.23}\text{Al}_{0.77}\text{As}_{0.75}\text{Sb}_{0.25}$  with  $E_g = 1.68\text{ eV}$ .<sup>205</sup> They again found that decreasing adatom mobility through decreased  $T_{sub}$  and increased group-V overpressure led to increased PL emission energy, suggesting reduced phase separation. However, these same growth conditions led to a roughened surface and decreased PL intensity. The presence of phase separation was confirmed via temperature-dependent PL measurements, which revealed the existence of an S-shaped temperature dependency rather than the expected Varshni curve. This has been observed previously in nitrides<sup>206,207</sup> and  $\text{In}_{0.31}\text{Al}_{0.69}\text{As}_{0.82}\text{Sb}_{0.18}$ <sup>208</sup> and has been explained by the development of local conduction band minima resulting from phase separation. As seen in Fig. 28, the S-shape arises from bulk carrier behavior at low and high temperatures where the carriers cannot diffuse far enough to reach the local minima and where they have enough thermal energy to escape the local minima, respectively. At moderate temperatures ( $100\text{--}200^{\circ}\text{C}$ ), the carriers recombine from the local minima, leading to a reduction in PL energy

and producing a dip in the temperature dependence. Ultimately, the authors found that the same growth conditions necessary to reduce phase separation led to rough surfaces and decreased PL intensity, and wide-bandgap InAlAsSb solar cells have not yet been demonstrated.

As research into wide-bandgap InAlAsSb for PV is still in relative infancy, there are clear directions on how to proceed. First, it is important to optimize the growth and anneal conditions for the desired 1.75 eV  $\text{In}_{0.19}\text{Al}_{0.81}\text{As}_{0.72}\text{Sb}_{0.28}$  to ensure the PL emission energy approaches the expected  $E_g$ . In addition to optimizing the optical properties of unintentionally doped InAlAsSb, it will be important to investigate doping in this novel alloy. Finally, as the desired InAlAsSb is one of the widest-bandgap materials at this lattice constant, the development of wider-bandgap material for window and back surface field layers (e.g., lattice-matched AlAsSb and strained InAlAs<sup>210</sup>) will be necessary to attain the highest efficiencies.

## B. Metamorphic AllnP

The widest direct-gap material among cubic III-Vs is  $\text{Al}_{1-x}\text{In}_x\text{P}$  ( $x = 0.55$ ,  $E_g = 2.33\text{ eV}$ ,  $a = 5.686\text{ \AA}$ ), but it is not lattice-matched to any conventional substrates.<sup>211</sup> However, it can be grown metamorphically on GaAs ( $a = 5.653\text{ \AA}$ ) or Ge ( $a = 5.658\text{ \AA}$ ), making it compatible with existing upright multi-junction technology. The Lee group investigated the viability of MM-AllnP, grown by MOCVD, for use as the top subcell in multi-junction devices.<sup>212</sup> In that work, the authors grew p-i-n-AllnP solar cells on GaInAs/GaAs CGBs with  $E_g = 2.07\text{ eV}$  ( $x = 0.64$ ) and  $E_g = 2.15\text{ eV}$  ( $x = 0.61$ ). Although  $\xi$  ranged from 0.6 to  $1.2\text{-}\mu\text{m}^{-1}$ , the TDD remained low at  $3\text{--}5 \times 10^6\text{ cm}^{-2}$ . The authors found that Zn from the p-emitter diffused into the i-region, effectively thickening the designed 280 emitter to 530 nm and thinning the designed 440 nm i-region to 180 nm, ultimately resulting in hampered current collection. To mitigate the severity of this effect, they wet-etched the emitter from 530 to 240 nm, which led to improved short wavelength collection and a 66% increase in  $J_{sc}$ . To prevent Zn diffusion from hindering future devices, the authors added an unintentionally doped spacer layer between the p-emitter and i-region to better balance the emitter- and i-region thicknesses following the expected Zn diffusion (emitter = 100 nm, spacer = 140 nm, i-region = 300 nm). Figure 29 shows SIMS profiles for the original sample (a) without a spacer vs the adapted design (b) showing improved control over the p-doping of the AllnP device.

This technique resulted in improved IQE over all wavelengths compared to the original device without a spacer layer. Results for all three cells are shown in Table XIII.

Furthermore, while the AllnP cells possessed high Al contents  $>35\%$ , SIMS showed fairly low  $[O] < 3.5 \times 10^{16}\text{ cm}^{-3}$ . This suggests that devices with such high Al contents may be more viable than previously thought, likely due to improvements in the purity of the TMAl precursor. Continued work for AllnP solar cells would include optimization of the device design by focusing on determining the appropriate spacer thickness to maximize current collection. Additionally, the inclusion of a tensile-strained AllnP WL would help to further improve short wavelength response.<sup>213</sup>

## C. GaNPAs

Rather than use a MM material for tandem applications on Si as in Sec. II D, researchers have also attempted to achieve the same top

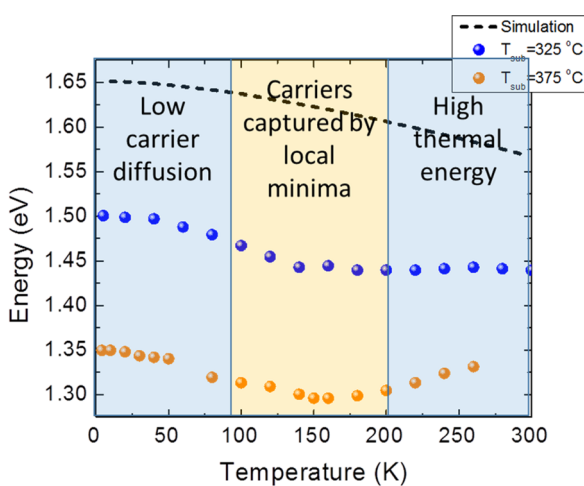
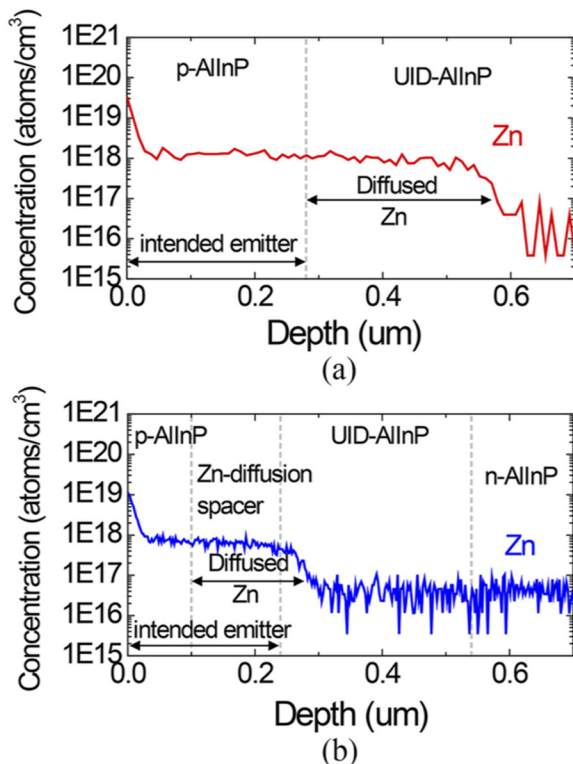


FIG. 28. PL energy as a function of measurement temperature of  $\text{In}_{0.31}\text{Al}_{0.69}\text{As}_{0.82}\text{Sb}_{0.18}$  grown at  $T_{sub} = 325^{\circ}\text{C}$  (blue symbols) and  $T_{sub} = 375^{\circ}\text{C}$  (orange symbols) revealing S-shape behavior indicative of phase separation. Dashed line represents simulated Varshni curve. Data from Ref. 208, figure from Ref. 209. Reproduced with permission from Tomasulo *et al.*, in *IEEE Proceedings of the 46th Photovoltaic Specialists Conference* (2019). Copyright 2019 IEEE.



**FIG. 29.** SIMS profiling of Zn in AlInP solar cells without (a) and with (b) a diffusion spacer layer. Spacer layer is critical to ensure that the grown device matches the intended device design.<sup>212</sup> Reproduced with permission from Vaisman *et al.*, IEEE J. Photovoltaics **6**, 571 (2016). Copyright 2016 IEEE.

cell  $E_g$  with a lattice-matched quaternary. By alloying N with GaAsP, the lattice constant can be matched with Si while the  $E_g$  can be tuned to 1.5–2.0 eV, making it an ideal candidate for tandem applications (lattice-matched  $\text{GaN}_x\text{P}_{1-x}\text{As}_y$ ,  $y = 4.7x - 0.1$ ). Of course, this material is not without its challenges. Nitrogen possesses an atomic radius nearly half that of As and P, presenting a large miscibility gap across nearly all N compositions and a significant challenge when attempting to grow the desired GaNPAs alloys. However, non-equilibrium growth techniques have been successful in alloying several % N into GaP and GaAsP despite the low solubility.<sup>214–217</sup>

NREL first investigated GaNPAs solar cells on GaP in the early-to-mid 2000s.<sup>218</sup> They grew heterojunction cells by MOCVD with various compositions of GaNPAs as the base and GaP as the emitter. Increasing the N content from 0.03 to 0.05 decreased the QE. To investigate the low QE and low minority carrier diffusion lengths, they

**TABLE XIII.** Summary of results for AlInP solar cells investigated in Ref. 212.

Cell	$E_g$ (eV)	$V_{oc}$ (V)	$J_{sc}$ ( $\text{mA}/\text{cm}^2$ )	FF	$W_{oc}$ (V)
No spacer—not etched	2.15	1.51	0.95	0.694	0.64
No spacer—etched	2.15	1.53	1.58	0.717	0.62
Spacer—not etched	2.07	1.50	3.14	0.739	0.57

performed capacitance-voltage measurements under various illumination conditions and found carrier concentration to be dependent on the incident light, which suggests the existence of a deep trap state in GaNPAs. Following this work, the same group developed a 1.8 eV  $\text{GaN}_{0.04}\text{P}_{0.86}\text{As}_{0.10}/\text{Si}$  2J device.<sup>219</sup> To enhance the electrical quality of the MOCVD-grown GaNPAs, the authors chose growth conditions ( $T_{sub} = 700^\circ\text{C}$ ,  $1 \mu\text{m}/\text{h}$ ) that minimize unintentional carbon and hydrogen contamination.<sup>220</sup> They utilized an n-i-p solar cell design for the top cell, in which  $1 \mu\text{m}$  of  $\text{GaN}_{0.04}\text{P}_{0.86}\text{As}_{0.10}$  is surrounded by thinner doped  $\text{GaN}_{0.02}\text{P}_{0.98}$  regions, to maximize QE. While the TDD of the devices on Si ( $5 \times 10^6 \text{ cm}^{-2}$ ) was over  $10\times$  higher than on GaP, it was still much lower than conventional GaAsP/Si of the mid-to-late 2000s ( $>1 \times 10^7 \text{ cm}^{-2}$ ). Figure 30 shows the (a) LIV and (b) IQE of the 2J device possessing  $V_{oc} = 1.53 \text{ V}$ ,  $J_{sc} = 6.3 \text{ mA}/\text{cm}^2$ , and FF = 0.54 ( $\eta = 5.2\%$ , no ARC), and mainly limited by the TJ and the top cell current density. A nearly identical device with an inactive bottom cell yielded a top cell with  $V_{oc} = 1.09 \text{ V}$  ( $W_{oc} = 0.71 \text{ V}$ ),  $J_{sc} = 5.7 \text{ mA}/\text{cm}^2$ ,

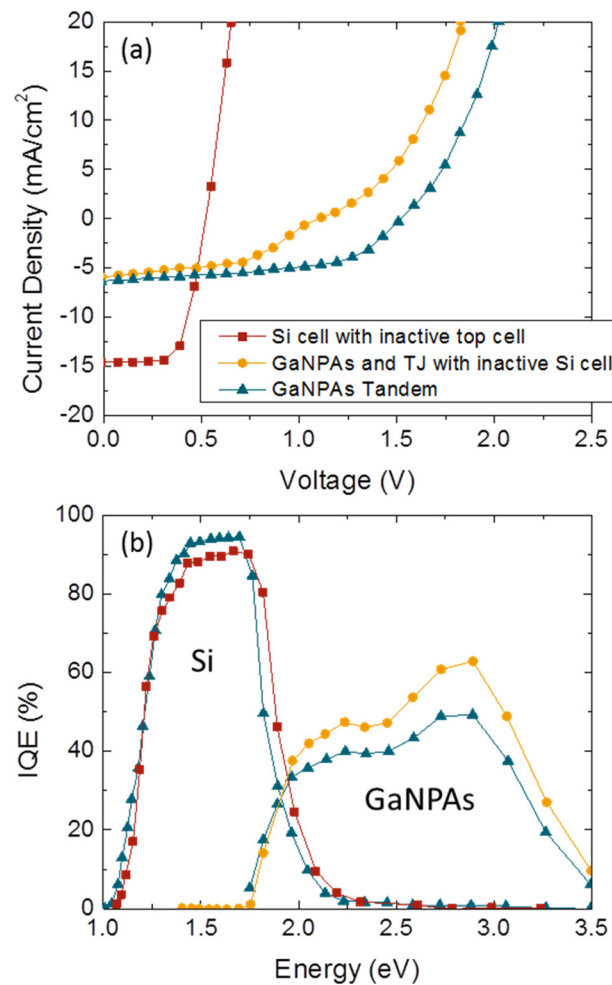


**FIG. 30.** (a) LIV curves of tandem and single-junction  $E_g = 1.8$  eV GaNPAs solar cells. (b) IQE of tandem and single-junction cells. Tandem results are light-biased to show both junctions.<sup>219</sup> Adapted from Ref. 219.

and  $\text{FF} = 0.48$ . Further research on GaNPAs growth should focus on identifying and controlling the formation of deep level defects<sup>221,222</sup> and improving the III-V on Si initiation to reduce TDD in the tandem. GaP-on-Si growth has matured substantially since this work<sup>107,223,224</sup> and may be beneficial for a return to GaNPAs research.

#### D. Summary and recommendations for future work on new materials systems

Novel materials spanning lattice constants from 5.43–5.87 Å and  $E_g = 1.8\text{--}2.2 \text{ eV}$  have been investigated for top cell applications, and most remain in a relatively immature state. Device details are limited, and ample opportunities exist for further research leveraging findings from other fields. For example, in the case of InAlAsSb, there are no obvious fundamental barriers to performance. Recent work on AlGaInP cells<sup>30,69,185</sup> proves that absorbers with significant %Al can provide excellent performance, while work on GaInAsP cells shows that challenges from miscibility gaps can be overcome. Furthermore, advances in digital alloy growth of InAlAsSb for high-performance infrared detectors could suppress phase separation and defect incorporation.<sup>225–227</sup> The case of GaNPAs may be more challenging due to the limited materials data on these highly mismatched alloys with three elements on the anion sub-lattice. Nevertheless, improvements in MBE growth of 1.0 eV InGaAsN absorbers<sup>58,228</sup> that took place after the initial investigations of GaNPAs in the early-to-mid 2000s suggest that considerably higher performance is achievable in dilute nitride materials.

#### VI. CONCLUSION

The III-V PV research community has consistently shown versatility and creativity in developing wide-bandgap absorber materials in response to application needs, often drawing on advances from other fields. For example, as the performance of single-junction GaAs solar cells improved throughout the 1970s and 1980s, the community went to work on AlGaAs/GaAs tandems. While AlGaAs was a well-developed material, much of the prior work had focused on its use as a barrier material in light emitters and transistors and as an undoped active region in red LEDs. Solar cells require doped, quasi-neutral active regions with long diffusion lengths (particularly in the base), making them distinct from virtually all other optoelectronic devices; most detectors leverage an undoped absorber region held at reverse bias for field-assisted carrier collection and do not consider FF. Furthermore, unlike lasers and LEDs, multi-junction solar cells are typically operated at low current densities of  $\sim 10\text{--}20 \text{ mA/cm}^2$  and low QFL splitting, which renders them more sensitive to trap-assisted recombination. Thus, PV researchers can encounter new challenges even when working on seemingly established materials. Despite these setbacks, Chung *et al.* were able to demonstrate an  $\sim 28\%$ -efficient 1.9 eV/1.4 eV tandem by MOCVD using an Al<sub>0.37</sub>Ga<sub>0.63</sub>As top cell by 1989.<sup>141</sup>

As AlGaInP red LEDs and laser diodes penetrated the market in the 1990s,<sup>229</sup> the PV community quickly pivoted. Again, the success of active regions based on undoped GaInP quantum wells did not guarantee high  $\eta$  in PV, and decades of research continue to reveal the complex dynamics of traps in these materials, particularly with annealing. It is also noteworthy that despite its  $E_g$  being slightly off for current-matching with GaAs, GaInP was adopted due to the serendipitous discovery of its radiation tolerance. Here, the research community

showed that simply using a thinner GaInP absorber to current-match with the underlying GaAs enabled very high  $\eta$  despite imperfect spectral matching. Another creative idea that leveraged gradual improvements in basic materials- and device-level understanding was Fraunhofer's demonstration of high-performance AlGaAs cells that utilized an n-GaInP emitter with a p-AlGaAs base to circumvent the deleterious effects of DX centers. Improved, albeit incomplete, understanding of the effects of doping, growth temperature, and annealing have enabled high performance in AlGaInP cells with  $E_g \leq 2.0 \text{ eV}$ , while wider-bandgap absorbers still suffer from the effects of poorly understood trap states. Finally, concomitant observations of unexpected misfit dislocations in III-V/Si lasers<sup>130</sup> and solar cells<sup>45</sup> led several groups to redesign heterojunction barrier layers used in their devices.<sup>129,133</sup>

Although this review has focused heavily on AlGaAs, GaInAsP, GaInP, and AlGaInP due to their high performance, the story is not yet complete for the less-developed absorber materials. Consider the case of 1.7 eV GaAsP single-junction cells on Si, where, until recently, the only reported efficiencies were  $< 10\%$ .<sup>73,116</sup> Taking advantage of fundamental advances in GaP/Si heteroepitaxy, GaAsP/Si single-junction cells can now attain efficiencies up to 17.6%,<sup>45</sup> TDDs as low as  $3 \times 10^6 \text{ cm}^{-2}$ ,<sup>123</sup> and  $W_{oc}$  values down to 0.44 V<sup>133</sup> (though no single device has attained all these values to date). While the performance of III-V/Si epitaxial tandem solar cells has not yet been high enough to warrant significant commercial interest, the rapid progress shows that issues such as MM growth and polar-on-nonpolar epitaxy can be overcome with a concerted research effort that emphasizes both materials science and device designs that account for the presence of defects.

The next generation of wide-bandgap PV materials and devices will likely encounter a combination of growth challenges that could include:

- (1) Al-containing growth;
- (2) Metamorphic growth;
- (3) III-V/Si growth;
- (4) Quaternary growth within miscibility gaps;
- (5) Complex doping and point defect effects, particularly in n-type phosphides;
- (6) Highly mismatched alloy growth.

In addition, other general materials and device trends will adversely affect wide-bandgap absorbers, such as decreased minority hole mobility and a wider spectrum of bulk and interfacial traps. Based on our review of over four decades of research, we deem that challenges 1–4 are tractable while understanding of topics 5–6 remains in their infancy.

#### SUPPLEMENTARY MATERIAL

See the [supplementary material](#) for Data and references from Fig. 6.

#### AUTHOR DECLARATIONS

##### Conflict of Interest

The authors have no conflicts to disclose.

##### Author Contributions

**Stephanie Tomasulo:** Conceptualization (equal); Data curation (lead); Formal analysis (equal); Investigation (equal); Visualization (lead); Writing – original draft (equal); Writing – review & editing (equal).

**Minjoo Larry Lee:** Conceptualization (equal); Data curation (supporting); Formal analysis (equal); Investigation (equal); Visualization (supporting); Writing – original draft (equal); Writing – review & editing (equal).

## DATA AVAILABILITY

Data sharing is not applicable to this article as no new data were created or analyzed in this study.

## REFERENCES

- <sup>1</sup>K. A. Horowitz, T. W. Remo, B. Smith, and A. J. Ptak, “A techno-economic analysis and cost reduction roadmap for III-V solar cells,” Tech. Rep., (National Renewable Energy Laboratory, Golden, CO, 2018).
- <sup>2</sup>D. Scheman, R. Hoheisel, D. Edwards, A. Paulsen, J. Lorentzen, W. Yoon *et al.*, “Solar technology comparison for wing integration in unmanned aerial vehicles,” in *Proceedings of the 2018 IEEE 7th World Conference on Photovoltaic Energy Conversion (WCPEC) (A Joint Conference of 45th IEEE PVSC, 28th PVSEC & 34th EU PVSEC)* (IEEE, 2018), pp. 3539–3544.
- <sup>3</sup>C. L. Stender, J. Adams, V. Elarde, T. Major, H. Miyamoto, M. Osowski *et al.*, “Flexible and lightweight epitaxial lift-off GaAs multi-junction solar cells for portable power and UAV applications,” in Proceedings of the 2015 IEEE 42nd Photovoltaic Specialist Conference (PVSC), 2015.
- <sup>4</sup>M. Yamaguchi, K. Nakamura, R. Ozaki, N. Kojima, Y. Ohshita, T. Masuda *et al.*, “Analysis for the potential of high-efficiency and low-cost vehicle-integrated photovoltaics,” *Sol. RRL* **7**, 2200556 (2023).
- <sup>5</sup>W. Metaferia, K. L. Schulte, J. Simon, S. Johnston, and A. J. Ptak, “Gallium arsenide solar cells grown at rates exceeding  $300 \mu\text{m h}^{-1}$  by hydride vapor phase epitaxy,” *Nat. Commun.* **10**, 3361 (2019).
- <sup>6</sup>Y. Shoji, R. Oshima, K. Makita, A. Ubukata, and T. Sugaya, “28.3% efficient III-V tandem solar cells fabricated using a triple-chamber hydride vapor phase epitaxy system,” *Sol. RRL* **6**, 2100948 (2022).
- <sup>7</sup>K. L. Schulte, S. W. Johnston, A. K. Braun, J. T. Boyer, A. N. Neumann, W. E. McMahon *et al.*, “GaAs solar cells grown on acoustically spalled GaAs substrates with 27% efficiency,” *Joule* **7**, 1529–1542 (2023).
- <sup>8</sup>J. Schube, O. Höhn, P. Schygulla, R. Müller, M. Jahn, G. Mikolasch *et al.*, “Mask and plate: A scalable front metallization with low-cost potential for III-V based tandem solar cells enabling 31.6% conversion efficiency,” *Sci. Rep.* **13**, 15745 (2023).
- <sup>9</sup>V. Daniel, T. Bidaud, J. Chretien, N. Paupy, A. Ayari, T. M. Diallo *et al.*, “High-efficiency GaAs solar cells grown on porous germanium substrate with PEELER technology,” *Sol. RRL* **8**, 2300643 (2024).
- <sup>10</sup>T. E. Saenz, D. Curry, A. Gray, R. Muzzio, J. W. Schall, and M. A. Steiner, “Lithography-free mesa isolation of III-V solar cells through laser ablation,” *IEEE J. Photovoltaics* **15**, 110–116 (2025).
- <sup>11</sup>C. Ballif, F.-J. Haug, M. Boccard, P. J. Verlinden, and G. Hahn, “Status and perspectives of crystalline silicon photovoltaics in research and industry,” *Nat. Rev. Mater.* **7**, 597–616 (2022).
- <sup>12</sup>H. Cotal, C. Fetzer, J. Boisvert, G. Kinsey, R. King, P. Hebert *et al.*, “III-V multijunction solar cells for concentrating photovoltaics,” *Energy Environ. Sci.* **2**, 174–192 (2009).
- <sup>13</sup>S. Kurtz and J. Geisz, “Multijunction solar cells for conversion of concentrated sunlight to electricity,” *Opt. Express* **18**, A73–A78 (2010).
- <sup>14</sup>D. Friedman, “Progress and challenges for next-generation high-efficiency multijunction solar cells,” *Curr. Opin. Solid State Mater. Sci.* **14**, 131–138 (2010).
- <sup>15</sup>M. Yamaguchi, F. Dimroth, J. F. Geisz, and N. J. Ekins-Daukes, “Multi-junction solar cells paving the way for super high-efficiency,” *J. Appl. Phys.* **129**, 240901 (2021).
- <sup>16</sup>M. Yamaguchi, F. Dimroth, N. J. Ekins-Daukes, N. Kojima, and Y. Ohshita, “Overview and loss analysis of III-V single-junction and multi-junction solar cells,” *EPJ Photovoltaics* **13**, 22 (2022).
- <sup>17</sup>A. Baiju and M. Yarema, “Status and challenges of multi-junction solar cell technology,” *Front. Energy Res.* **10**, 971918 (2022).
- <sup>18</sup>S. Rühle, “Tabulated values of the Shockley–Queisser limit for single junction solar cells,” *Sol. Energy* **130**, 139–147 (2016).
- <sup>19</sup>C. H. Henry, “Limiting efficiencies of ideal single and multiple energy gap terrestrial solar cells,” *J. Appl. Phys.* **51**, 4494–4500 (1980).
- <sup>20</sup>D. J. Aiken, A. B. Cornfeld, M. A. Stan, and P. R. Sharps, “Consideration of high bandgap subcells for advanced multijunction solar cells,” in *Proceedings of the Conference Record of the 2006 IEEE 4th World Conference on Photovoltaic Energy Conversion (IEEE, 2006)*, pp. 838–841.
- <sup>21</sup>M. A. Green, E. D. Dunlop, M. Yoshita, N. Kopidakis, K. Bothe, G. Siefer *et al.*, “Solar cell efficiency tables (version 65),” *Prog. Photovoltaics Res. Appl.* **33**, 3–15 (2025).
- <sup>22</sup>F. Dimroth, see <https://www.ise.fraunhofer.de/en/press-media/press-releases/2022/fraunhofer-ise-develops-the-worlds-most-efficient-solar-cell-with-47-comma-6-percent-efficiency.html> for “Fraunhofer ISE Develops the World’s Most Efficient Solar Cell with 47.6 Percent Efficiency.”
- <sup>23</sup>J. F. Geisz, R. M. France, K. L. Schulte, M. A. Steiner, A. G. Norman, H. L. Guthrey *et al.*, “Six-junction III-V solar cells with 47.1% conversion efficiency under 143 Suns concentration,” *Nat. Energy* **5**, 326–335 (2020).
- <sup>24</sup>D. C. Law, T. P. C. C. M. Fetzer, M. Haddad, S. Mesropian, R. Cravens *et al.*, “Development of XTJ targeted environment (XTE) solar cells for specific space applications,” in *Proceedings of the 2018 IEEE 7th World Conference on Photovoltaic Energy Conversion (WCPEC) (A Joint Conference of 45th IEEE PVSC, 28th PVSEC & 34th EU PVSEC)* (IEEE, 2018), pp. 3360–3363.
- <sup>25</sup>X. Q. Liu, C. Fetzer, P. Chiu, M. Haddad, X. Zhang, R. Cravens *et al.*, “Large area multijunction III-V space solar cells over 31% efficiency,” in *Proceedings of the 2017 IEEE 44th Photovoltaic Specialist Conference (PVSC)*, (IEEE, 2017), pp. 2094–2098.
- <sup>26</sup>See <https://www.nrel.gov/grid/solar-resource/spectra-am1.5.html> for Reference Air Mass 1.5 Spectra.”
- <sup>27</sup>R. R. King, D. Bhusari, A. Boca, D. Larrabee, X. Q. Liu, W. Hong *et al.*, “Band gap-voltage offset and energy production in next-generation multijunction solar cells,” *Prog. Photovoltaics Res. Appl.* **19**(7), 797–812 (2010).
- <sup>28</sup>M. A. Green, “Accuracy of analytical expressions for solar cell fill factors,” *Sol. Cells* **7**, 337–340 (1982).
- <sup>29</sup>M. A. Steiner, R. M. France, E. E. Perl, D. J. Friedman, J. Simon, and J. F. Geisz, “Reverse heterojunction (Al)GaInP solar cells for improved efficiency at concentration,” *IEEE J. Photovoltaics* **10**, 487–494 (2020).
- <sup>30</sup>Y. Sun, S. Fan, J. Faucher, R. D. Hool, B. D. Li, P. Dhingra *et al.*, “2.0–2.2 eV AlGaInP solar cells grown by molecular beam epitaxy,” *Sol. Energy Mater. Sol. Cells* **219**, 110774 (2021).
- <sup>31</sup>F. Feldmann, M. Simon, M. Bivour, C. Reichel, M. Hermle, and S. W. Glunz, “Carrier-selective contacts for Si solar cells,” *Appl. Phys. Lett.* **104**, 181105 (2014).
- <sup>32</sup>J. F. Geisz, M. A. Steiner, I. García, S. R. Kurtz, and D. J. Friedman, “Enhanced external radiative efficiency for 20.8% efficient single-junction GaInP solar cells,” *Appl. Phys. Lett.* **103**, 041118 (2013).
- <sup>33</sup>M. P. Lumb, M. A. Steiner, J. F. Geisz, and R. J. Walters, “Incorporating photon recycling into the analytical drift-diffusion model of high efficiency solar cells,” *J. Appl. Phys.* **116**, 194504 (2014).
- <sup>34</sup>S.-T. Hwang, S. Kim, H. Cheun, H. Lee, B. Lee, T. Hwang *et al.*, “Bandgap grading and  $\text{Al}_{0.3}\text{Ga}_{0.7}\text{As}$  heterojunction emitter for highly efficient GaAs-based solar cells,” *Sol. Energy Mater. Sol. Cells* **155**, 264–272 (2016).
- <sup>35</sup>Y. Sun, B. D. Li, R. D. Hool, S. Fan, M. Kim, and M. L. Lee, “Improving the performance of GaInP solar cells through rapid thermal annealing and delta doping,” *Sol. Energy Mater. Sol. Cells* **241**, 111725 (2022).
- <sup>36</sup>M. A. Steiner, J. F. Geisz, I. García, D. J. Friedman, A. Duda, and S. R. Kurtz, “Optical enhancement of the open-circuit voltage in high quality GaAs solar cells,” *J. Appl. Phys.* **113**, 123109 (2013).
- <sup>37</sup>E. A. Fitzgerald, “Dislocations in strained-layer epitaxy: Theory, experiment, and applications,” *Mater. Sci. Rep.* **7**, 87–142 (1991).
- <sup>38</sup>E. A. Fitzgerald, A. Y. Kim, M. T. Currie, T. A. Langdo, G. Taraschi, and M. T. Bulsara, “Dislocation dynamics in relaxed graded composition semiconductors,” *Mater. Sci. Eng. B* **67**, 53–61 (1999).
- <sup>39</sup>N. J. Quitoriano and E. A. Fitzgerald, “Relaxed, high-quality InP on GaAs by using InGaAs and InGaP graded buffers to avoid phase separation,” *J. Appl. Phys.* **102**, 033511 (2007).

- <sup>40</sup>R. M. France, I. García, W. E. McMahon, A. G. Norman, J. Simon, J. F. Geisz *et al.*, "Lattice-mismatched 0.7-eV GaInAs solar cells grown on GaAs using GaInP compositionally graded buffers," *IEEE J. Photovoltaics* **4**, 190–195 (2014).
- <sup>41</sup>R. M. France, J. F. Geisz, M. A. Steiner, B. To, M. J. Romero, W. J. Olavarria *et al.*, "Reduction of crosshatch roughness and threading dislocation density in metamorphic GaInP buffers and GaInAs solar cells," *J. Appl. Phys.* **111**, 103528 (2012).
- <sup>42</sup>K. L. Schulte, R. M. France, and J. F. Geisz, "Highly transparent compositionally graded buffers for new metamorphic multijunction solar cell designs," *IEEE J. Photovoltaics* **7**, 347–353 (2017).
- <sup>43</sup>M. Yamaguchi, "Dislocation density reduction in heteroepitaxial III-V compound films on Si substrates for optical devices," *J. Mater. Res.* **6**, 376–384 (1991).
- <sup>44</sup>C. L. Andre, A. Khan, M. Gonzalez, M. K. Hudait, E. A. Fitzgerald, J. A. Carlin *et al.*, "Impact of threading dislocations on both n/p and p/n single junction GaAs cells grown on Ge/SiGe/Si substrates," in *Proceedings of the Conference Record of the 29th IEEE Photovoltaic Specialists Conference* (IEEE, 2002), pp. 1043–1046.
- <sup>45</sup>S. Fan, Z. J. Yu, R. D. Hool, P. Dhingra, W. Weigand, M. Kim *et al.*, "Current-matched III-V/Si epitaxial tandem solar cells with 25.0% efficiency," *Cell Rep. Phys. Sci.* **1**, 100208 (2020).
- <sup>46</sup>D. L. Lepkowski, T. J. Grassman, J. T. Boyer, D. J. Chmielewski, C. Yi, M. K. Juhl *et al.*, "23.4% monolithic epitaxial GaAsP/Si tandem solar cells and quantification of losses from threading dislocations," *Sol. Energy Mater. Sol. Cells* **230**, 111299 (2021).
- <sup>47</sup>A. W. Bett, F. Dimroth, W. Guter, R. Hoheisel, E. Oliva, S. P. Philipps *et al.*, "Highest efficiency multi-junction solar cell for terrestrial and space applications," in *Proceedings of the 24th European Photovoltaic Solar Energy Conference Hamburg, Germany* (2009).
- <sup>48</sup>K. Sasaki, T. Agui, K. Nakaido, N. Takahashi, R. Onitsuka, and T. Takamoto, "Development of InGaP/GaAs/InGaAs inverted triple junction concentrator solar cells," *AIP Conf. Proc.* **1556**, 22–25 (2013).
- <sup>49</sup>R. M. France, J. F. Geisz, I. García, M. A. Steiner, W. E. McMahon, D. J. Friedman *et al.*, "Quadrapole-junction inverted metamorphic concentrator devices," *IEEE J. Photovoltaics* **5**, 432–437 (2015).
- <sup>50</sup>R. M. France, J. F. Geisz, I. García, M. A. Steiner, W. E. McMahon, D. J. Friedman *et al.*, "Design flexibility of ultrahigh efficiency four-junction inverted metamorphic solar cells," *IEEE J. Photovoltaics* **6**, 578–583 (2016).
- <sup>51</sup>F. Dimroth, M. Grave, P. Beutel, U. Fiedeler, C. Karcher, T. N. D. Tibbits *et al.*, "Wafer bonded four-junction GaInP/GaAs/GaInAsP/GaInAs concentrator solar cells with 44.7% efficiency," *Prog. Photovoltaics Res. Appl.* **22**, 277–282 (2014).
- <sup>52</sup>P. Schygulla, R. Müller, O. Höhn, M. Schachtner, D. Chojniak, A. Cordaro *et al.*, "Wafer-bonded two-terminal III-V/Si triple-junction solar cell with power conversion efficiency of 36.1% at AM1.5g," *Prog. Photovoltaics Res. Appl.* **33**, 100–108 (2025).
- <sup>53</sup>G. B. Stringfellow, *Organometallic Vapor-Phase Epitaxy: Theory and Practice* (Academic Press, 1999).
- <sup>54</sup>M. Henini, *Molecular Beam Epitaxy: From Research to Mass Production* (Elsevier Science, 2012).
- <sup>55</sup>J. Simon, K. L. Schulte, K. A. W. Horowitz, T. Remo, D. L. Young, and A. J. Ptak, "III-V-based optoelectronics with low-cost dynamic hydride vapor phase epitaxy," *Crystals* **9**, 3 (2018).
- <sup>56</sup>R. Lang, C. Klein, J. Ohlmann, F. Dimroth, and D. Lackner, "Review on ultrahigh growth rate GaAs solar cells by metalorganic vapor-phase epitaxy," *J. Vacuum Sci. Technol. A* **42**, 020801 (2024).
- <sup>57</sup>J. R. Lang and J. S. Speck, "NH<sub>3</sub>-rich growth of InGaN and InGaN/GaN superlattices by NH<sub>3</sub>-based molecular beam epitaxy," *J. Cryst. Growth* **346**, 50–55 (2012).
- <sup>58</sup>M. Wiemer, V. Sabnis, and H. Yuen, *43.5% Efficient Lattice Matched Solar Cells* (SPIE, 2011), Vol. 8108.
- <sup>59</sup>J. T. Boyer, K. L. Schulte, M. R. Young, A. J. Ptak, and J. Simon, "AlInP-passivated III-V solar cells grown by dynamic hydride vapor-phase epitaxy," *Prog. Photovoltaics Res. Appl.* **31**, 230–236 (2023).
- <sup>60</sup>R. Oshima, A. Ogura, Y. Shoji, K. Makita, A. Ubukata, S. Koseki *et al.*, "Ultrahigh-speed growth of GaAs solar cells by triple-chamber hydride vapor phase epitaxy," *Crystals* **13**, 370 (2023).
- <sup>61</sup>A. Rockett, *The Materials Science of Semiconductors* (Springer, New York, NY, 2008).
- <sup>62</sup>W. C. Liu, "Investigation of electrical and photoluminescent properties of MBE-grown Al<sub>x</sub>Ga<sub>1-x</sub>As layers," *J. Mater. Sci.* **25**, 1765–1772 (1990).
- <sup>63</sup>T. Shitara and K. Eberl, "Electronic properties of InGaP grown by solid-source molecular-beam epitaxy with a GaP decomposition source," *Appl. Phys. Lett.* **65**, 356–358 (1994).
- <sup>64</sup>M. Ikeda and K. Kaneko, "Selenium and zinc doping in Ga<sub>0.5</sub>In<sub>0.5</sub>P and (Al<sub>0.5</sub>Ga<sub>0.5</sub>)<sub>0.5</sub>In<sub>0.5</sub>P grown by metalorganic chemical vapor deposition," *J. Appl. Phys.* **66**, 5285–5289 (1989).
- <sup>65</sup>S. Adachi, "Material parameters of In<sub>1-x</sub>Ga<sub>x</sub>As<sub>y</sub>P<sub>1-y</sub> and related binaries," *J. Appl. Phys.* **53**, 8775–8792 (1982).
- <sup>66</sup>A. K. Saxena, "Electron mobility in Ga<sub>1-x</sub>Al<sub>x</sub>As alloys," *Phys. Rev. B* **24**, 3295–3302 (1981).
- <sup>67</sup>D. C. Loo, D. K. Lorance, J. R. Sizelove, C. E. Stutz, K. R. Evans, and D. W. Whitson, "Alloy scattering in p-type Al<sub>x</sub>Ga<sub>1-x</sub>As," *J. Appl. Phys.* **71**, 260–266 (1992).
- <sup>68</sup>P. M. Mooney, "Deep donor levels (DX centers) in III-V semiconductors," *J. Appl. Phys.* **67**, R1–R26 (1990).
- <sup>69</sup>E. E. Perl, J. Simon, J. F. Geisz, W. Olavarria, M. Young, A. Duda *et al.*, "Development of high-bandgap AlGaInP solar cells grown by organometallic vapor-phase epitaxy," *IEEE J. Photovoltaics* **6**, 770–776 (2016).
- <sup>70</sup>R. R. King, J. H. Ermer, D. E. Joslin, M. Haddad, J. W. Eldredge, N. Karam *et al.*, "Double heterostructures for characterization of bulk lifetime and interface recombination velocity in III-V multijunction solar cells," in *Proceedings of the 2nd World Conference on Photovoltaic Solar Energy Conversion* (NREL, 1998), pp. 86–90.
- <sup>71</sup>N. Jain, J. F. Geisz, R. M. France, A. G. Norman, and M. A. Steiner, "Enhanced current collection in 1.7 eV GaInAsP solar cells grown on GaAs by metalorganic vapor phase epitaxy," *IEEE J. Photovoltaics* **7**, 927–933 (2017).
- <sup>72</sup>J. F. Geisz and D. J. Friedman, "III-N-V semiconductors for solar photovoltaic applications," *Semicond. Sci. Technol.* **17**, 769 (2002).
- <sup>73</sup>J. F. Geisz, J. M. Olson, M. J. Romero, C. s Jiang, and A. G. Norman, "Lattice-mismatched GaAsP solar cells grown on silicon by OMVPE," in *Proceedings of the 2006 IEEE 4th World Conference on Photovoltaic Energy Conference* (IEEE, 2006), pp. 772–775.
- <sup>74</sup>T. J. Grassman, M. R. Brenner, S. Rajagopalan, R. Unocic, R. Dehoff, M. Mills *et al.*, "Control and elimination of nucleation-related defects in GaP/Si(001) heteroepitaxy," *Appl. Phys. Lett.* **94**, 232106 (2009).
- <sup>75</sup>I. Németh, B. Kunert, W. Stoltz, and K. Volz, "Heteroepitaxy of GaP on Si: Correlation of morphology, anti-phase-domain structure and MOVPE growth conditions," *J. Cryst. Growth* **310**, 1595–1601 (2008).
- <sup>76</sup>W. Guter, J. Schöne, S. P. Philipps, M. Steiner, G. Siefer, A. Wekkeli *et al.*, "Current-matched triple-junction solar cell reaching 41.1% conversion efficiency under concentrated sunlight," *Appl. Phys. Lett.* **94**, 223504 (2009).
- <sup>77</sup>R. R. King, D. C. Law, K. M. Edmondson, C. M. Fetzer, G. S. Kinsey, H. Yoon *et al.*, "40% efficient metamorphic GaInP/GaInAs/Ge multijunction solar cells," *Appl. Phys. Lett.* **90**, 183516 (2007).
- <sup>78</sup>P. R. Sharps, M. L. Timmons, R. Venkatasubramanian, R. Pickett, J. S. Hills, J. Hancock *et al.*, "Development of 20% efficient GaInAsP solar cells," in *Proceedings of the Conference Record of the 23rd IEEE Photovoltaic Specialists Conference - 1993 (Cat. No.93CH3283-9)* (IEEE, 1993), pp. 633–638.
- <sup>79</sup>N. Jain, J. Simon, K. L. Schulte, P. Dippo, M. Young, D. L. Young *et al.*, "InGaAsP solar cells grown by hydride vapor phase epitaxy," in *Proceedings of the 2016 IEEE 43rd Photovoltaic Specialists Conference (PVSC)* (IEEE, 2016), pp. 1090–1094.
- <sup>80</sup>N. Jain, R. Oshima, R. France, J. Geisz, A. Norman, P. Dippo *et al.*, "Development of lattice-matched 1.7 eV GaInAsP solar cells grown on GaAs by MOVPE," in *Proceedings of the 2016 IEEE 43rd Photovoltaic Specialists Conference (PVSC)* (IEEE, 2016), pp. 46–51.
- <sup>81</sup>R. Oshima, R. M. France, J. F. Geisz, A. G. Norman, and M. A. Steiner, "Growth of lattice-matched GaInAsP grown on vicinal GaAs(001) substrates within the miscibility gap for solar cells," *J. Cryst. Growth* **458**, 1–7 (2017).
- <sup>82</sup>N. Jain, K. L. Schulte, J. F. Geisz, D. J. Friedman, R. M. France, E. E. Perl *et al.*, "High-efficiency inverted metamorphic 1.7/1.1 eV GaInAsP/GaInAs dual-junction solar cells," *Appl. Phys. Lett.* **112**, 053905 (2018).

- <sup>83</sup>M. A. Steiner, R. M. France, J. Buencuerpo, J. F. Geisz, M. P. Nielsen, A. Pusch *et al.*, "High efficiency inverted GaAs and GaInP/GaAs solar cells with strain-balanced GaInAs/GaAsP quantum wells," *Adv. Energy Mater.* **11**, 2002874 (2021).
- <sup>84</sup>S. M. Bedair, M. F. Lamorte, and J. R. Hauser, "A two-junction cascade solar-cell structure," *Appl. Phys. Lett.* **34**, 38–39 (1979).
- <sup>85</sup>R. P. Gale, J. C. C. Fan, G. W. Turner, R. L. Chapman, and J. V. Pantano, "Efficient AlGaAs shallow-homojunction solar cells," *Appl. Phys. Lett.* **44**, 632–634 (1984).
- <sup>86</sup>G. F. Virshup, C. W. Ford, and J. G. Werthen, "A 19% efficient AlGaAs solar cell with graded band gap," *Appl. Phys. Lett.* **47**, 1319–1321 (1985).
- <sup>87</sup>M. Umeno, T. Kato, Y. Mingui, Y. Azuma, T. Soga, and T. Jimbo, "High efficiency AlGaAs/Si tandem solar cell over 20%," in *Proceedings of 1994 IEEE 1st World Conference on Photovoltaic Energy Conversion - WCPEC (A Joint Conference of PVSC, PVSEC and PSEC)* (IEEE, 1994), Vol. 2, pp. 1679–1684.
- <sup>88</sup>T. Soga, T. Kato, M. Yang, M. Umeno, and T. Jimbo, "High efficiency AlGaAs/Si monolithic tandem solar cell grown by metalorganic chemical vapor deposition," *J. Appl. Phys.* **78**, 4196–4199 (1995).
- <sup>89</sup>M. Umeno, T. Kato, T. Egawa, T. Soga, and T. Jimbo, "High efficiency AlGaAs/Si tandem solar cell over 20%," *Sol. Energy Mater. Sol. Cells* **41–42**, 395–403 (1996).
- <sup>90</sup>Y. Yazawa, T. Kitatani, J. Minemura, K. Tamura, K. Mochizuki, and T. Warabisako, "AlGaAs solar cells grown by MBE for high-efficiency tandem cells," *Sol. Energy Mater. Sol. Cells* **35**, 39–44 (1994).
- <sup>91</sup>S. Heckelmann, D. Lackner, C. Karcher, F. Dimroth, and A. W. Bett, "Investigations on AlGaAs solar cells grown by MOVPE," *IEEE J. Photovoltaics* **5**, 446–453 (2015).
- <sup>92</sup>C. Amano, K. Ando, and M. Yamaguchi, "The effect of oxygen on the properties of AlGaAs solar-cells grown by molecular-beam epitaxy," *J. Appl. Phys.* **63**, 2853–2856 (1988).
- <sup>93</sup>S. Heckelmann, D. Lackner, F. Dimroth, and A. W. Bett, "Material quality frontiers of MOVPE grown AlGaAs for minority carrier devices," *J. Cryst. Growth* **464**, 49–53 (2017).
- <sup>94</sup>A. Onno, M. Tang, L. Oberbeck, J. Wu, and H. Liu, "Impact of the growth temperature on the performance of 1.70-eV Al<sub>0.22</sub>Ga<sub>0.78</sub>As solar cells grown by MBE," *J. Cryst. Growth* **475**, 322–327 (2017).
- <sup>95</sup>H. Morkoç, T. J. Drummond, W. Kopp, and R. Fischer, "Influence of substrate temperature on the morphology of Al<sub>x</sub>Ga<sub>1-x</sub>As grown by molecular beam epitaxy," *J. Electrochem. Soc.* **129**, 824–826 (1982).
- <sup>96</sup>F. Alexandre, L. Goldstein, G. Leroux, M. C. Joncour, H. Thibierge, and E. V. K. Rao, "Investigation of surface roughness of molecular beam epitaxy Ga<sub>1-x</sub>Al<sub>x</sub>As layers and its consequences on GaAs/Ga<sub>1-x</sub>Al<sub>x</sub>As heterostructures," *J. Vacuum Sci. Technol. B: Microelectron. Process. Phenom.* **3**, 950–955 (1985).
- <sup>97</sup>A. Ben Slimane, A. Michaud, O. Mauguin, X. Lafosse, A. Bercegol, L. Lombez *et al.*, "1.73 eV AlGaAs/InGaP heterojunction solar cell grown by MBE with 18.7% efficiency," *Prog. Photovoltaics Res. Appl.* **28**, 393–402 (2020).
- <sup>98</sup>Y. J. Chung, A. Gupta, K. W. Baldwin, K. W. West, M. Shayegan, and L. N. Pfeiffer, "Understanding limits to mobility in ultrahigh-mobility GaAs two-dimensional electron systems: 100 million cm<sup>2</sup>/Vs and beyond," *Phys. Rev. B* **106**, 075134 (2022).
- <sup>99</sup>H. C. Chui, B. E. Hammons, N. E. Harff, J. A. Simmons, and M. E. Sherwin, "2 × 10<sup>6</sup> cm<sup>2</sup>/Vs electron mobility by metalorganic chemical vapor deposition with tertiarybutylarsine," *Appl. Phys. Lett.* **68**, 208–210 (1996).
- <sup>100</sup>R. W. Hoffman, N. S. Fatemi, M. A. Stan, P. Jenkins, V. G. Weizer, D. A. Scheiman *et al.*, "High efficiency monolithic multi-junction solar cells using lattice-mismatched growth," *MRS Online Proc. Library* **551**, 51–62 (1998).
- <sup>101</sup>F. Dimroth, U. Schubert, and A. W. Bett, "25.5% efficient Ga<sub>0.35</sub>In<sub>0.65</sub>P/Ga<sub>0.83</sub>In<sub>0.17</sub>As tandem solar cells grown on GaAs substrates," *IEEE Electron Device Lett.* **21**, 209–211 (2000).
- <sup>102</sup>F. Dimroth, P. Lanyi, U. Schubert, and A. W. Bett, "MOVPE grown Ga<sub>1-x</sub>In<sub>x</sub>As solar cells for GaInP/GaInAs tandem applications," *J. Electron. Mater.* **29**, 42–46 (2000).
- <sup>103</sup>R. H. van Leest, D. Fuhrmann, A. Frey, M. Meusel, G. Siefer, and S. K. Reichmuth, "Recent progress of multi-junction solar cell development for CPV applications at AZUR SPACE," *AIP Conf. Proc.* **2149**, 020007 (2019).
- <sup>104</sup>M. Kim, Y. Sun, R. D. Hool, and M. L. Lee, "Metamorphic front- and rear-junction 1.7 eV GaInP solar cells with high open-circuit voltage," *Sol. Energy Mater. Sol. Cells* **259**, 112435 (2023).
- <sup>105</sup>C. L. Andre, D. M. Wilt, A. J. Pitera, M. L. Lee, E. A. Fitzgerald, and S. A. Ringel, "Impact of dislocation densities on n+/p and p+/n junction GaAs diodes and solar cells on SiGe virtual substrates," *J. Appl. Phys.* **98**, 014502 (2005).
- <sup>106</sup>B. Kunert, I. Németh, S. Reinhard, K. Volz, and W. Stoltz, "Si (001) surface preparation for the antiphase domain free heteroepitaxial growth of GaP on Si substrate," *Thin Solid Films* **517**, 140–143 (2008).
- <sup>107</sup>K. Volz, A. Beyer, W. Witte, J. Ohlmann, I. Németh, B. Kunert *et al.*, "GaP-nucleation on exact Si (001) substrates for III/V device integration," *J. Cryst. Growth* **315**, 37–47 (2011).
- <sup>108</sup>S. Fan, Z. J. Yu, Y. Sun, W. Weigand, P. Dhingra, M. Kim *et al.*, "20%-efficient epitaxial GaAsP/Si tandem solar cells," *Sol. Energy Mater. Sol. Cells* **202**, 110144 (2019).
- <sup>109</sup>D. L. Barton and L. C. Olsen, "Solar cells based on GaP<sub>x</sub>As<sub>1-x</sub> compounds," in *Proceedings of the 13th IEEE Photovoltaic Specialists Conference* (IEEE, 1978), pp. 972–977.
- <sup>110</sup>L. M. Fraas, J. A. Cape, P. S. McLeod, and L. D. Partain, "High-efficiency GaAs<sub>0.7</sub>P<sub>0.3</sub> solar cell on a transparent GaP wafer," *J. Appl. Phys.* **57**, 2302–2304 (1985).
- <sup>111</sup>G. H. Negley, J. B. McNeely, P. G. Lasswell, E. A. Gartley, A. M. Barnett, and T. M. Trumble, "Design and development of GaAsP on GaP/Silicon mechanically stacked, multijunction solar cells," in *Proceedings of the IEEE Photovoltaic Specialists Conference* (IEEE, 1987), p. 119.
- <sup>112</sup>S. M. Vernon, S. P. Tobin, V. E. Haven, R. G. Wolfson, M. W. Wanlass, and R. J. Matson, "Development of high-efficiency GaAsP solar cells on compositionally graded buffer layers," in *Proceedings of the 19th IEEE Photovoltaic Specialists Conference, New Orleans, LA* (IEEE, 1987), p. 108.
- <sup>113</sup>M. W. Wanlass, K. A. Emery, M. M. Al-Jassim, and A. R. Mason, "Effects of defect density and compositional grading on GaAsP photovoltaic performance," in *Proceedings of the 19th IEEE Photovoltaic Specialists Conference, New Orleans, LA* (IEEE, 1987), p. 530.
- <sup>114</sup>K. Hayashi, T. Soga, H. Nishikawa, T. Jimbo, and M. Umeno, "MOCVD growth of GaAsP on Si for tandem solar cell application," in *Proceedings of the 1994 IEEE 1st World Conference on Photovoltaic Energy Conversion - WCPEC (A Joint Conference of PVSC, PVSEC and PSEC)* (IEEE, 1994), Vol. 2, pp. 1890–1893.
- <sup>115</sup>T. J. Grassman, M. R. Brenner, A. M. Carlin, S. Rajagopalan, R. Unocic, R. Dehoff *et al.*, "Toward metamorphic multijunction GaAsP/Si photovoltaics grown on optimized GaP/Si virtual substrates using anion-graded GaAsP buffers," in *2009 34th IEEE Photovoltaic Specialists Conference (PVSC)* (IEEE, 2009), pp. 2016–2021.
- <sup>116</sup>T. J. Grassman, M. R. Brenner, M. Gonzalez, A. M. Carlin, R. R. Unocic, R. R. Dehoff *et al.*, "Characterization of metamorphic GaAsP/Si materials and devices for photovoltaic applications," *IEEE Trans. Electron Devices* **57**, 3361–3369 (2010).
- <sup>117</sup>T. J. Grassman, J. A. Carlin, C. Ratcliff, D. J. Chmielewski, and S. A. Ringel, "Epitaxially-grown metamorphic GaAsP/Si dual-junction solar cells," in *Proceedings of the 2013 IEEE 39th Photovoltaic Specialists Conference (PVSC)* (IEEE, 2013), pp. 149–153.
- <sup>118</sup>D. L. Lepkowski, J. T. Boyer, D. J. Chmielewski, A. C. Silvaggio, S. A. Ringel, and T. J. Grassman, "Investigation of rear-emitter GaAsP top cells for use in III-V/Si Tandem photovoltaics," in *Proceedings of the 2018 IEEE 7th World Conference on Photovoltaic Energy Conversion (WCPEC) (A Joint Conference of 45th IEEE PVSC, 28th PVSEC & 34th EU PVSEC)* (IEEE, 2018), pp. 2642–2647.
- <sup>119</sup>T. J. Grassman, D. J. Chmielewski, S. D. Carnevale, J. A. Carlin, and S. A. Ringel, "GaAs<sub>0.75</sub>P<sub>0.25</sub>/Si dual-junction solar cells grown by MBE and MOCVD," *IEEE J. Photovoltaics* **6**, 326–331 (2016).
- <sup>120</sup>M. A. Green, E. D. Dunlop, D. H. Levi, J. Hohl-Ebinger, M. Yoshita, and A. W. Y. Ho-Baillie, "Solar cell efficiency tables (version 54)," *Prog. Photovoltaics Res. Appl.* **27**, 565–575 (2019).
- <sup>121</sup>T. J. Grassman, D. L. Lepkowski, J. T. Boyer, D. J. Chmielewski, C. Yi, N. Western *et al.*, "Toward >25% efficient monolithic epitaxial GaAsP/Si tandem

- solar cells," in *Proceedings of the 2019 IEEE 46th Photovoltaic Specialists Conference (PVSC)* (IEEE, 2019), pp. 734–737.
- <sup>122</sup>D. L. Lepkowski, J. T. Boyer, C. Yi, A. H. Soeriyadi, Z. H. Blumer, M. K. Juhl *et al.*, "Loss analysis and design strategies enabling >23% GaAsP/Si tandem solar cells," in *Proceedings of the IEEE Photovoltaic Specialists Conference*, 2020.
- <sup>123</sup>J. T. Boyer, A. N. Blumer, Z. H. Blumer, D. L. Lepkowski, and T. J. Grassman, "Reduced dislocation introduction in III-V/Si heterostructures with glide-enhancing compressively strained superlattices," *Cryst. Growth Des.* **20**, 6939–6946 (2020).
- <sup>124</sup>S. Tomasulo, K. N. Yaung, J. Simon, and M. L. Lee, "GaAsP solar cells on GaP substrates by molecular beam epitaxy," *Appl. Phys. Lett.* **101**, 033911 (2012).
- <sup>125</sup>J. R. Lang, J. Faucher, S. Tomasulo, K. N. Yaung, and M. L. Lee, "Comparison of GaAsP solar cells on GaP and GaP/Si," *Appl. Phys. Lett.* **103**, 092102 (2013).
- <sup>126</sup>K. N. Yaung, M. Vaisman, J. Lang, and M. L. Lee, "GaAsP solar cells on GaP/Si with low threading dislocation density," *Appl. Phys. Lett.* **109**, 032107 (2016).
- <sup>127</sup>M. Vaisman, S. Fan, K. Nay Yaung, E. Perl, D. Martín-Martín, Z. J. Yu *et al.*, "15.3%-efficient GaAsP solar cells on GaP/Si templates," *ACS Energy Lett.* **2**, 1911–1918 (2017).
- <sup>128</sup>S. Fan, Z. J. Yu, R. D. Hool, P. Dhingra, W. Weigand, M. Kim *et al.*, "Epitaxial GaAsP/Si solar cells with high quantum efficiency," in *Proceedings of the IEEE Photovoltaic Specialists Conference*, 2020.
- <sup>129</sup>T. E. Saenz, J. Boyer, J. S. Mangum, A. N. Neumann, J. Selvidge, S. A. Collins *et al.*, "GaAs solar cells grown directly on V-Groove Si substrates," *ACS Appl. Mater. Interfaces* **17**, 1341–1349 (2025).
- <sup>130</sup>J. Selvidge, J. Norman, E. T. Hughes, C. Shang, D. Jung, A. A. Taylor *et al.*, "Defect filtering for thermal expansion induced dislocations in III-V lasers on silicon," *Appl. Phys. Lett.* **117**, 122101 (2020).
- <sup>131</sup>B. Li, Y. Wang, A. Birge, B. Kim, X. Fang, and M. L. Lee, "AlGaAsP distributed Bragg reflectors for GaAsP/Si solar cells," *IEEE J. Photovoltaics* **15**, 87–94 (2025).
- <sup>132</sup>D. L. Lepkowski, T. Kasher, T. J. Grassman, and S. A. Ringel, "Designing an epitaxially-integrated DBR for dislocation mitigation in monolithic GaAsP/Si tandem solar cells," *IEEE J. Photovoltaics* **11**, 400–407 (2021).
- <sup>133</sup>T. Kasher, L. M. Kaliszewski, D. L. Lepkowski, J. T. Boyer, M. Baan, T. J. Grassman *et al.*, "Design for increased defect tolerance in metamorphic GaAsP-on-Si top cells," *IEEE J. Photovoltaics* **14**, 911–919 (2024).
- <sup>134</sup>J. Faucher, A. Gerger, S. Tomasulo, C. Ebert, A. Lochtefeld, A. Barnett *et al.*, "Single-junction GaAsP solar cells grown on SiGe graded buffers on Si," *Appl. Phys. Lett.* **103**, 191901 (2013).
- <sup>135</sup>T. Milakovich, R. Shah, S. Hadi, M. Bulsara, A. Nayfeh, and E. Fitzgerald, "Growth and characterization of GaAsP top cells for high efficiency III-V/Si tandem PV," in *Proceedings of the 2015 IEEE 42nd Photovoltaic Specialist Conference (PVSC)* (IEEE, 2015), pp. 1–4.
- <sup>136</sup>K. J. Schmieder, A. Gerger, M. Diaz, Z. Pulwin, M. Curtin, L. Wang *et al.*, "GaAsP on SiGe/Si material quality improvements with in-situ stress sensor and resulting tandem device performance," *Mater. Sci. Semicond. Process.* **39**, 614–620 (2015).
- <sup>137</sup>S. P. Philippss and A. W. Bett, "III-V Multi-junction solar cells and concentrating photovoltaic (CPV) systems," *Adv. Opt. Technol.* **3**, 469–478 (2014).
- <sup>138</sup>S. G. Bailey and D. J. Flood, "Space photovoltaics," *Prog. Photovoltaics Res. Appl.* **6**, 1–14 (1998).
- <sup>139</sup>S. R. Kurtz, J. M. Olson, and A. Kibbler, "Effect of growth rate on the band gap of  $\text{Ga}_{0.5}\text{In}_{0.5}\text{P}$ ," *Appl. Phys. Lett.* **57**, 1922–1924 (1990).
- <sup>140</sup>K. Streubel, N. Linder, R. Wirth, and A. Jaeger, "High brightness AlGaInP light-emitting diodes," *IEEE J. Sel. Top. Quantum Electron.* **8**, 321–332 (2002).
- <sup>141</sup>B. C. Chung, G. F. Virshup, S. Hikido, and N. R. Kaminar, "27.6% efficiency (1 sun, air mass 1.5) monolithic  $\text{Al}_{0.37}\text{Ga}_{0.63}\text{As}/\text{GaAs}$  two-junction cascade solar cell with prismatic cover glass," *Appl. Phys. Lett.* **55**, 1741–1743 (1989).
- <sup>142</sup>J. M. Olson, S. R. Kurtz, A. E. Kibbler, and P. Faine, "A 27.3% efficient  $\text{Ga}_{0.5}\text{In}_{0.5}\text{P}/\text{GaAs}$  tandem solar cell," *Appl. Phys. Lett.* **56**, 623–625 (1990).
- <sup>143</sup>K. A. Bertness, S. R. Kurtz, D. J. Friedman, A. E. Kibbler, C. Kramer, and J. M. Olson, "29.5%-efficient GaInP/GaAs tandem solar cells," *Appl. Phys. Lett.* **65**, 989–991 (1994).
- <sup>144</sup>P. K. Chiang, P. S. Vijayakumar, and B. T. Cavicchi, "Large area GaInP/sub 2GaAs tandem cell development for space power systems," in *Proceedings of the Conference Record of the 23rd IEEE Photovoltaic Specialists Conference - 1993 (Cat. No.93CH3283-9)* (IEEE, 1993), pp. 659–664.
- <sup>145</sup>S. R. Kurtz, J. M. Olson, K. A. Bertness, D. J. Friedman, A. Kibbler, B. T. Cavicchi *et al.*, "Radiation Hardness of GaInP/GaAs Tandem Solar Cells," in *Proceedings of the Space Photovoltaic Research and Technology Conference*, 1991.
- <sup>146</sup>Y. C. M. Yeh, C. L. Chu, J. Kroger, F. F. Ho, G. C. Datum, S. Billets *et al.*, "Production experience with large area, dual junction space cells," in *Proceedings of the Conference Record of the 25th IEEE Photovoltaic Specialists Conference* (IEEE, 1996), pp. 187–190.
- <sup>147</sup>N. H. Karam, R. R. King, B. T. Cavicchi, D. D. Krut, J. H. Ermer, M. Haddad *et al.*, "Development and characterization of high-efficiency  $\text{Ga}_{0.5}\text{In}_{0.5}\text{P}/\text{GaAs}/\text{Ge}$  dual- and triple-junction solar cells," *IEEE Trans. Electron. Devices* **46**, 2116–2125 (1999).
- <sup>148</sup>P. K. Chiang, C. L. Chu, Y. C. M. Yeh, P. Iles, and F. Ho, "Progress toward high-efficiency (>24%) and low-cost multi-junction solar cell production," *Sol. Energy Mater. Sol. Cells* **66**, 615–620 (2001).
- <sup>149</sup>T. Takamoto, E. Ikeda, H. Kurita, and M. Ohmori, "Over 30% efficient InGaP/GaAs tandem solar cells," *Appl. Phys. Lett.* **70**, 381–383 (1997).
- <sup>150</sup>T. Takamoto, H. Washio, and H. Juso, "Application of InGaP/GaAs/InGaAs triple junction solar cells to space use and concentrator photovoltaic," in *Proceedings of the 2014 IEEE 40th Photovoltaic Specialist Conference (PVSC)* (IEEE, 2014), pp. 1–5.
- <sup>151</sup>J. N. Baillargeon, A. Y. Cho, and R. J. Fischer, "Evaluation of the performance and operating characteristics of a solid phosphorus source valved cracking cell for molecular beam epitaxy growth of III-V compounds," *J. Vacuum Sci. Technol. B: Microelectron. Nanometer Struct. Process., Meas., Phenom.* **13**, 64–68 (1995).
- <sup>152</sup>C. L. Andre, *III-V Semiconductors on SiGe Substrates for Multi-Junction Photovoltaics* (The Ohio State University, 2004).
- <sup>153</sup>M. A. Steiner, J. F. Geisz, R. C. Reedy, and S. Kurtz, "A direct comparison of inverted and non-inverted growths of GaInP solar cells," in *Proceedings of the 2008 33rd IEEE Photovoltaic Specialists Conference* (IEEE, 2008), pp. 1–6.
- <sup>154</sup>S. Lu, L. Ji, W. He, P. Dai, H. Yang, M. Arimotochi *et al.*, "High-efficiency GaAs and GaInP solar cells grown by all solid-state molecular-beam-epitaxy," *Nanoscale Res. Lett.* **6**, 576 (2011).
- <sup>155</sup>P. Dai, S. L. Lu, Y. Q. Zhu, L. Ji, W. He, M. Tan *et al.*, "The investigation of GaInP solar cell grown by all-solid MBE," *J. Cryst. Growth* **378**, 604–606 (2013).
- <sup>156</sup>O. D. Miller, E. Yablonovitch, and S. R. Kurtz, "Strong internal and external luminescence as solar cells approach the Shockley–Queisser limit," *IEEE J. Photovoltaics* **2**, 303–311 (2012).
- <sup>157</sup>M. A. Green, E. D. Dunlop, J. Hohl-Ebinger, M. Yoshita, N. Kopidakis, and X. Hao, "Solar cell efficiency tables (Version 58)," *Prog. Photovoltaics Res. Appl.* **29**, 657–667 (2021).
- <sup>158</sup>M. Hinojosa, I. García, I. Rey-Stolle, and C. Algora, "Inverted rear-heterojunction GaInP solar cells using Te memory effect," *Sol. Energy Mater. Sol. Cells* **205**, 110235 (2020).
- <sup>159</sup>R. Oshima, K. Makita, A. Ubukata, and T. Sugaya, "Fabrication of GaAs solar cells grown with InGaP layers by hydride vapor-phase epitaxy," *Japanese J. Appl. Phys.* **57**, 08RD06 (2018).
- <sup>160</sup>K. L. Schulte, J. Simon, J. Mangum, C. E. Packard, B. P. Gorman, N. Jain *et al.*, "Development of GaInP solar cells grown by hydride vapor phase epitaxy," *IEEE J. Photovoltaics* **7**, 1153–1158 (2017).
- <sup>161</sup>K. L. Schulte, J. Simon, M. R. Young, and A. J. Ptak, "Improvement of short-circuit current density in GaInP solar cells grown by dynamic hydride vapor phase epitaxy," *IEEE J. Photovoltaics* **8**, 1616–1620 (2018).
- <sup>162</sup>K. L. Schulte, W. Metaferia, J. Simon, D. Guiling, K. Udwary, G. Dodson *et al.*, "Growth of AlGaAs, AlInP, and AlGaInP by hydride vapor phase epitaxy," *ACS Appl. Energy Mater.* **2**, 8405–8410 (2019).
- <sup>163</sup>Y. Shoji, R. Oshima, K. Makita, A. Ubukata, and T. Sugaya, "InGaP/GaAs dual-junction solar cells with AlInGaP passivation layer grown by hydride vapor phase epitaxy," *Prog. Photovoltaics Res. Appl.* **29**, 1285–1293 (2021).
- <sup>164</sup>Y. Shoji, R. Oshima, K. Makita, A. Ubukata, S. Koseki, and T. Sugaya, "Performance of hydride vapor phase epitaxy-grown GaInP photovoltaics with

- double-sided Al-containing passivation layers under air mass 1.5 global solar irradiation and low-intensity indoor light irradiation," *Sol. RRL* **8**, 2300845 (2024).
- <sup>165</sup>R. M. France, M. Hinojosa, S. P. Ahrenkiel, M. R. Young, S. W. Johnston, H. L. Guthrey *et al.*, "Improvement of front-junction GaInP by point-defect injection and annealing," in *Proceedings of the 2021 IEEE 48th Photovoltaic Specialists Conference (PVSC)* (IEEE, 2021), pp. 2522–2524.
- <sup>166</sup>B. Li, P. Dhingra, R. D. Hool, S. Fan, and M. L. Lee, "Effect of threading dislocations on GaInP front- and rear-junction solar cells grown on Si," *IEEE J. Photovoltaics* **14**, 616–622 (2024).
- <sup>167</sup>B. C. Chung, H. C. Hamaker, G. F. Virshup, and J. G. Werthen, "15% efficiency (1 sun, air mass 1.5), large-area, 1.93 eV  $\text{Al}_x\text{Ga}_{1-x}\text{As}$  ( $x=0.37$ ) n-p solar cell grown by metalorganic vapor phase epitaxy," *Appl. Phys. Lett.* **52**, 631–633 (1988).
- <sup>168</sup>R. A. LaRue, P. G. Borden, M. J. Ludowise, P. E. Gregory, and W. T. Dietz, "The metal interconnected cascade solar cell," in *Proceedings of the Photovoltaic Specialists Conference*, San Diego, CA (1982).
- <sup>169</sup>C. Amano, H. Sugiura, K. Ando, M. Yamaguchi, and A. Saletes, "High-efficiency  $\text{Al}_{0.3}\text{Ga}_{0.7}\text{As}$  solar cells grown by molecular beam epitaxy," *Appl. Phys. Lett.* **51**, 1075–1077 (1987).
- <sup>170</sup>M. J. Ludowise, R. A. LaRue, P. G. Borden, P. E. Gregory, and W. T. Dietz, "High-efficiency organometallic vapor phase epitaxy AlGaAs/GaAs monolithic cascade solar cell using metal interconnects," *Appl. Phys. Lett.* **41**, 550–552 (1982).
- <sup>171</sup>C. Amano, H. Sugiura, A. Yamamoto, and M. Yamaguchi, "20.2% efficiency  $\text{Al}_{0.4}\text{Ga}_{0.6}\text{As}/\text{GaAs}$  tandem solar cells grown by molecular beam epitaxy," *Appl. Phys. Lett.* **51**, 1998–2000 (1987).
- <sup>172</sup>M. G. Crawford and W. O. Groves, "Vapor phase epitaxial materials for LED applications," *Proc. IEEE* **61**, 862–880 (1973).
- <sup>173</sup>M. S. Abrahams, L. R. Weisberg, C. J. Buiocchi, and J. Blanc, "Dislocation morphology in graded heterojunctions:  $\text{GaAs}_{1-x}\text{P}_x$ ," *J. Mater. Sci.* **4**, 223–235 (1969).
- <sup>174</sup>V. Sabnis, H. Yuen, and M. Wiemer, "High-efficiency multijunction solar cells employing dilute nitrides," *AIP Conf. Proc.* **1477**, 14–19 (2012).
- <sup>175</sup>C. T. Foxon, J. B. Clegg, K. Woodbridge, D. Hilton, P. Dawson, and P. Blood, "The effect of the oxygen concentration on the electrical and optical-properties of AlGaAs films grown by Mbe," *J. Vacuum Sci. Technol. B* **3**, 703 (1985).
- <sup>176</sup>T. Achtnich, G. Burri, and M. Illegems, "Study of oxygen incorporation in AlGaAs layers grown by molecular-beam epitaxy," *J. Vacuum Sci. Technol. A-Vacuum Surf. Films* **7**, 2537–2541 (1989).
- <sup>177</sup>T. Agui, T. Takamoto, and M. Kaneiwa, "Investigation on AlInGaP solar cells for current matched multijunction cells," in *Proceedings of the 3rd World Conference on Photovoltaic Energy Conversion* (IEEE, 2003), Vol. 1, pp. 670–672.
- <sup>178</sup>C. Morioka, M. Imaizumi, T. Ohshima, H. Itoh, and K. Kibe, "Study on optimum structure of AlInGaP top cell for triple-junction space solar cell," in *Proceedings of the 2006 IEEE 4th World Conference on Photovoltaic Energy Conference* (IEEE, 2006), pp. 1846–1849.
- <sup>179</sup>R. Campesato, M. Casale, G. Gori, G. Gabetta, R. Colletto, and S. Taylor, "High efficiency solar cells based on AlInGaP," in *Proceedings of the 34th IEEE Photovoltaic Specialists Conference (PVSC)* (IEEE, 2009), pp. 1112–1117.
- <sup>180</sup>A. Le Donne, M. Acciarri, G. Gori, R. Colletto, R. Campesato, and S. Binetti, "Optical and electrical characterization of AlGaInP solar cells," *Sol. Energy Mater. Sol. Cells* **94**, 2002–2006 (2010).
- <sup>181</sup>A. B. Cornfeld, P. Patel, J. Spann, D. Aiken, and J. McCarty, "Evolution of a 2.05 eV AlGaInP top sub-cell for 5 and 6J-IMM applications," in *Proceedings of the 38th IEEE Photovoltaic Specialists Conference (PVSC)* (IEEE, 2012), pp. 2788–2791.
- <sup>182</sup>T. Masuda, S. Tomasulo, J. R. Lang, and M. L. Lee, "Comparison of single junction AlGaInP and GaInP solar cells grown by molecular beam epitaxy," *J. Appl. Phys.* **117**, 094504 (2015).
- <sup>183</sup>J. Faucher, Y. Sun, D. Jung, D. Martin, T. Masuda, and M. L. Lee, "High-efficiency AlGaInP solar cells grown by molecular beam epitaxy," *Appl. Phys. Lett.* **109**, 172105 (2016).
- <sup>184</sup>E. E. Perl, J. Simon, J. F. Geisz, W. Olavarria, M. Young, A. Duda *et al.*, "Development of a 2.0 eV AlGaInP solar cell grown by OMVPE," in *Proceedings of the 42nd IEEE Photovoltaic Specialist Conference (PVSC)* (IEEE, 2015), pp. 1–6.
- <sup>185</sup>M. W. Wanlass, S. P. Ahrenkiel, J. J. Carapella, D. J. Friedman, C. R. Osterwald, and M. Romero, "Progress toward an advanced four-subcell inverted metamorphic multi-junction (IMM) solar cell," *Prog. Photovoltaics Res. Appl.* **24**, 139–149 (2016).
- <sup>186</sup>M. A. Steiner, R. M. France, M. W. Wanlass, J. F. Geisz, W. J. Olavarria, J. J. Carapella *et al.*, "2.0–2.1 eV  $\text{Ga}_x\text{In}_{1-x}\text{P}$  solar cells grown on relaxed GaAsP step grades," in *Proceedings of the 35th IEEE Photovoltaic Specialists Conference* (IEEE, 2010), pp. 2111–2116.
- <sup>187</sup>J. Simon, S. Tomasulo, P. J. Simmonds, M. Romero, and M. L. Lee, "Metamorphic GaAsP buffers for growth of wide-bandgap InGaP solar cells," *J. Appl. Phys.* **109**, 13708–13706 (2011).
- <sup>188</sup>S. Tomasulo, K. N. Yaung, and M. L. Lee, "Metamorphic GaAsP and InGaP solar cells on GaAs," *Photovoltaics, IEEE J.* **2**, 56–61 (2012).
- <sup>189</sup>J. Simon, S. Tomasulo, P. J. Simmonds, M. Romero, and M. L. Lee, "Metamorphic InGaP on GaAs and GaP for widebandgap photovoltaic junctions," in *Proceedings of the 35th IEEE Photovoltaic Specialists Conference* (IEEE, 2010), p. 3760.
- <sup>190</sup>S. Tomasulo, J. Simon, P. J. Simmonds, J. Biagiotti, and M. L. Lee, "Molecular beam epitaxy of metamorphic  $\text{In}_x\text{Ga}_{1-y}\text{P}$  solar cells on mixed anion  $\text{GaAs}_x\text{P}_{1-x}/\text{GaAs}$  graded buffers," *J. Vacuum Sci. Technol. B* **29**, 03C118 (2011).
- <sup>191</sup>S. Tomasulo, J. Faucher, J. R. Lang, K. N. Yaung, and M. L. Lee, "2.19 eV InGaP solar cells on GaP substrates," in *Proceedings of the 39th IEEE Photovoltaic Specialists Conference*, Tampa, FL (2013).
- <sup>192</sup>S. Tomasulo, K. Nay Yaung, J. Faucher, M. Vaisman, and M. L. Lee, "Metamorphic 2.1–2.2 eV InGaP solar cells on GaP substrates," *Appl. Phys. Lett.* **104**, 173903 (2014).
- <sup>193</sup>D. W. Cardwell, N. Vaughn, P. Paul, C. Ratcliff, D. Chmielewski, S. Carnevale *et al.*, "Investigations of metamorphic (Al)GaInP for III–V multijunction photovoltaics," in *Proceedings of the 42nd IEEE Photovoltaic Specialist Conference (PVSC)* (IEEE, 2015), pp. 1–4.
- <sup>194</sup>C. R. Allen, J.-H. Jeon, and J. M. Woodall, "Simulation assisted design of a gallium phosphide n-p photovoltaic junction," *Sol. Energy Mater. Sol. Cells* **94**(5), 865–868 (2010).
- <sup>195</sup>C. R. Allen, J. M. Woodall, and J. H. Jeon, "Results of a gallium phosphide photovoltaic junction with an AR coating under concentration of natural sunlight," *Sol. Energy Mater. Sol. Cells* **95**, 2655–2658 (2011).
- <sup>196</sup>X. Lu, S. R. Huang, M. Diaz, R. L. Opila, and A. Barnett, "Wide band gap Gallium Phosphide solar cells for multi-junction solar cell system," in *Proceedings of the 35th IEEE Photovoltaic Specialists Conference (PVSC)* (IEEE, 2010), pp. 2079–2083.
- <sup>197</sup>X. Lu, M. Diaz, N. Kotulak, R. L. Opila, and A. Barnett, "Quantum efficiency model driven design for wide band gap gallium phosphide solar cells," in *Proceedings of the 2011 37th IEEE Photovoltaic Specialists Conference* (IEEE, 2011), pp. 507–512.
- <sup>198</sup>X. Lu, S. Huang, M. B. Diaz, N. Kotulak, R. Hao, R. Opila *et al.*, "Wide band gap gallium phosphide solar cells," *Photovoltaics, IEEE J.* **2**, 214–220 (2012).
- <sup>199</sup>X. Lu, H. Ruiying, M. Diaz, R. L. Opila, and A. Barnett, "Improving GaP solar cell performance by passivating the surface using  $\text{Al}_x\text{Ga}_{1-x}\text{P}$  epi-layer," *IEEE J. Electron Devices Soc.* **1**, 111–116 (2013).
- <sup>200</sup>M. Vaisman, S. Tomasulo, T. Masuda, J. R. Lang, J. Faucher, and M. L. Lee, "Effects of growth temperature and device structure on GaP solar cells grown by molecular beam epitaxy," *Appl. Phys. Lett.* **106**, 063903 (2015).
- <sup>201</sup>R. J. Walters, M. González, J. G. Tischler, M. P. Lumb, J. R. Meyer, I. Vurgaftman *et al.*, "Design of an achievable, all lattice-matched multijunction solar cell using InGaAlAsSb," in *Proceedings of the 2011 37th IEEE Photovoltaic Specialists Conference* (IEEE, 2011), pp. 122–126.
- <sup>202</sup>M. González, M. Lumb, M. Yakes, J. Abell, J. Tischler, C. Bailey *et al.*, "Modeling, design and experimental results for high efficiency multi-junction solar cells lattice matched to InP," in *Physics, Simulation, and Photonic Engineering of Photovoltaic Devices III* (SPIE, 2014), Vol. 8981.
- <sup>203</sup>S. Tomasulo, M. Gonzalez, J. G. Tischler, J. Abell, M. P. Lumb, M. K. Yakes *et al.*, "Molecular beam epitaxy of InAlAsSb for the top cell in high-efficiency InP-based lattice-matched triple-junction solar cells," in *Proceedings of the*

- <sup>2015</sup> IEEE 42nd Photovoltaic Specialist Conference (PVSC) (IEEE, 2015), pp. 1–4.
- <sup>204</sup>M. González, M. P. Lumb, L. C. Hirst, S. Tomasulo, J. G. Tischler, W. Yoon *et al.*, “Rapid thermal annealing of InAlAsSb lattice-matched to InP for top cell applications,” in *Proceedings of the 2015 IEEE 42nd Photovoltaic Specialist Conference (PVSC)* (IEEE, 2015), pp. 1–4.
- <sup>205</sup>S. Tomasulo, M. Gonzalez, M. P. Lumb, C. R. Brown, A. H. Dicarlo, I. R. Sellers *et al.*, “Effect of molecular beam epitaxy growth conditions on phase separation in wide-bandgap InAlAsSb lattice-matched to InP,” *J. Cryst. Growth* **548**, 125826 (2020).
- <sup>206</sup>Y.-H. Cho, G. H. Gainer, A. J. Fischer, J. J. Song, S. Keller, U. K. Mishra *et al.*, “S-shaped” temperature-dependent emission shift and carrier dynamics in InGaN/GaN multiple quantum wells,” *Appl. Phys. Lett.* **73**, 1370–1372 (1998).
- <sup>207</sup>S. Mazzucato, R. J. Potter, A. Erol, N. Balkan, P. R. Chalker, T. B. Joyce *et al.*, “S-shaped behaviour of the temperature-dependent energy band gap in dilute nitrides,” *Phys. E* **17**, 242–244 (2003).
- <sup>208</sup>L. C. Hirst, M. P. Lumb, J. Abell, C. T. Ellis, J. G. Tischler, I. Vurgaftman *et al.*, “Spatially indirect radiative recombination in InAlAsSb grown lattice-matched to InP by molecular beam epitaxy,” *J. Appl. Phys.* **117**, 215704 (2015).
- <sup>209</sup>S. Tomasulo, M. Gonzalez, M. P. Lumb, M. E. Twigg, I. Vurgaftman, J. R. Meyer *et al.*, “Molecular beam epitaxy of wide-bandgap InAlAsSb on InP substrates for an all lattice-matched triple-junction solar cell,” in *Proceedings of the 2019 IEEE 46th Photovoltaic Specialists Conference (PVSC)* (IEEE, 2019), pp. 3187–3190.
- <sup>210</sup>M. K. Yakes, K. J. Schmieder, M. P. Lumb, M. F. Bennett, M. Gonzalez, P. D. Cunningham *et al.*, “Evaluation of strained InAlAs as a window layer for wide bandgap materials lattice matched to InP,” in *Proceedings of the 2015 IEEE 42nd Photovoltaic Specialist Conference (PVSC)* (IEEE, 2015), pp. 1–4.
- <sup>211</sup>D. A. Beaton, T. Christian, K. Alberi, A. Mascarenhas, K. Mukherjee, and E. A. Fitzgerald, “Determination of the direct to indirect bandgap transition composition in  $\text{Al}_x\text{In}_{1-x}\text{P}$ ,” *J. Appl. Phys.* **114**, 203504 (2013).
- <sup>212</sup>M. Vaisman, K. Mukherjee, T. Masuda, K. N. Yauing, E. A. Fitzgerald, and M. L. Lee, “Direct-Gap 2.1–2.2 eV AlInP solar cells on GaInAs/GaAs metamorphic buffers,” *IEEE J. Photovoltaics* **6**, 571–577 (2016).
- <sup>213</sup>J. T. Boyer, D. L. Lepkowski, D. J. Chmielewski, and T. J. Grassman, “Modeling and experimental demonstration of short-wavelength carrier collection enhancement in  $\text{Ga}_{0.51}\text{In}_{0.49}\text{P}$  solar cells using graded  $(\text{Al}_z\text{Ga}_{1-z})_x\text{In}_{1-x}\text{P}$  window-emitter structures,” *Sol. Energy Mater. Sol. Cells* **202**, 110133 (2019).
- <sup>214</sup>S. Miyoshi, H. Yaguchi, K. Onabe, R. Ito, and Y. Shiraki, “Metalorganic vapor phase epitaxy of  $\text{GaP}_{1-x}\text{N}_x$  alloys on GaP,” *Appl. Phys. Lett.* **63**, 3506–3508 (1993).
- <sup>215</sup>W. G. Bi and C. W. Tu, “N incorporation in GaP and band gap bowing of  $\text{GaN}_x\text{P}_{1-x}$ ,” *Appl. Phys. Lett.* **69**, 3710–3712 (1996).
- <sup>216</sup>G. Biwa, H. Yaguchi, K. Onabe, and Y. Shiraki, “Metalorganic vapor-phase epitaxy of  $\text{GaP}_{1-x-y}\text{As}_y\text{N}_x$  quaternary alloys on GaP,” *J. Cryst. Growth* **189–190**, 485–489 (1998).
- <sup>217</sup>Y. Fujimoto, H. Yonezu, A. Utsumi, K. Momose, and Y. Furukawa, “Dislocation-free  $\text{GaAs}_y\text{P}_{1-x-y}\text{N}_x/\text{GaP}_{0.98}\text{N}_{0.02}$  quantum-well structure lattice-matched to a Si substrate,” *Appl. Phys. Lett.* **79**, 1306–1308 (2001).
- <sup>218</sup>J. F. Geisz, D. J. Friedman, and S. Kurtz, “GaNPAs solar cells lattice-matched to GaP,” in *Proceedings of the Conference Record of the 29th IEEE Photovoltaic Specialists Conference* (IEEE, 2002), pp. 864–867.
- <sup>219</sup>J. F. Geisz, J. M. Olson, D. J. Friedman, K. M. Jones, R. C. Reedy, and M. J. Romero, “Lattice-matched GaNPAs-on-silicon tandem solar cells,” in *Proceedings of the Conference Record of the 31st IEEE Photovoltaic Specialists Conference* (IEEE, 2005), pp. 695–698.
- <sup>220</sup>J. F. Geisz, R. C. Reedy, B. M. Keyes, and W. K. Metzger, “Unintentional carbon and hydrogen incorporation in GaNP grown by metal-organic chemical vapor deposition,” *J. Cryst. Growth* **259**, 223–231 (2003).
- <sup>221</sup>S. Ilahi, S. Almosni, F. Chouchane, M. Perrin, K. Zelazna, N. Yacoubi *et al.*, “Optical absorption and thermal conductivity of GaAsPN absorbers grown on GaP in view of their use in multijunction solar cells,” *Sol. Energy Mater. Sol. Cells* **141**, 291–298 (2015).
- <sup>222</sup>S. Almosni, C. Robert, T. N. Thanh, C. Cornet, A. Létoublon, T. Quinci *et al.*, “Evaluation of InGaN and GaAsPN materials lattice-matched to Si for multijunction solar cells,” *J. Appl. Phys.* **113**, 123509 (2013).
- <sup>223</sup>M. Feifel, J. Ohlmann, R. M. France, D. Lackner, and F. Dimroth, “Electron channeling contrast imaging investigation of stacking fault pyramids in GaP on Si nucleation layers,” *J. Cryst. Growth* **532**, 125422 (2020).
- <sup>224</sup>R. D. Hool, Y. Chai, Y. Sun, B. C. Eng, P. Dhingra, S. Fan *et al.*, “Relaxed GaP on Si with low threading dislocation density,” *Appl. Phys. Lett.* **116**, 042102 (2020).
- <sup>225</sup>S. J. Maddox, S. D. March, and S. R. Bank, “Broadly tunable AlInAsSb digital alloys grown on GaSb,” *Cryst. Growth Des.* **16**, 3582–3586 (2016).
- <sup>226</sup>M. E. Woodson, M. Ren, S. J. Maddox, Y. Chen, S. R. Bank, and J. C. Campbell, “Low-noise AlInAsSb avalanche photodiode,” *Appl. Phys. Lett.* **108**, 081102 (2016).
- <sup>227</sup>B. Guo, M. Schwartz, S. H. Kodati, K. M. McNicholas, H. Jung, S. Lee *et al.*, “InGaAs/AlInAsSb avalanche photodiodes with low noise and strong temperature stability,” *APL Photonics* **8**, 116112 (2023).
- <sup>228</sup>D. B. Jackrel, S. R. Bank, H. B. Yuen, M. A. Wistey, J. S. Harris, Jr., A. J. Ptak *et al.*, “Dilute nitride GaInNAs and GaInNAsSb solar cells by molecular beam epitaxy,” *J. Appl. Phys.* **101**, 114916 (2007).
- <sup>229</sup>D. A. Vanderwater, I. H. Tan, G. E. Hofler, D. C. Defevere, and F. A. Kish, “High-brightness AlGaInP light emitting diodes,” *Proc. IEEE* **85**, 1752–1764 (1997).